QUANTIFYING IMPACTS OF GLOBAL CHANGE ON HYDROLOGY AND SEDIMENT

By

Travis A. Dahl

A DISSERTATION

Submitted to
Michigan State University
in partial fulfillment of the requirements
for the degree of

Environmental Geosciences—Doctor of Philosophy

2019

ABSTRACT

QUANTIFYING IMPACTS OF GLOBAL CHANGE ON HYDROLOGY AND SEDIMENT

By

Travis A. Dahl

The hydrologic cycle evolves over time, with landscape changes driving differences in evapotranspiration, runoff, and groundwater recharge while climate change affects the timing and magnitude of precipitation as well as temperature. These changes also affect how sediment moves across the landscape and through watersheds. In this dissertation, I examine how land use changes and climate change both affect the movement of water and sediment through watersheds in the Great Lakes Basin.

Extreme cases of land use change, such as the logging and forest fires that affected large swaths of the Great Lakes in the late 19th and early 20th centuries, can greatly increase both streamflow and sediment transport. Chapter 1 utilizes the process-based Landscape Hydrologic Model (LHM) to examine the hydrologic effects of land use change from the forested pre-settlement condition to clearcut, burned, and modern land uses in the northwestern corner of Michigan's Lower Peninsula. I show that extensive fires could have increased streamflow by 160% relative to the virgin forest landscape and 96% relative to the logged scenario. Chapter 2 focuses on modeling of the Jordan River watershed, showing that logging may have increased sediment transport in the river by up to 34% compared to pre-settlement conditions and a watershed-wide fire could have increased the sediment transport capacity by as much as 166% above the pre-settlement levels. A reach-based sediment budgeting tool, the Sediment Impact Assessment Methods (SIAM), highlights the possibility of complex system responses to land use change over time.

Chapter 3 explores the potential impacts of climate change on sediment yield and dredging costs in the adjacent Maumee and St. Joseph River watersheds where I project that dredging costs may change in opposite directions (-8 to -16% in the St. Joseph but +1 to +6% in the Maumee). This difference between the two watersheds is driven by differences in the proportion of farmland and assumptions about how farmers will

respond to a changing climate. I also show that there is a large variation in sediment yield and sediment discharge predictions because of the differences among the various Global Climate Model (GCM) projections.

Rather than downscale and run all of the GCM projections, many researchers average a subset of the projections together and use the ensembled climate data as the input to hydrologic models. In Chapter 4, I compare different climate change scenario ensembling methodologies to determine if they produce the same results. I show that a climate ensemble produces significantly ($p < 0.05$) different hydrologic model results than the ensemble of the hydrologic model results based on the individual climate scenarios. I also demonstrate a method for selecting a subset of climate ensemble members that captures most of the range of the hydrology outputs while also matching the hydrologic and sediment results from the entire set.

Global change causes complex hydrologic and sediment responses that need to be carefully considered in modeling and management. Land use mediates the effects of climate change and there are potential feedback mechanisms that will depend on how farmers and other land managers respond to the changing climate. This dissertation provides some of the information needed to identify and understand these interactions.

This dissertation is dedicated to Ken and Chris Dahl, who have always believed in me; to Jodi Ryder who showed me it could be done; and to Rachel and Lexi, whom I hope to continue inspiring.

ACKNOWLEDGEMENTS

This dissertation would not have been possible without the direct and indirect support of my friends and colleagues. My advisor, David Hyndman, has provided advice and guidance not just on navigating a Ph.D. at MSU but research in general. Anthony Kendall, in addition to serving on my committee, has been an invaluable collaborator on coding, writing, and research. My remaining committee members, Phanikumar Mantha and Jay Zarnetske, have both provided timely advice that has kept me moving forward towards my academic and professional goals.

A number of people have provided informal mentoring to me before and during this process, whether they know it or not. I would like to particularly recognize Steve Daly, Grahame Larson, and David Biedenharn. Tom Willemain was my master's advisor for a thesis that I finished but a degree that I didn't. Jim Selegean not only provided mentoring but actively helped to arrange work projects that could support my academic goals. Tim Calappi, Calvin Creech, and Stanford Gibson all showed me that it is possible to finish a Ph.D. while working at the U.S. Army Corps of Engineers. Kate White provided encouragement and funding for the initial phases of the climate change portions of my dissertation.

My family has supported me emotionally and, occasionally, financially throughout my time in graduate school. I am incredibly lucky to have been supported by my parents, Ken and Chris Dahl, throughout my life. My wife, Jodi Ryder, provided emotional support and the occasional kick in the pants to keep me moving. My path through the Ph.D. was significantly easier and more productive because of lessons learned from her academic experiences. Finally, I have to thank my daughters for being the wonderful, supportive, curious, and thoughtful people that they are. Rachel probably can't remember a time when I wasn't in graduate school and Lexi wasn't even born when I started this process. They have been needed distractions and reminders of what is important as I toiled away.

"Got to pay your dues if you wanna sing the blues and you know it don't come easy."
–Ringo Starr

"Look! A trickle of water running through some dirt! I'd say our afternoon just got booked solid!"
–Calvin & Hobbes (Bill Waterson)

TABLE OF CONTENTS

LIST OF TABLES

LIST OF FIGURES

CHAPTER 1:
MODELED EFFECTS OF HISTORICAL LAND USE CHANGE ON REGIONAL HYDROLOGY USING AN INTEGRATED HYDROLOGIC MODEL

Abstract

Humans have been altering the landscape for thousands of years. These changes affect the hydrologic cycle by altering evapotranspiration, runoff, and groundwater recharge. We used the process-based Landscape Hydrology Model to examine the impact that widespread logging, forest fires, and landscape recovery likely had in the northern portion of Michigan's Lower Peninsula. Compared to the pre-settlement landcover, a clearcut landscape would have reduced evapotranspiration, leading to increased groundwater recharge (+19%) and streamflow (+5 to +37%) in the model. Fires likely amplified this trend, with an extreme modeled burn scenario resulting in very large increases to groundwater recharge (+99%) and streamflow (+68 to +160%) relative to pre-settlement. Our model results indicate that the modern landscape has slightly lower levels of evapotranspiration, but greater groundwater recharge (+2%) and streamflow (+2.1 to 5.8%) than it did pre-settlement.

1. Introduction

Humans can profoundly affect the hydrologic cycle through land use change. Urbanization is often mentioned in the context of changing hydrology but logging and wildfire can affect much greater areas. Examples of these impacts exist from antiquity (Abrams and Rue, 1988; Ellis et al., 2013; Rothacker et al., 2018), but there is evidence that forest clearing and wildfires have accelerated in modern times (Gentry and Lopez-Parodi, 1980; Hansen et al., 2010; Kalamandeen et al., 2018; Potapov et al., 2017). It is important for mankind to have a better understanding of the hydrologic impacts of this land use change.

Mature forests, like those that covered large portions of North America prior to European settlement, tend to produce little runoff due to their high rates of evapotranspiration. Logging removes this evapotranspiration demand and reduces canopy interception of rainfall for a period of time until the vegetation recovers, leading to increased streamflow for a period of time (Bosch and Hewlett, 1982; Bowling et al., 2000; Gentry and Lopez-Parodi, 1980; Li et al., 2007; Zhang and Wei, 2014). This increase in streamflow can last for several decades (Hicks et al., 1991; Lewis et al., 2001; Zhang et al., 2012).

In a comprehensive review of the effects of fire on hydrology, Moody et al. (2013) describe the bare-ground hypothesis for the primary effect of wildfire on runoff as due to the removal of vegetation. This is supported by numerous papers that have found a significant linkage between vegetated area and runoff, both immediately post-fire and during the recovery process (Cerda, 1998; Johansen et al., 2001). The increase in runoff after a forest fire tends to last until a sufficient amount of vegetation regrows (Helvey, 1980). Regrowth can take more than 7 years, although many authors report shorter recovery times (Ebel et al., 2016; Moody and Martin, 2001b; Moody et al., 2013; Shin et al., 2013). Another, often cited effect of wildfires is an increase in the water repellency of soils that can decrease infiltration (Shakesby and Doerr, 2006). This phenomena can be highly variable in both space and time, although the most extreme effects may only last minutes to months (Doerr et al., 2000; Doerr and Thomas, 2000). Additionally, there appears to be a critical threshold of soil moisture below which water repellency can become a significant issue, reducing its importance in humid environments (Dekker et al., 2001; Doerr and Thomas, 2000).

The Great Lakes region of North America experienced both extensive logging and fires followed by a range of land use changes that include agricultural expansion, urbanization, and forest regrowth over the last 150 years and can help us to understand the potential effects of similar events in other non-alpine parts of the world. Forests covered most of Michigan into the mid-19th century (Comer and Albert, 1998). Large-scale logging operations in the late 19th century removed almost all of the native forests (Dickmann, 2009), starting with the easily accessible softwoods and then moving on to the hardwoods and wooded wetlands as technology improved (Whitney, 1987). The logging industry often left behind branches, stumps, and other debris that provided fuel for large fires, some of which were started on purpose (Dickmann, 2009). Haines and Sando (1969) note that at one point, in October, 1871, more than 10,000 km^2 were burning across the Great Lakes states. Some of these same areas were also part of a 4,000 km^2 fire in 1881. The mix of tree species that eventually repopulated these areas were often different than the original forests (Whitney, 1987).

Directly measuring the impact of multiple land use changes is often impossible because the change has already occurred or will have undesirable consequences. Instead, researchers often use hydrologic models to simulate the effects of land use changes. Hydrologic models have been used extensively to look at the effects of logging on evapotranspiration and streamflow (Bowling et al., 2000; Matheussen et al., 2000; Swank et al., 2001; Whitaker et al., 2002). Twine et al. (2004) examined the hydrologic impact of converting forests and grassland to agriculture in the Mississippi River Basin, while other researchers modeled the hydrologic differences between pre-settlement and modern landcovers in the Upper Midwest and Great Lakes region of the United States (Fitzpatrick and Knox, 2000; Frans et al., 2013; Mao and Cherkauer, 2009). A number of researchers have also used hydrologic models to examine post-fire impacts on hydrology, although much of this work has been focused in the mountainous western United States (Gould et al., 2016; Larsen and MacDonald, 2007; Litschert et al., 2014; Miller et al., 2003) or the Mediterranean (Fernandez et al., 2010; Karamesouti et al., 2016; Rulli et al., 2013; Terranova et al., 2009) where fires have been more prevalent in recent decades.

This study uses the process-based Landscape Hydrology Model (LHM) to examine the water balance and streamflow impacts of three large-scale anthropogenic disturbances in the Great Lakes region: logging, forest fire, and modern land use. The model was run with the same 30 year meteorological forcing for each of the three scenario. The effects of these disturbances are compared to model results for the pre-settlement landcover of the early 19^{th} century.

2. Methods

2.1 Site Description

The Extended Boardman-Charlevoix Watershed (EBCW) model covers the northwestern corner of Michigan's Lower Peninsula. The model is designed to capture all of the watersheds draining to Grand Traverse and Little Traverse Bays. The model domain is bounded by Lake Michigan on the north and west, by the Muskegon River to the south, and the Sturgeon and North Branch Au Sable Rivers to the east (Figure 1.1). This larger domain ensures that both the surface watersheds and groundwatersheds are fully captured by the model. The surficial geology of this area is dominated by glacial deposits and landforms (Blewett et al., 2009). The soils tend have high sand content. The dominant modern land use is 47% forest (40% deciduous and 7% coniferous) with an additional 12% occupied by woody wetlands (Fry et al., 2013). The remainder of the area is composed of grassland (13%), agriculture (10%), urban (8%), and open water (6%), with shrublands, wetlands, and barren areas each contributing less than 5% each.

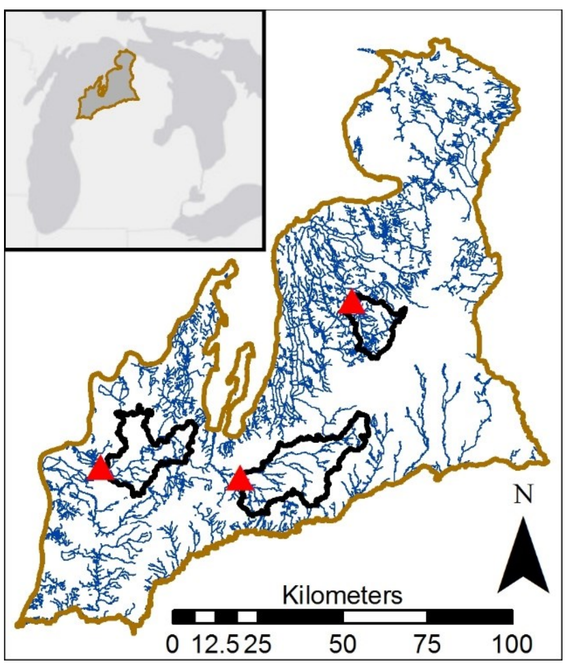

Figure 1.1. Extended Boardman Charlevoix Watershed Model location map. The Jordan, Boardman, and Platte River watersheds are outlined in black. USGS gages are indicated by red triangles.

The study area received an average of 842 mm of precipitation per year between

1986 and 2015 (Figure S1.1, left). There is some spatial variation in precipitation, with the western portions of the EBCW receiving more precipitation (up to 914 mm/year), and the northern portions receiving the least (as low as 734 mm/year). The mean annual temperature for the EBCW over the same time period was 7.3 °C (Figure S1.1, right). The areas close to Lake Michigan on the west side of the model domain generally have warmer mean air temperatures (up to 8.4 °C) than the inland areas (as low as 6.1 °C), due to the moderating effect of the lake on winter temperatures.

2.2. LHM Model Setup

LHM is a process-based, gridded model that utilizes commonly available GIS data combined with energy and mass-balance equations to simulate evapotranspiration, groundwater recharge, and streamflow (Hyndman et al., 2007). LHM can simulate snowmelt and other hydrologic pathways, including canopy growth and interception. The model can also be linked to MODFLOW (Harbaugh et al., 2000) to allow groundwater to move beyond the limits of individual surface watersheds. LHM has been successfully applied to multiple watersheds in the Great Lakes Region (Luscz et al., 2017; Wiley et al., 2010).

The EBCW LHM model is based on 1/3 arc-second (10 m) resolution digital elevation model data from the National Elevation Dataset, as well as data from the National Hydrography Dataset, and the National Wetlands Inventory. Soil data were extracted from the Soil Survey Geographic Database (SSURGO) using the procedures described above. The model uses a uniform grid cell size of 432 m.

The base model simulation used the pre-settlement land-cover described by the General Land Office surveys [Figure 1.2.a; Comer and Albert (1998)]. We then modified the pre-settlement land cover data set to create a post-logging scenario by converting all the forested areas (deciduous and coniferous) to grasslands and all of the woody wetlands to wetlands (Figure 1.2.b). We used a similar process to create the post-fire land use, converting all of the grasslands in the post-logging scenario to barren areas (Figure 1.2.c). This accounts for the major impacts of fire (removal of canopy interception and transpiration effects) but does not account for any impacts of fire-induced soil hydrophobicity. We assumed that any impact of fires on soil hydrophobicity would be negligible due to the humid nature and coarse-textured soils of the study area, an idea supported by two previous studies of fire-induced hydrophobicity in the Great Lakes (Reeder and Jurgensen, 1979; Richardson and Hole, 1978). Finally, we modeled the modern land use scenario using the 2006 National Land Cover Dataset [Figure 1.2.d; Fry et al. (2013)] because it was representative of the 1988-2017 time period used for model validation. Table S1.1 lists the proportions of each land use class for the modeled land use scenarios.

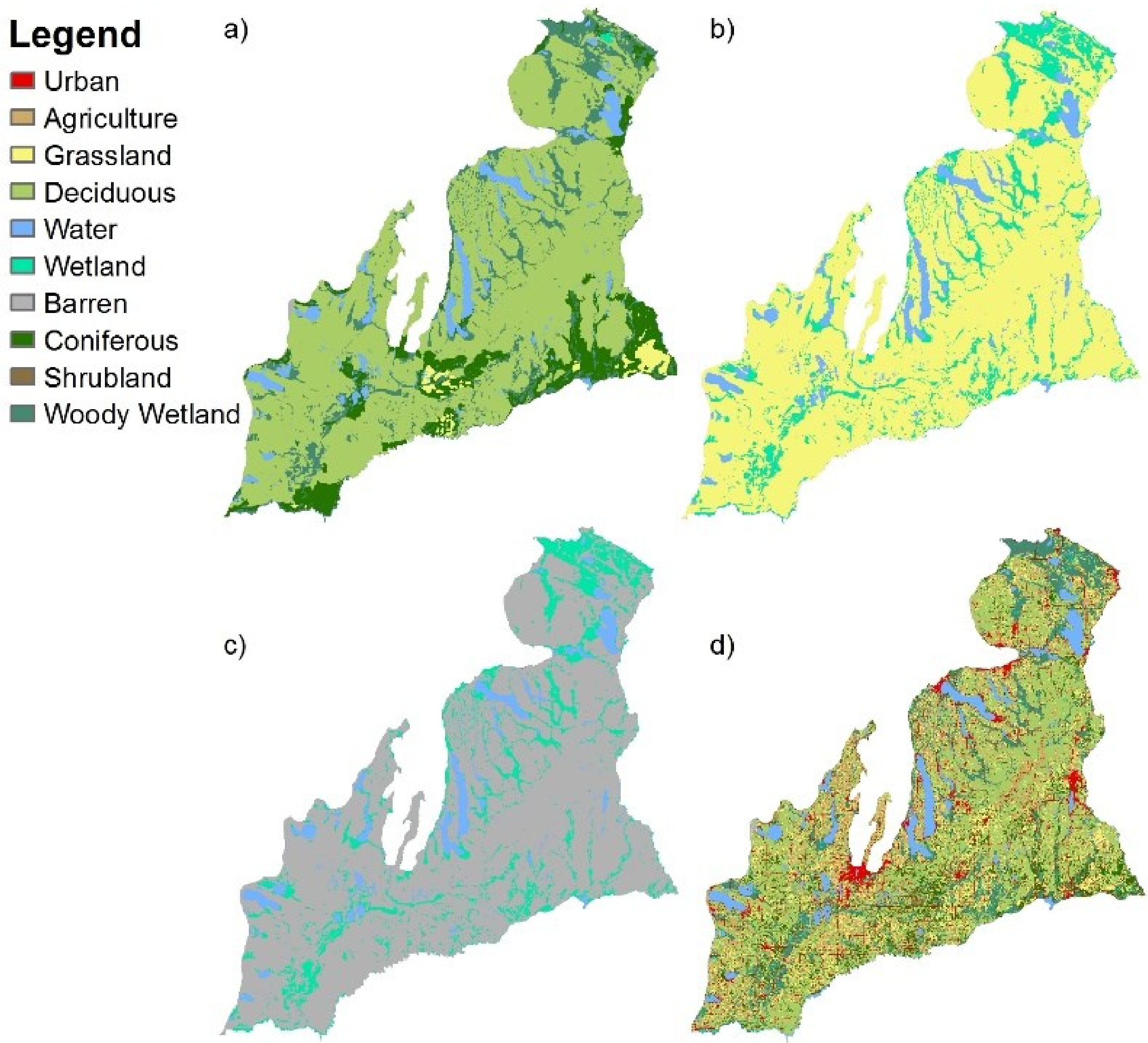

Figure 1.2. The modeled land use scenarios used for comparison to modern land use consisted of: (a) pre-settlement; (b) post-logging; (c) post-fire; and (d) modern land use.

The model was run using the same climate inputs for each land use scenario. Climate data were obtained from the North American Land Data Assimilation System (NLDAS) 2a forcing dataset for 1988-2017 (Xia et al., 2012). The input climate parameters included precipitation; temperature; shortwave and longwave radiation; specific humidity, and wind speed. We wanted to look at the likely effects of land use change based a range of climate scenarios. Our simulations used a thirty year period to capture a wide range of climate variability for each fixed land use case; this is the standard climatology length recommended by the World Meteorological Organization to calculate average conditions.

2.3 LAI Model

Typically, the vegetation components of LHM would be driven by Leaf Area Index (LAI) data from satellite remote sensing products, such as NASA's Moderate Resolution Imaging Spectroradiometer (MODIS). These allow for vegetation to dynamically respond to climate conditions during the simulation period, without requiring that LHM dynamically model vegetation. However, when conducting scenarios involving land transformation (or altered climate), we need an alternate means of assigning LAI values. LAI then in turn controls landscape albedo, canopy height, stomatal conductance, and other aspects of the landscape.

We validated the LAI model using the MODIS MCD15A2H and MCD15A3H products for 2000 – 2014. These are Collection 6 products produced using the MODIS instruments on both the Terra and Aqua satellites. They have a 500 meter spatial resolution and sub-weekly time scale.

3. Results and Discussion

3.1 Model Validation

The EBCW model was validated by comparing observed data to modeled data when using the modern land use with NLDAS climate inputs for years 2000-2014.

Streamflow and Groundwater Head Validation

We obtained observed groundwater head data from the State of Michigan's Wellogic database and the USGS. Our simulated groundwater head data matches the observed heads for years 2000-2014 with an r^2 of 0.98 (Figure 1.3, left). The median head residual is -1.63 m for all observations with 10% and 90% values of -13.65 m and 8.69 m, respectively. The median decreases slightly over this validation time period, but remains centered near zero (Figure 1.3, right).

We validated streamflow using three rivers in the EBCW model domain: the Jordan (174 km^2), in the eastern portion of the domain; the Boardman (482 km^2), in the central portion; and the Platte (325 km^2), in the western portion (Figure 1.1). When compared to monthly average gaged flows from the USGS for 2000-2014, this uncalibrated model reasonably matches the baseflows and the major rises on two of the rivers (Figure 1.4). The Jordan and Boardman Rivers have Nash-Sutcliffe Efficiencies (NSE) of 0.42 and 0.52, respectively, for mean monthly flows. The Platte, where the model overpredicts flows due to the spring freshet, has a NSE of -0.26 but maintains an r^2 of 0.45.

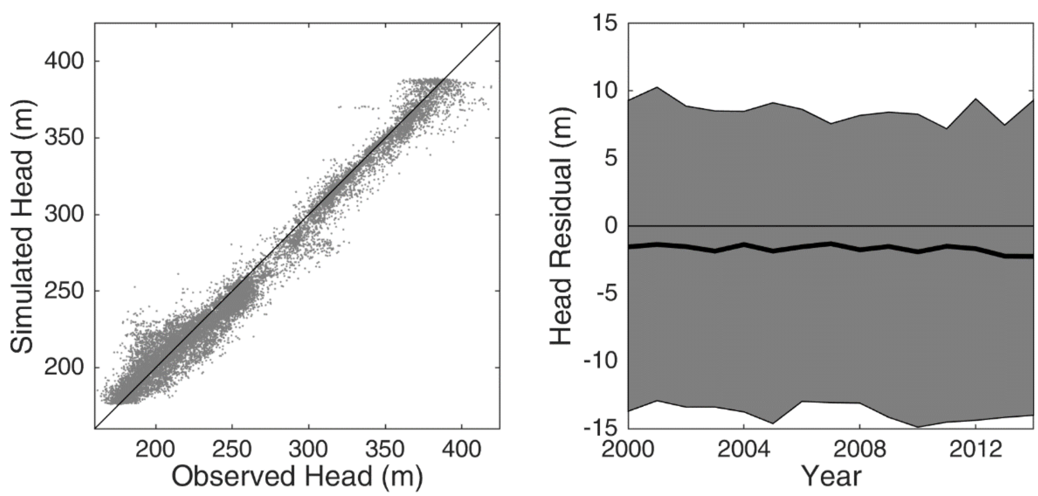

Figure 1.3. Comparing simulated and observed groundwater head for years 2000-2014 demonstrates the validity of the EBCW groundwater model. The figure on the left shows simulated and observed heads along with the line of perfect agreement. The figure on the right shows the time series of the residual mean with the grey-shaded area representing the 10th and 90th percentiles.

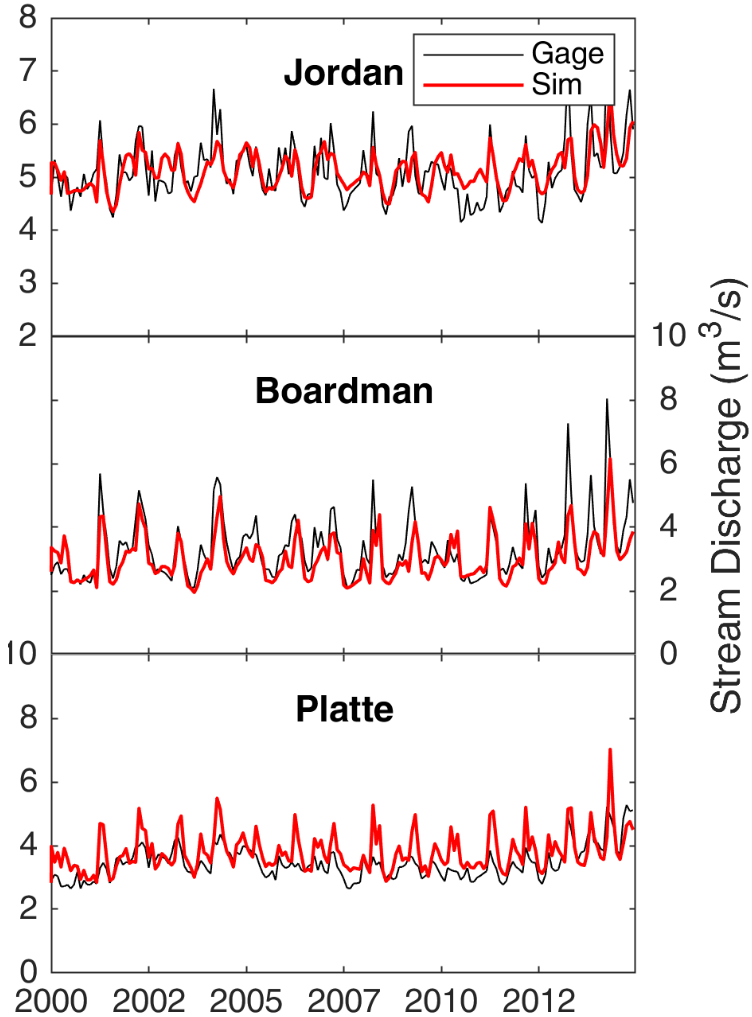

Figure 1.4. A comparison of gaged (black line) and simulated (red line) streamflows in three rivers (Jordan, a; Boardman, b; Platte, c) demonstrates the validity of the modern land use scenario model for years 2000-2014.

LAI Validation

The simulated LAI generally agrees with the observed data (Figure 1.5) and captures the annual vegetative growth dynamics (Figure 1.6). Several of the land use types have a maximum modeled LAI value, which is visible in Figure 1.5 and Figure 1.6 (e.g., shrubland in the middle of the bottom row in both figures).

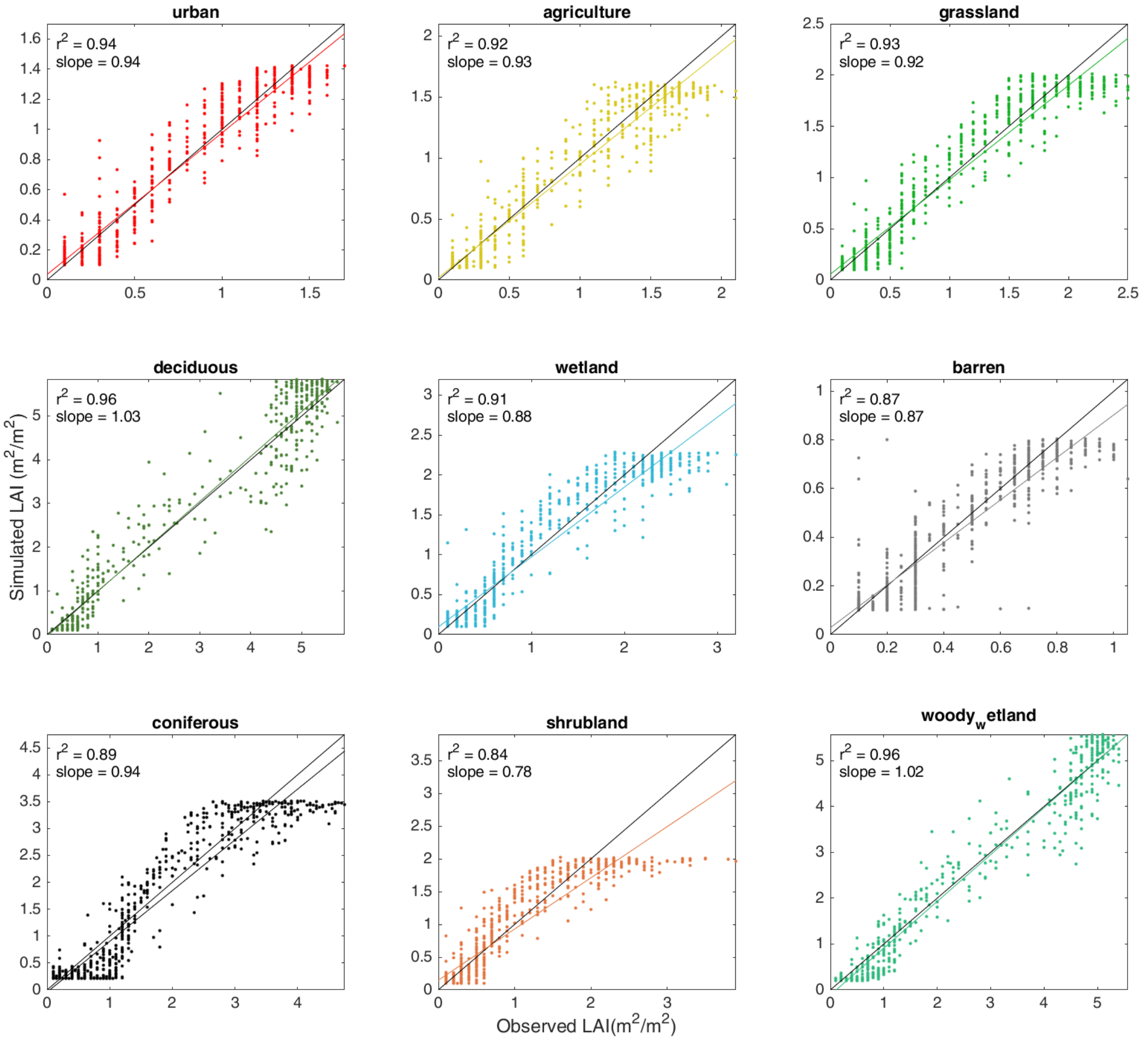

Figure 1.5. Comparison of observed (horizontal axis) and simulated (vertical axis) LAI values for each land cover type. The effect of the maximum LAI value in the model is visible for several of the cover types.

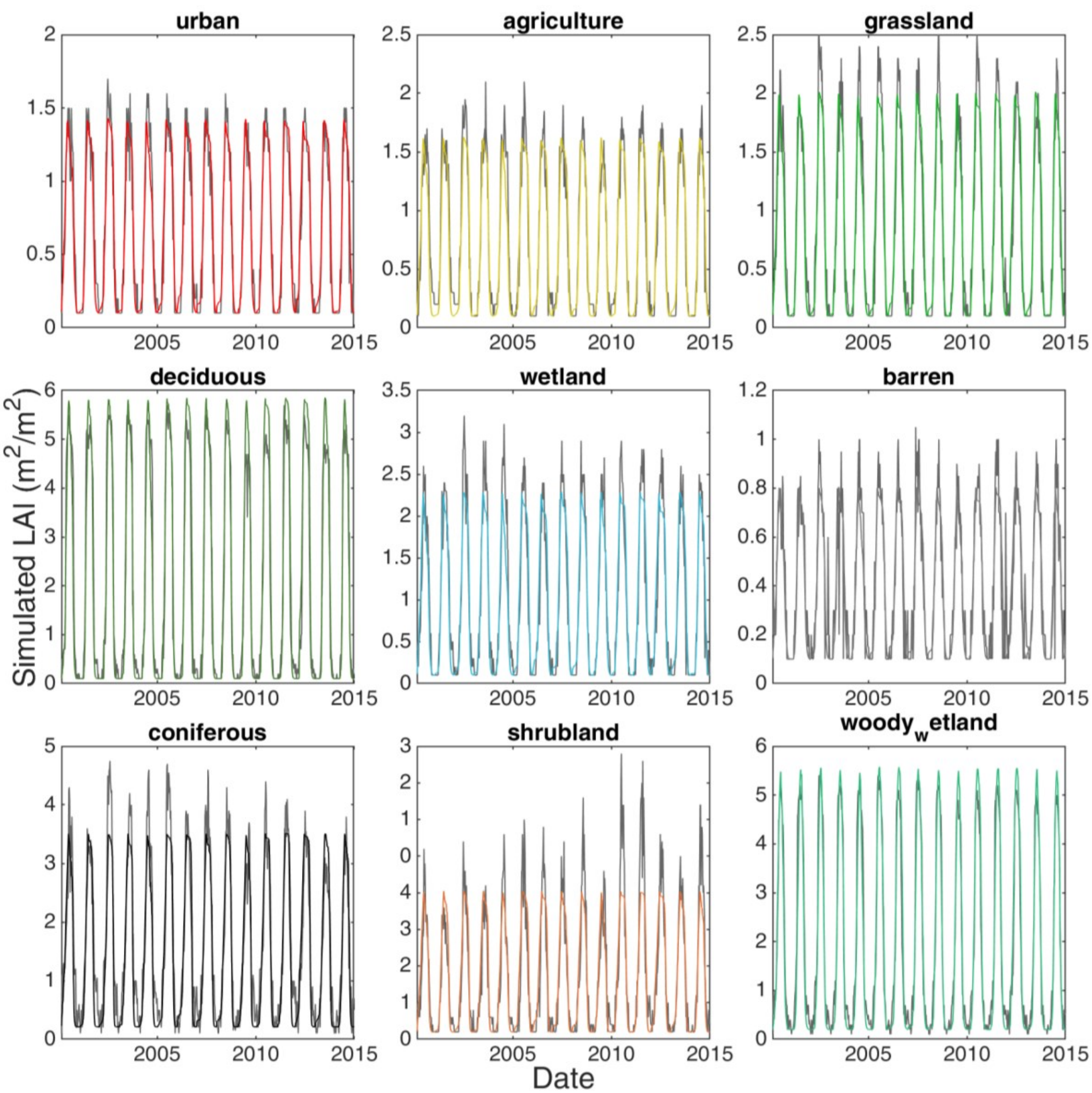

Figure 1.6. Comparison between observed (grey lines) and simulated (colored lines) LAI values shows that LHM reasonably captures the annual dynamics of vegetative growth.

3.3 Land Use Scenarios

Modeled pre-settlement groundwater recharge values ranged from 110 mm/yr (13.1% of precipitation) for the 10th percentile to 440 mm/yr (52.3% of precipitation) for the 90th percentile and a median of 36 0 mm/yr (42.8% of precipitation; Figure 1.7, top left), with the areas of coniferous forest generally producing greater recharge than adjacent deciduous forest areas and woody wetlands. The pre-settlement scenario serves as a baseline for comparison for the other three land use scenarios (logging, fire, and current).

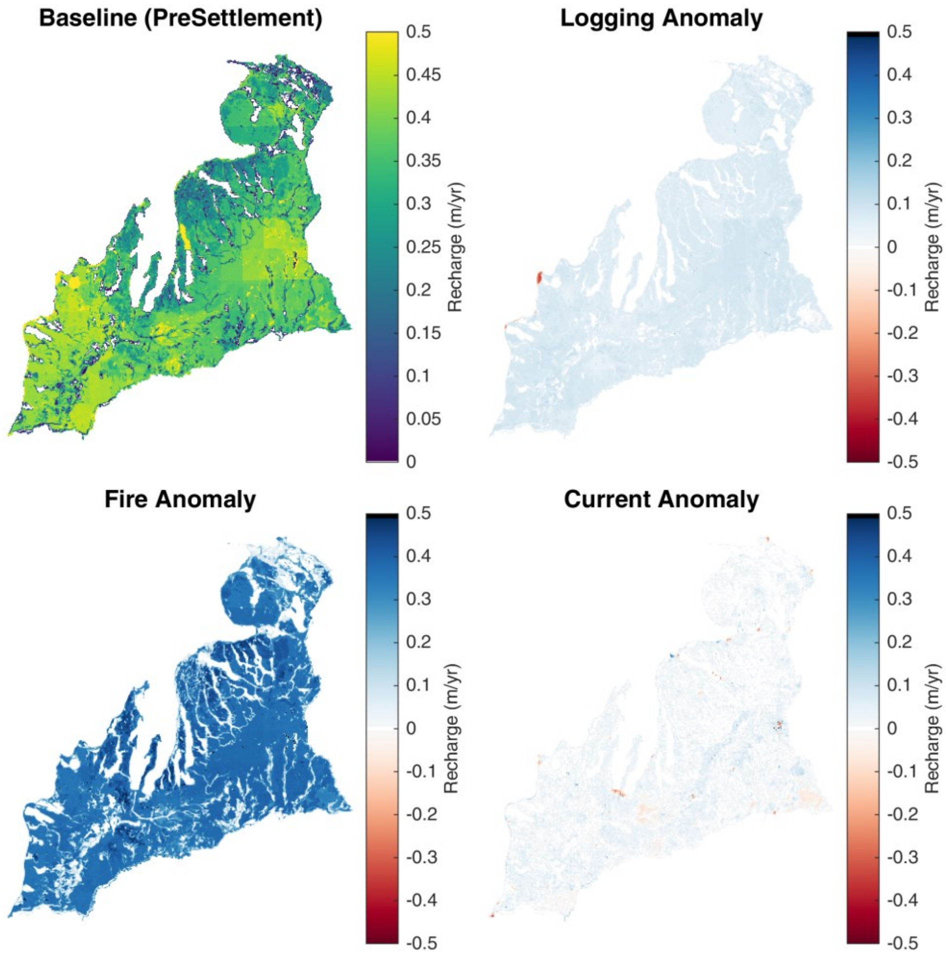

Figure 1.7. Map of the average annual groundwater recharge over the 30 year model run for the pre-settlement scenario (top left) and anomalies from pre-settlement for the post-logging (top right), post-fire (bottom left), and modern land use scenarios (bottom right).

Widespread land use change substantially can substantially shift the water balance across a large area like the EBCW. Logging, converting the woodlands to grasslands and wetlands, changed the recharge values for those areas by +8 mm/yr (+7%; 10th percentile) to +84 mm/yr (+19%; 90th percentile), with a median change of +64 mm/yr (+19%; Figure 1.7, top right). The scenario simulating a widespread fire, where most of the vegetation was removed, resulted in even greater recharge values [+27 (+24%) , +354 (+99%), and +395 (+92%) mm/yr above pre-settlement for the 10th, 50th, and 90th percentiles, respectively; Figure 1.7, bottom left]. This burned scenario is extreme, demonstrating that watershed-scale fires (e.g., the 4,000 to 10,000 km^2 fires in 19th Century Michigan) can have a large impact on individual river basins. Modern land use mostly increased the groundwater recharge above pre-settlement levels, but not as much as the post-logging or post-fire scenarios [-4 (-3%), +6 (+2%), and +39 (+9%) mm/yr for the 10^{th}, 50^{th}, and 90^{th} percentiles, respectively; Figure 1.7, bottom right]. The moderated response is likely due to the similarity between the modern land use (Figure 1.2.d) and the pre-settlement condition (Figure 1.2.a), with only a few, localized areas of intense urbanization and patchy conversion of forest to grassland and pasture.

LHM simulates the complete terrestrial hydrologic budget, and there are numerous components of the water balance affected by these scenarios. Two of these components, ET and runoff, are shown in the Supplement. Figure S1.1.2 displays similar patterns of increased runoff. Ultimately, changes in both recharge and runoff are largely due to decreases in modeled evapotranspiration (Figure S1.1.3), which are examined in greater detail below.

Pre-settlement flows across the EBCW were lower than in any of subsequent land use scenarios (Figure 1.8). Median flows were 5.1, 2.7, and 3.6 m^3/s for the Jordan, Boardman, and Platte Rivers, respectively. The baseflow-dominated Jordan River has a 10%-90% flow range of 1.1 m^3/s, while that range was 1.8 m^3/s for the Boardman and 1.7 m^3/s for the Platte.

The logged scenario had increased flows (16%, 33%, and 14% increases to median flows) and more variability of those flows as evidenced by increases in the 10%-90% range of 0.1, 1.9, and 0.6 m^3/s (5%, 37%, and 14% more than pre-settlement) for the Jordan, Boardman, and Platte Rivers, respectively. The increases in annual streamflows are similar to measured increases reported in the literature for other logged watersheds, which range from 8% to 80% (Lewis et al., 2001; Moore and Wondzell, 2005). In a paper focused on the Great Lakes states, Verry (1986) summarizes previous work that observed increases in annual streamflow of 30 to 80% due to clearcutting of upland hardwoods, depending on the forest density.

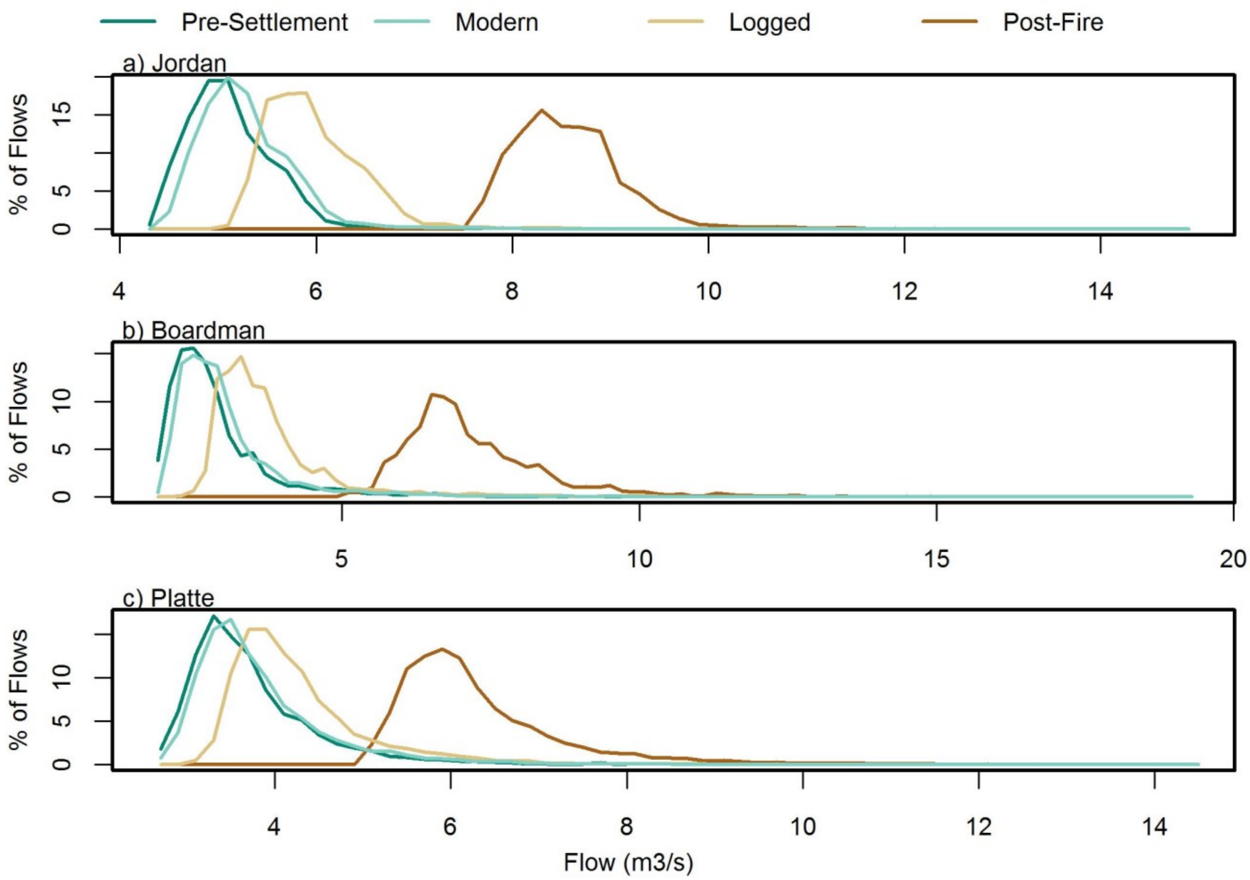

Figure 1.8. Flow duration curves for the Jordan (a), Boardman (b), and Platte Rivers (c) indicate both the increase in flow and variability associated with land use change. The light green bars depict modern land use scenario results in comparison to pre-settlement (dark green), post-logging (light brown), and post-fire (dark brown) results. Additional shading in the figure indicates locations of overlap in the flow histograms.

The post-fire scenario is a substantial shock to the system, resulting in median flows 68%, 160%, and 70% higher than during the pre-settlement period and an increased range between the 10% and 90% values, effects that are within the range of annual flow changes reported in the literature for the first year after a fire (Moody and Martin, 2001b; Scott, 1993). In the Great Lakes region, Miesel et al. (2012) cite three studies with post-fire increases in water yield of 28-98%; Kolka (2012) gives a range of 60-80%; and Wright (1976) attributes increases of 30-80% to fires in Northern Minnesota. As noted above, our fire scenario is extreme, and is used to illustrate the potential of the landscape to respond to alterations. Given the scale of each of these river systems (174 to 482 km^2), historically observed fires may have burned much of these or other similar basins. Thus changes of this magnitude likely occurred during this period.

The effects of fire on hydrology are often temporary, but the short-term increase in streamflow can cause long-term impacts to stream sediment budgets, morphology, and ecosystem structure. The effects of the historical fires in the EBCW were compounded by the fact that they occurred during and after essentially complete logging of the landscape. Logging altered riparian and in-stream structure as timber companies widened and channeled rivers to allow the transport of timber and stream beds were disturbed by log drives (Nilsson et al., 2005; Vincent, 1962). The paired disturbances of logging and fire likely profoundly altered water and sediment budgets across the region, forcing large-scale ecosystem alterations.

The current land use still has elevated streamflows across the EBCW relative to the pre-settlement condition, although the increases in median flow are minor (2.8%, 5.8%, and 2.1% for the Jordan, Boardman, and Platte Rivers, respectively). These changes are roughly in proportion to the modeled difference between current and pre-settlement recharge—suggesting that most of the streamflow change can be attributed to shifts in groundwater sourced waters. While urbanization can cause increased runoff, the small differences in the EBCW are unsurprising both because of the extent of reforestation and the areas of urbanization tend to be at the river mouths, downstream from the gaged locations summarized in Figure 1.8. Mao and Cherkauer (2009) also show only small differences in evapotranspiration and runoff in this area of Michigan.

Ultimately, changes in evapotranspiration and canopy cover drive much of the change in the major remaining water balance components (runoff and recharge), an effect that is well-documented in the literature (Bowling et al., 2000). To examine these changes in greater detail, Figure 1.9 plots monthly-averaged values for each of six distinct categories of evaporation and transpiration in the model: open water evaporation, ice/snow sublimation, direct evaporation from the soil, canopy evaporation (i.e. water intercepted and stored in the canopy, which is subsequently evaporated), wetland transpiration, and upland transpiration. Note that on an hourly basis, all of the evaporation and sublimation terms can be negative as water condenses or deposits onto water/ice surfaces due to reversed vapor pressure gradients. For two of these terms, open water evaporation and ice/snow sublimation, during the spring the net balance shifts negative, as relatively warm and humid air masses contribute additional water to the land and water surfaces in addition to what would otherwise come as precipitation.

In this heavily forested region, canopy evaporation can account for as much as 48% of the monthly evapotranspiration in the winter (Figure 1.9, top left). This proportion falls to 26-28% during the peak of the growing season (June, July, and August), as transpiration in both the upland and wetland portions of the model increase to account for 56-58% of the total evapotranspiration.

The primary modeled impact of logging and fire is to reduce vegetation and the associated canopy. This reduction in canopy reduces both the evaporation directly from the canopy and the transpiration from the plants (Figure 1.9, top right and bottom left), effects also noted by other researchers in the Great Lakes region (Mao and Cherkauer, 2009; Twine et al., 2004; Verry, 1986). Once the EBCW recovered from logging and fire impacts, as seen in the current land use case, the reduction in the evapotranspiration components is on the order of the land-use that shifted from forest to urban. While the modeling of Mao and Cherkauer (2009) indicated decreased evapotranspiration led to increased runoff across Michigan's Lower Peninsula, their model results show relatively small decreases in evapotranspiration in the EBCW, and are consistent with our results.

The impacts of the land use change on evapotranspiration are the largest during the growing season months of April through October. Comparable modeling of the conversion from pre-settlement forest to grassland in the Great Lakes region indicated approximately a one month delay in peak evapotranspiration was associated with increased runoff in April to June (Mao and Cherkauer, 2009). These results are similar to a study of a logged watershed in the Pacific Northwest of the United States where observed August flows increased for the first 8 years post-harvest (Hicks et al., 1991).

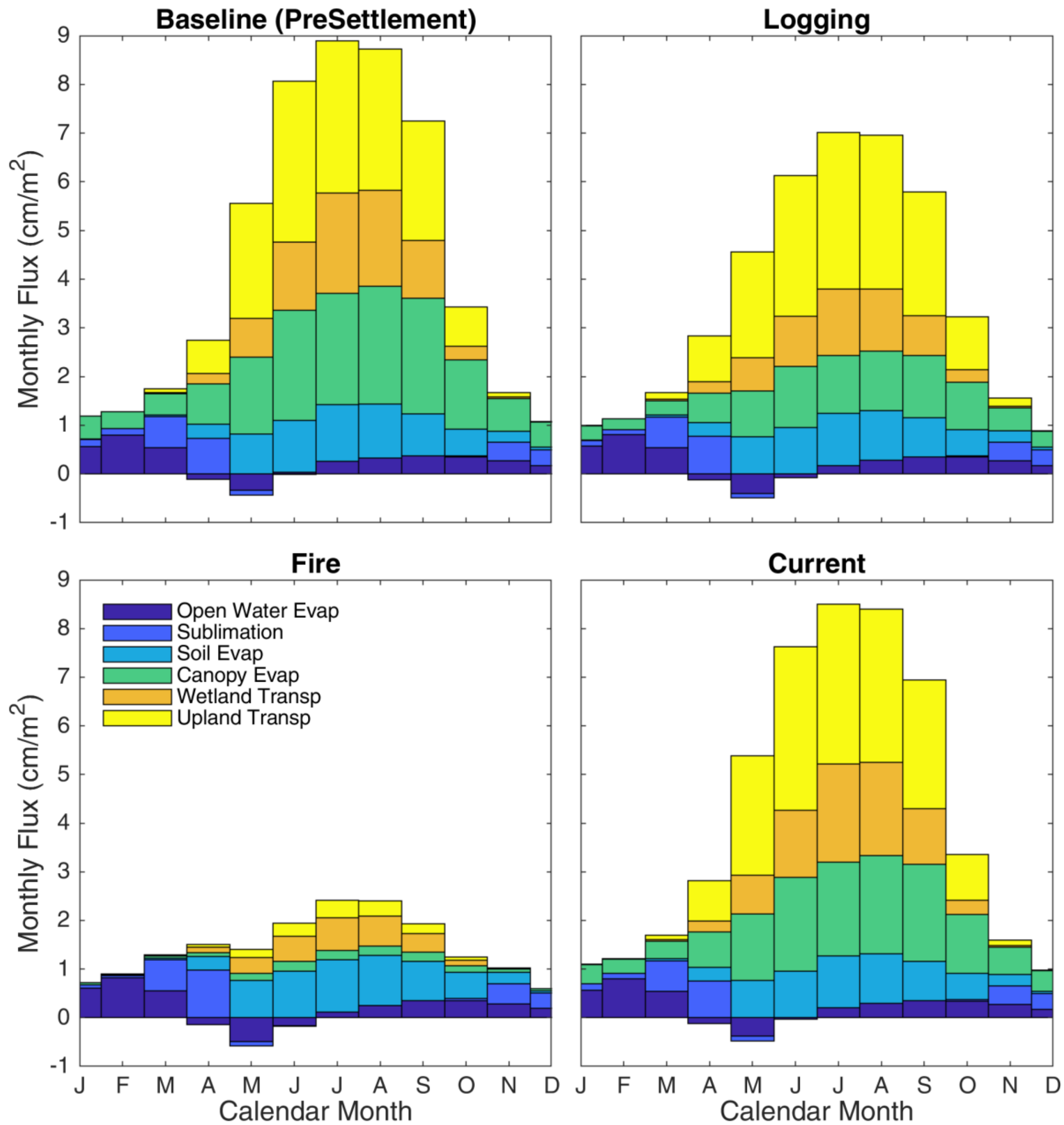

Figure 1.9. The largest impacts of shifting land use are due to changes in evapotranspiration during the growing season and, for the post-fire scenario, a reduction in canopy evaporation throughout the year.

4. Conclusions

Michigan's Lower Peninsula has experienced a series of dramatic land use changes over the last 150 years; our models show that these changes led to major shifts in the regional hydrology. In the EBCW, the extensively forested landscape that existed prior to

European settlement had relatively high evapotranspiration and low streamflow. The virtually complete logging of these forests removed a significant portion of the vegetative canopy. Our models demonstrate that this led to decreased evapotranspiration and increased streamflow. Fires, the extent and timing of which are largely undocumented, burned large tracts of Michigan during and immediately after logging. The most extreme of these fires would have left barren soil with little transpiration; this could have resulted in increases in streamflows up to 96% greater than those of the logged condition and 160% more than those simulated for the virgin forest landscape. Over the succeeding decades, much of the forest regrew, increasing evapotranspiration rates and leading to streamflows that are only slightly increased from the pre-settlement conditions.

Land use and land cover changes similar to those experienced in the EBCW are still happening throughout the world. As shown in this study, it is important to consider not just the visible impact of these changes, but the larger temporal effects on hydrology. It is encouraging that the modern land use in the EBCW, which incorporates farming and small urban areas, exhibits similar simulated hydrology to the pre-settlement condition.

Acknowledgements

This chapter will be submitted for publication, co-authored by Anthony Kendall, Sherry Martin, and David Hyndman. Funding was provided by the Friends of the Jordan and the U.S. Army Corps of Engineers Great Lakes Tributary Modeling Program. Any opinions, findings, and conclusions or recommendations expressed in this material are those of the authors and do not necessarily reflect the views of USACE or the Friends of the Jordan.

APPENDIX

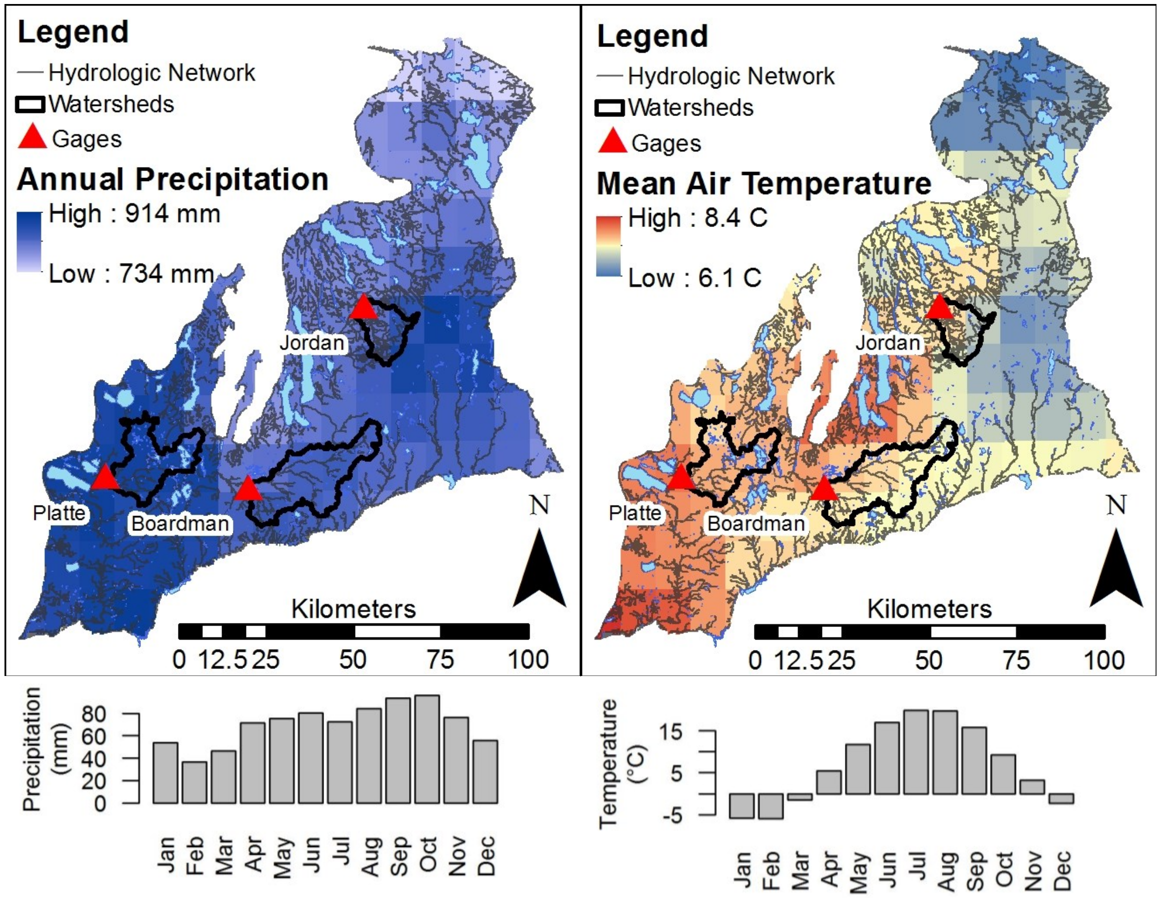

Figure S1.1. The average annual precipitation across the EBCW from 1986 to 2015 ranged from 734 mm to 914 mm, based on data from the NLDAS (top left). The precipitation is usually greatest in September and October and lowest in February and March (bottom left). The mean air temperature across the EBCW from 1986 to 2015, based on NLDAS data, shows the moderating effects of Lake Michigan along the western edge of the model domain (top right). The mean air temperature across the basin is lowest in February and peaks in August (bottom right).

Table S1.1. Percentage of each land use type for each of the modeled scenarios.

	Land Use Scenario			
	Pre-Settlement	Logged	Post-Fire	Modern
Urban	0%	0%	0%	8%
Agriculture	0%	0%	0%	10%
Grassland	2%	81%	0%	13%
Deciduous	68%	0%	0%	40%
Water	6%	6%	6%	6%
Wetland	0%	13%	13%	1%
Barren	0%	0%	81%	1%
Coniferous	11%	0%	0%	7%
Shrubland	0%	0%	0%	3%
Woody Wetland	13%	0%	0%	12%

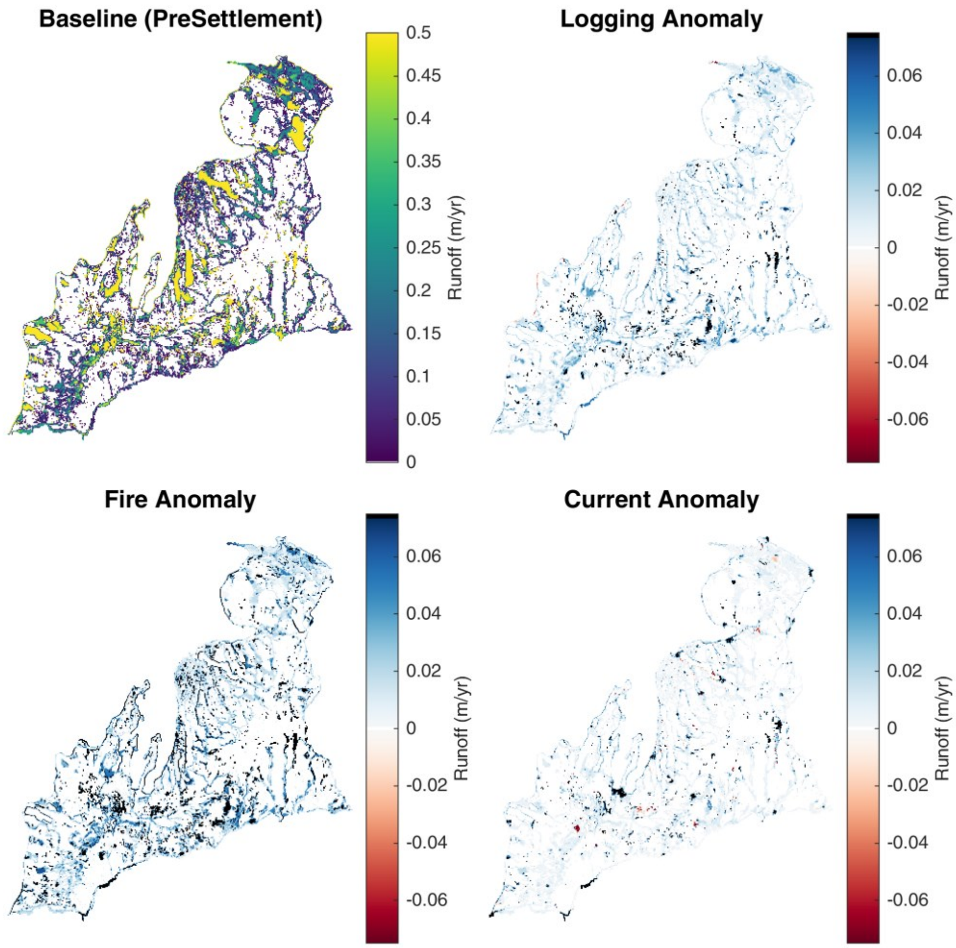

Figure S1.1.2. Map of average annual runoff over the 30 year model run for the pre-settlement scenario (top left) and anomalies from pre-settlement for the post-logging (top right), post-fire (bottom left), and modern land use scenarios (bottom right).

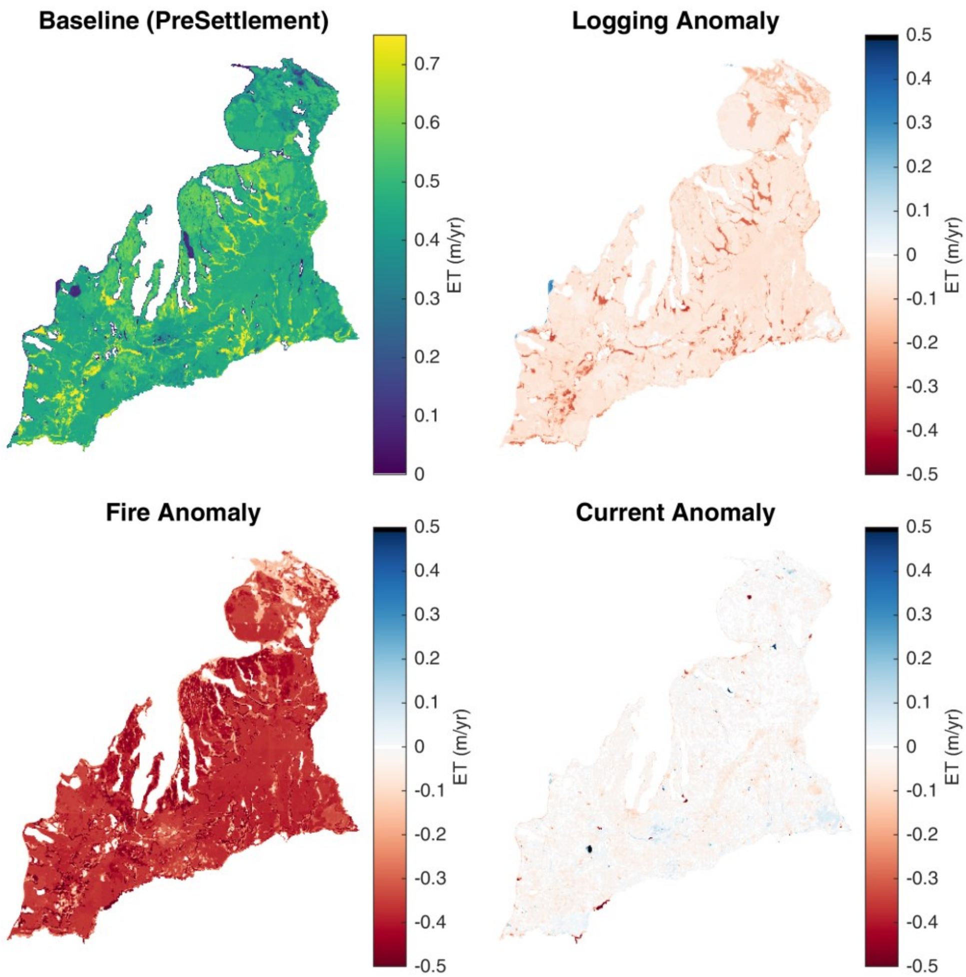

Figure S1.1.3. Map of average annual evapotranspiration over the 30 year model run for the pre-settlement scenario (top left) and anomalies from pre-settlement for the post-logging (top right), post-fire (bottom left), and modern land use scenarios (bottom right).

CHAPTER 2:

MODELED IMPACT OF HISTORICAL DEFORESTATION AND FOREST FIRE ON SEDIMENT TRANSPORT CAPACITY IN A BASEFLOW DOMINATED RIVER USING AN INTEGRATED HYDROLOGIC MODEL

Abstract

Globally, deforestation and forest fires are two of the most dramatic land use changes occurring today, but they also occurred in the past. The legacy of these changes is often visible in the modern landscape due to the movement of water and sediment through the affected watersheds. We present results from the Landscape Hydrology Model (LHM) that integrate both surface and groundwater flows through the Jordan River watershed in northern Michigan for a range of historical land use scenarios. These include the pre-settlement, forested land cover; a post-logging scenario; a severe post-fire scenario; and the modern land cover. We used the simulated surface runoff produced by LHM to estimate in-channel sediment transport using the sediment transport capacity calculator and the Sediment Impact Analysis Methods (SIAM) incorporated in the one-dimensional hydraulic model, HEC-RAS. Our modeling suggests that logging increased sediment transport capacities as much as 34% relative to pre-settlement conditions. Sediment transport capacity increased by up to 166% for the post-fire scenario. The current sediment transport capacities are only slightly elevated relative to the pre-settlement condition. The SIAM results show that the effects of land use change are not uniform along the river and can lead to complex responses. Our findings demonstrate the importance of considering the effects of land use change on in-channel transport in addition to the overland erosion.

1. Introduction

Large tracts of North America experienced significant land use change over the last two centuries. These changes include logging of old growth forests and forest fires. While some parts of North America, particularly the northern portions of Michigan's Lower Peninsula, are now partially reforested, the same large-scale land use changes are occurring throughout the world. It is important to understand the impacts of such land use changes on the hydrology and sediment of rivers in the impacted areas.

Mature forests produce very little sediment during rain events (Neary et al., 2009). Wide-scale logging removes the trees, reducing canopy interception and moving the interception much closer to the ground. This effect, combined with disturbance of the soil from the logging activity, can result in greatly increased sediment yield initially (Bathurst and Iroume, 2014; Beschta, 1978). Logging activities are also often followed by an increase in streamflow due to reduced evapotranspiration as well as increased snow accumulation and melt rates. This streamflow difference can be more noticeable during peak flows (Lewis et al., 2001). Sediment production can take decades to recover to its former levels after logging (Klein et al., 2012) and the sediment can remain in the channel for even longer (Roberts and Church, 1986).

The primary focus of most post-fire sediment research has been on overland erosion or debris flows (Moody et al., 2013; Shakesby and Doerr, 2006). Surface erosion is a function of overland flow and therefore depends on the same drivers. Fires remove vegetation that would normally slow the velocity of overland flows and reinforce the soil matrix (Moody et al., 2013). Such denuded soil is then more readily eroded. Fires can also affect the physical and chemical properties of the soil. Hydrophobicity, which causes water to more readily run off than to infiltrate, is sometimes cited as a potential effect of forest fires (e.g., (Huffman et al., 2001; Litschert et al., 2014; Robichaud, 2000)), but it is also highly variable in both space and time (Doerr et al., 2000; Doerr and Thomas, 2000). Shakesby and Doerr (2006) state that sediment erosion rates from burned areas generally return to undisturbed levels in 3-10 years, although watershed sediment yields may lag because of in-channel storage. This in-channel storage can lead to complex responses as accumulations of post-fire sediment move through the river network (Benda et al., 2003; Legleiter et al., 2003; Moody and Martin, 2001a).

Michigan's Lower Peninsula was covered by extensive forests prior to settlement by Europeans (Comer and Albert, 1998). The logging activity that accompanied and sometimes preceded European settlement began in the mid-19th century and peaked in the northern parts of the Lower Peninsula in the 1880s to 1890s (Dickmann, 2009). The initial phases of logging focused on white and red pine (*pinus strobus* and *pinus resinosa*). As the stands of softwood were exhausted, the logging industry turned to hemlock and other hardwoods. This shift was aided by changes in technology, such as railroads, that allowed for easier harvesting and transport of the denser wood (Whitney, 1987). In many places, farms moved in to the cut-over areas. In some cases, the poor soils that had supported large forests were not sufficient to sustain the agricultural practices of the day and the farms were eventually abandoned.

The brush, branches, and stumps left behind after logging were easily ignited either intentionally by settlers or accidentally by sparks from wood-burning locomotives and other sources of fire (Dickmann, 2009). Six discrete fires burned over 10,000 km^2 of the Great Lakes Region in early October, 1871 (Haines and Sando, 1969). In September of 1881, the Thumb Fire in Michigan's Lower Peninsula burned over 4,000 km^2, including some of the same areas that burned in earlier fires. Fires were more common among the former softwood forests than the hardwood forests and coniferous swamps. In some places, the fires were so severe that they burned all of the organics in the area, leaving just the mineral soil. In these locations, the dominant trees in the forests were different after recovery, with aspen (*Populus* sp.), oaks (*Quercus* sp.), and jack pines (*Pinus banksiana*) taking the place of the mixed white and red pines (*Pinus strobus* and *Pinus resinosa*) (Whitney, 1987).

The goal of this paper is to quantify the likely effects of land use change on sediment yield and in-channel transport. To accomplish these goals, we modeled four different phases of land use (pre-settlement, logging, post-fire, and current) in Michigan's Jordan River watershed using an integrated hydrologic model. We then combined the resulting hydrologic and sediment yield information with a hydraulic model of the river mainstem to estimate sediment transport capacity and geomorphic impacts at the reach scale for each land use scenario.

2. Methods

2.1. Site Description

The Jordan River watershed occupies 333 km^2 in the northwestern part of Michigan's Lower Peninsula. Approximately the upper half of the 56 km-long mainstem generally runs southwest before it is captured by a glacial valley and turns northward. The lower, navigable portion of the river is much less sinuous than the upper reaches. A significant tributary, Deer Creek, enters the Jordan River 2.6 km before the river empties into Lake Charlevoix at the town of East Jordan. Elevations in the watershed range from 177 to 415 m above sea level (Figure 2.1).

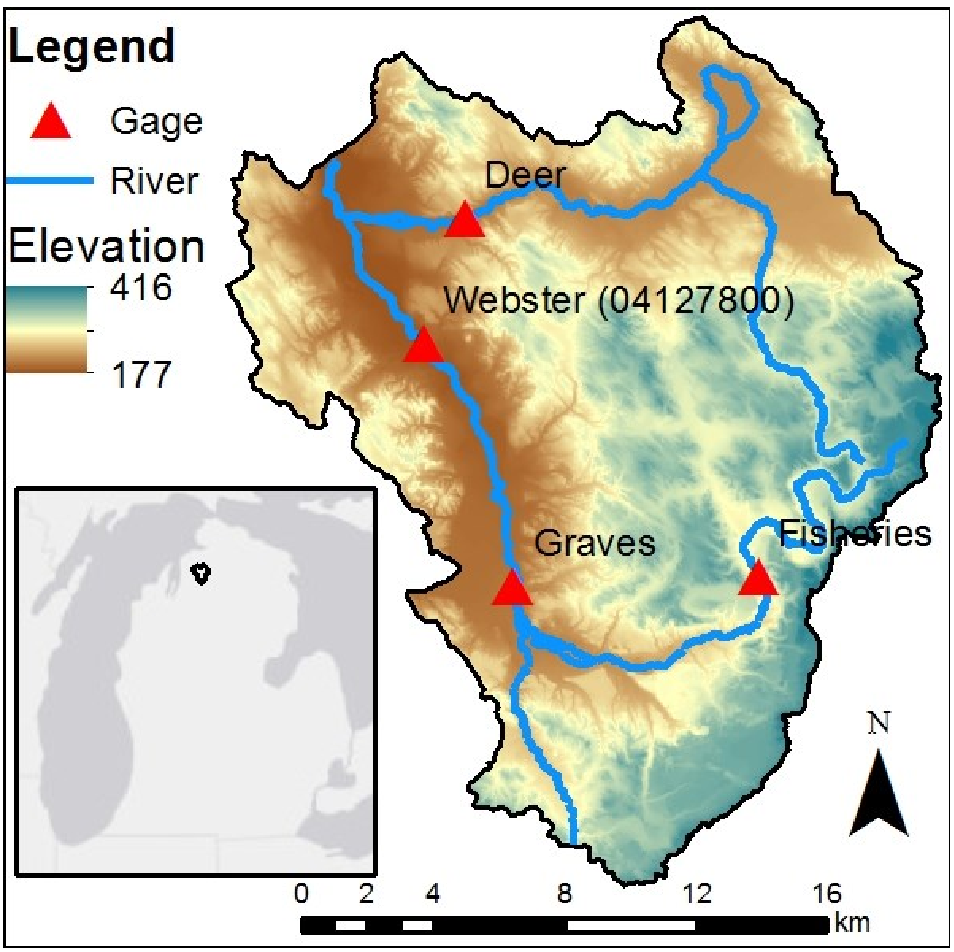

Figure 2.1. There are four stream gages in the Jordan River watershed in the northwestern portion of Michigan's Lower Peninsula. The Webster gage is maintained by the USGS. The remaining gages (Fisheries, Graves, and Deer) are maintained by the Michigan State University Hydrogeology research group.

Prior to European settlement, the Jordan River watershed was dominated by old-growth forest (Figure 2.2.a; (Comer and Albert, 1998)). These forests succumbed to the same fate as others in Michigan, with the first sawmill opening in East Jordan at the mouth of the Jordan River in 1879 when the timber near the mill in Leland, Michigan was exhausted (Powers and Cutler, 1912). Like most of the Great Lakes region, the Jordan River was impacted by the extensive historic trapping of beavers followed by their recovery in the modern era (Martin et al., 2015). The Jordan River Watershed, like many other areas in Michigan, suffered from multiple wildfires after logging (Hay and Meriwether, 2004). Eventually, the farms and second-growth forests came to dominate the watershed (Figure 2.2.d). The land use in 2006 was 61% forest, with an additional 14% woody wetlands, 12% cultivated crops, 8% herbaceous/grassland, and 5% developed (Fry et al., 2013).

The coarse-texture glacial sediments that form the majority of the Jordan River watershed allow rapid infiltration of rainfall and promote a very stable flow regime in the river. Groundwater is the dominant source of water in the river, with a baseflow index of 87-89% (Wolock, 2003). A United States Geological Survey gage (#04127800) was established in 1966 and the record of daily discharge since that time shows that the river experiences a small range of flows. The median daily flow recorded at the gage for water years 1967-2017 was 5.7 m^3/s, with a standard deviation of 1.2 m^3/s. The minimum daily flow was 4.2 m^3/s and the maximum was 26.8 m^3/s. The low variation in flow is a feature of groundwater-dominated systems, although the prevalence of small beaver ponds in the upper reaches of the watershed may also play a role (Martin et al., 2015).

2.2. Field Data Collection

We collected elevation, flow, and bathymetry data during a canoe trip on 13-15 July, 2011. Elevation data were collected using a Global Positioning System (GPS) receiver. Flow and bathymetry data were collected using a Sontek ADCP at 11 locations along the Jordan River (Figure S2.1). We also used a total station to survey a subset of the cross sections used for flow measurement.

To obtain bed material gradations, we collected grab samples at evenly spaced intervals along representative transects at 4 locations along the river on 13-14 October, 2011. After these samples were dried and sieved, the volume of the particles in each size class was measured by displacement in a graduated cylinder to calculate the sediment density (ρ).

We measured sediment transport during base flow at two sites, Graves Crossing and Webster Bridge, on June 23rd, 2014, following the methods described in (Edwards and Glysson, 1999). Suspended sediment sampling utilized the equal-discharge increment and a DH-81 sampler. We collected bed load with a BLH-84 sampler, using the Multiple Equal-Width Increment method and ensured that at least 35 evenly-spaced vertical samples were collected.

2.3. Landscape Hydrology Model (LHM)

Process-based hydrology models allow researchers to simulate the streamflows that would result from alternate land uses. This study uses the Landscape Hydrology Model (LHM), a gridded model that couples surface and groundwater processes to simulate evapotranspiration, groundwater recharge, and streamflow (Hyndman et al., 2007; Kendall, 2009). LHM simulates a number of physical processes to support these hydrologic calculations, including canopy interception and snowmelt. Groundwater flow in LHM is calculated using MODFLOW (Harbaugh et al., 2000). Several previous implementations of LHM in the Great Lakes region are documented in the literature (Luscz et al., 2017; Wiley et al., 2010).

LHM Sediment Yield Module

We developed a new sediment yield module for LHM based on the Modified Universal Soil Loss Equation (MUSLE; (Williams, 1975; Williams, 1995)). The MUSLE is also the sediment yield algorithm implemented in the Soil and Water Assessment Tool (SWAT; (Neitsch et al., 2011)). It utilizes the peak runoff rate for a given day in conjunction with the total runoff volume to estimate the sediment yield for a given location. LHM calculates the peak hourly runoff (mm/hr) and the total daily runoff volume (mm) to calculate a daily sediment yield (t/ha) from each grid cell according to Equation 1.

$$Sediment\ Yield = 1.586 * (Q * q_{Peak})^{0.56} * A^{0.12} * K * C * P * LS * ROKF \qquad (1)$$

where, Q is the total daily runoff volume (mm), q_{Peak} is the peak hourly runoff rate (mm/hr), A is the watershed area (ha), K is the soil erodibility factor, C is the cover and management factor, P is the support practice factor, LS is the topographic (land slope) factor, and ROKF is coarse fragment factor. We set the P factor to 1 for this simulation, because no permanent support practices (such as terracing) have been implemented in the Jordan River watershed.

The K used by LHM is calculated from the fractions of sand, silt, clay, and organic carbon according to the equation provided by Williams (1995). The LS factor is estimated in the model based on the average flowpath length to the stream within each grid cell and the average slope within the grid cell, according to the equations suggested by (Williams, 1995). The coarse fragment is calculated based on the percentage of rock in the top layer of soil, as shown in Equation 2 (Williams, 1995).

$$ROKF = \mathrm{e}^{-0.03*\mathrm{Pct\_Rock}} \qquad (2)$$

The C factor for each model grid cell is determined based on the area-weighted average from the individual land use types present. LHM assumes that water and wetland areas produce negligible amounts of sediment (C=0). We assume barren areas have no appreciable canopy or ground cover and assign them a C factor of 0.45 based on (Wischmeier and Smith, 1978). Both coniferous and deciduous forests are assigned C values of 0.001, based on the assumption that they are fully mature. The model calculates the C factor for vegetated land uses (agricultural, grassland, and shrubland) from the percentages of canopy cover, litter cover, and canopy height. These values are linearly interpolated from the data in (Wischmeier and Smith, 1978) when the canopy height is 1 m or less. In cases where the canopy height is greater than 1 m, LHM multiplies the C factor for 0% canopy cover by the data in (Wischmeier and Smith, 1978) regarding the effect of fall height (the distance from the canopy to the ground). LHM calculates the C factor for urban areas as an area-weighted combination of the impervious surface area (C=0.001) and the remaining area (calculated in the same manner as the vegetated land uses).

To estimate the proportions of sand, silt, and clay in the eroded material, we implemented the method described by (Foster et al., 1980; Foster et al., 1981). We assumed that the large and small sediment aggregates calculated by this method would break apart into their constituent sand, silt, and clay particles when they enter the river. This algorithm has been successfully implemented in several other models, such as SWAT and AGNPS (Neitsch et al., 2011; Young et al., 1989).

LHM Model Setup

The groundwatershed for the Jordan River is much larger than the surface watershed. We used a model domain that covered the entire Extended Boardman-Charlevoix Watershed (EBCW) to appropriately capture the groundwater impacts on the hydrology of the Jordan River. This model was validated using both groundwater heads and streamflows in the Jordan River. Additional details of the creation and validation of this model are described in Chapter 1. We used soils data, including the proportions of sand, silt, and clay, from the Soil Survey Geographic Database (SSURGO).

Land Use Scenarios

We simulated four different land use scenarios (Figure 2.2). The General Land Office surveyed Michigan in the early 19th century. The Michigan Natural Features Inventory (MNFI) used this information to create maps of land use (Comer and Albert, 1998). We used the MNFI maps for our pre-settlement condition (Figure 2.2.a). We simulated the post-logging condition by converting all of the deciduous and coniferous forests from the pre-settlement map to grassland and the woody wetlands to wetlands (Figure 2.2.b). Since large tracts of Michigan burned during and immediately after logging, we created a post-fire scenario where all of the grassland from the post-logging scenario was converted to a barren land use (Figure 2.2.c). Finally, we used the 2006 National Land Cover Dataset to represent the modern land use in the Jordan River watershed (Figure 2.2.d).

A number of studies that simulated soil loss after forest fires using the Revised Universal Soil Loss Equation relied on changes in the cover factor to account for most of the effect of fire (Larsen and MacDonald, 2007; Litschert et al., 2014). Some studies also incorporated changes to the soil erodibility factor (e.g., Miller et al. (2003)). Larsen et al. (2009) make a convincing argument that hydrophobic effects are both short-lived and often minor relative to the impact of changes to the hydrologic cycle associated with altered vegetative cover. Reeder and Jurgensen (1979) examined fire-induced hydrophobicity in the Upper Peninsula of Michigan and found that it was not a long-term issue based on the soils of the region. Richardson and Hole (1978) found that even if fire-induced water-repellency is present, water can still percolate rapidly into coarse-textured soils in Wisconsin. We assumed that in the humid environment and coarse-textured soils of Northwestern Michigan the potential hydrophobicity was unlikely to have long-lasting effects and could be disregarded in our model.

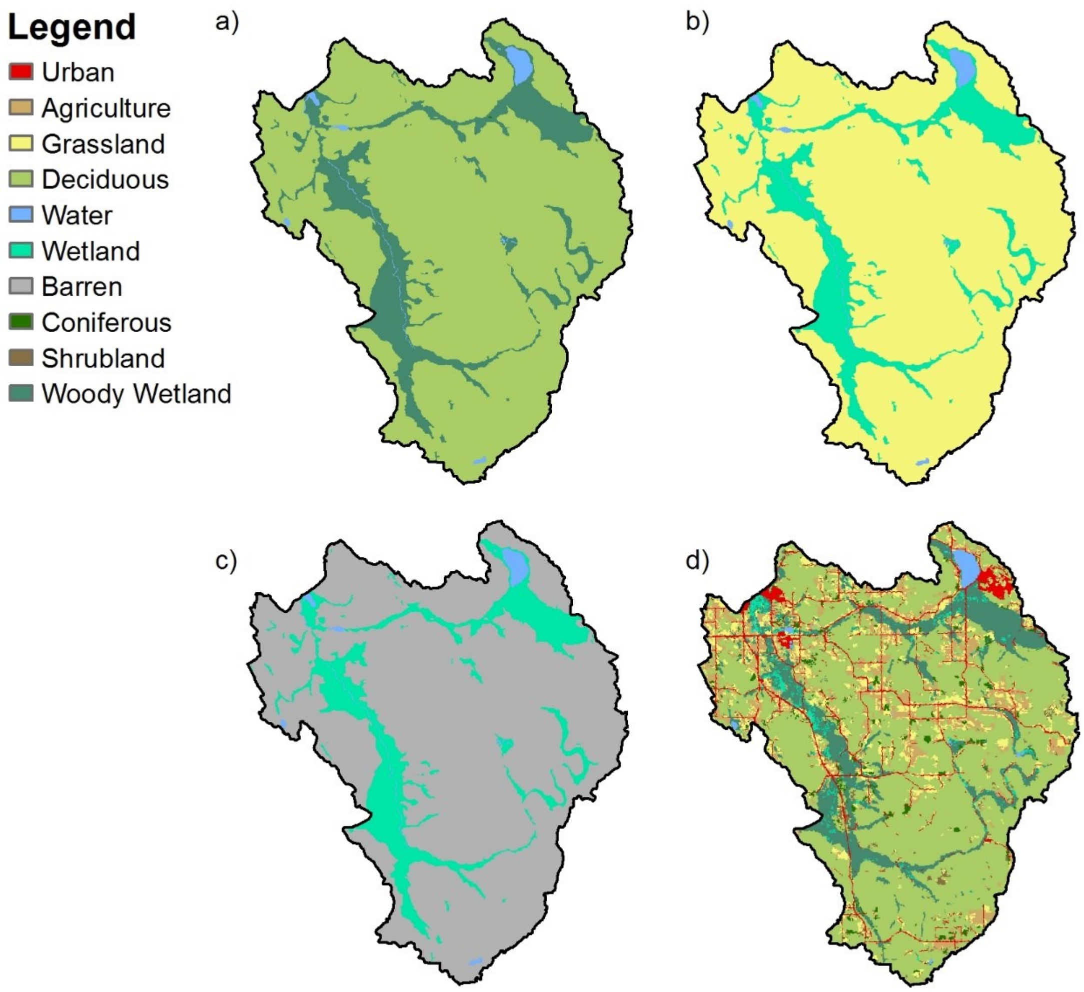

Figure 2.2. The modeled land use scenarios were (a) pre-settlement; (b) post-logging; (c) post-fire; and (d) modern land use.

2.4. Hydraulic Model

We developed a one-dimensional hydraulic model of the lower 17.5 km of the Jordan River using the Hydrologic Engineering Center River Analysis System (HEC-RAS; Brunner, 2018). As shown in Figure 2.3, the model covers the area from Graves Crossing to the mouth of the river at Lake Charlevoix. Initial elevations for the model cross sections were extracted from a commercially-available 5m resolution Digital Terrain Model (NEXTMAP, Intermap Technologies, Inc.). This data had noticeable "stair-stepping" that coincided with the contour lines from the source topographic maps.

The artificial "stair-steps" were smoothed out of the DTM by combining GPS elevation data with ADCP depths to better estimate the true thalweg elevation at various points along the river. After fitting several regressions to this thalweg elevation data, we decided to represent the data were by two equations: one for the upper channel and one for the lower channel. A third-order polynomial was used to interpolate between points above Webster Bridge and a second-order polynomial was used downstream of this point. These regressions show a generalized elevation change along the length of the modeled portion of the river (Figure S2.2).

The NEXTMAP based cross-sections from GeoRAS show a distinct water surface from the confluence with Deer Creek, downstream to Lake Charlevoix (Figure S2.3). For the cross-sections in this area, the nearest surveyed bathymetry was applied based on this water surface. Bathymetry for cross-sections upstream of this point were modeled using the nearest surveyed bathymetry with a constant bank height (above the thalweg). Inspection of the surveyed data indicated two distinct bank height regimes. A bank height of 1.26m was used between Deer Creek and approximately 1 km downstream of Webster Bridge, while a bank height of 1.05m was used from this point upstream. This dividing point was based on the qualitative fit from the cross-section surveys that extended past the top of the banks. Once the bathymetry was applied to each cross-section, we adjusted the entire cross-section vertically so the channel thalweg elevation was aligned with the regression equations.

The Jordan River HEC-RAS model uses a fixed water level elevation, the average level of Lake Charlevoix, as the downstream boundary condition. The upstream boundary condition is the flow provided by LHM at Graves Crossing. We also incorporated flow changes at Old State, Webster, and the confluence with Deer Creek to account for increases in flow due to small tributaries and groundwater inputs, as modeled by LHM. The LHM provided Jordan River streamflows under each land use scenario and we assumed the same Lake Charlevoix level for each scenario.

We calibrated the model longitudinally to water depths and flows collected during a site visit on 13-15 July, 2011 by adjusting the in-channel Manning's roughness values. We also calibrated the model to observed depths reported by the USGS at the Webster Gage (#04127800) within two years of our site visit. USGS flow and stage measurements below the bank height were used as validation for the previously determined in-channel roughness values. We adjusted the overbank roughness values separately to match the observed USGS data for out of bank flows. More details are available in the Appendix, under Hydraulic and Sediment Transport Model Validation.

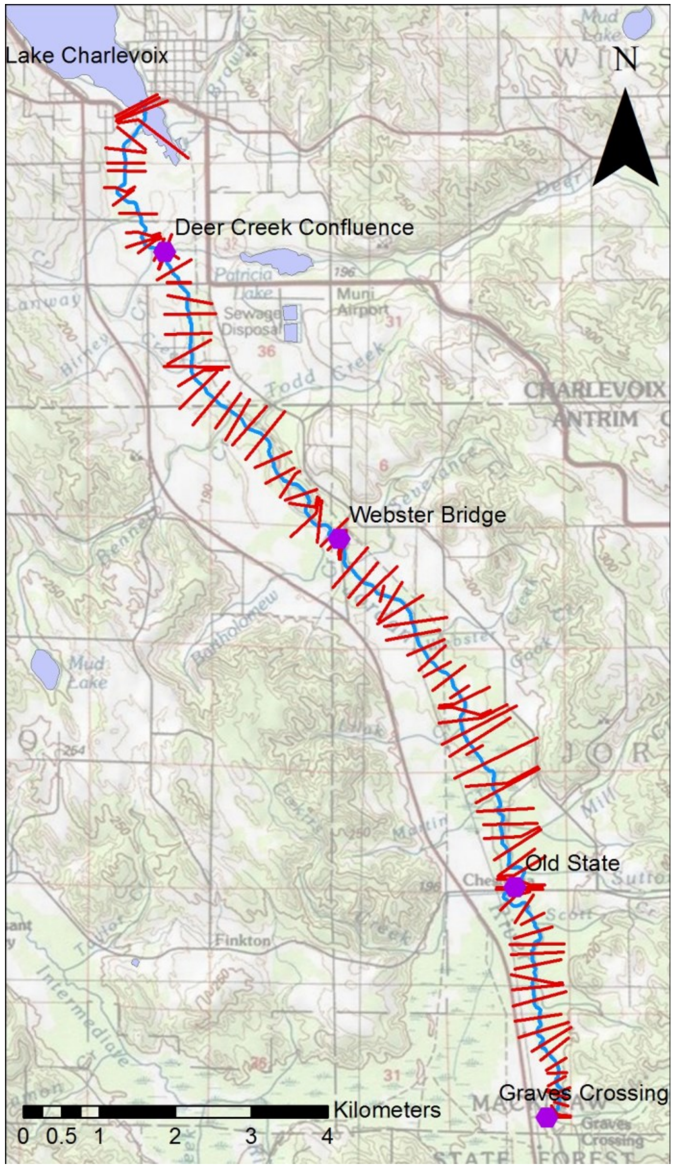

Figure 2.3. HEC-RAS model cross-section and flow change locations on the lower Jordan River. The river flows from South to North.

2.5. HEC-RAS Sediment Transport Capacity Calculator

We used the Sediment Transport Capacity Hydraulic Design Tool in HEC-RAS to compute transport potential at each cross-section in the model. We selected sediment transport functions based on their appropriateness for the bed material gradation. Calculations were made with 10%, 50%, and 90% exceedance flows from the LHM model for each land use scenario. We ran the transport capacity tool with $\rho = 2.65$ g/cm^3, which is typical of silica and the sand-sized particles from the bed of the Jordan River. Finally, we compared the current low flow transport capacity to bedload measurements collected in the field at the same flows.

2.6. Sediment Impact Assessment Methods (SIAM)

The Sediment Impact Assessment Methods (SIAM) were developed to estimate reach-based, in-channel sediment budgets and subsequently incorporated into HEC-RAS (Gibson and Little, 2006; Little and Jonas, 2010; Mooney, 2006; Mooney, 2007). SIAM was developed to compare the effects of different scenarios on sediment continuity and budgets for individual river reaches. SIAM allows the user to define the local inputs of sediment to a reach and the wash load threshold. SIAM uses the hydraulics provided by HEC-RAS to calculate the total sediment transport based on an annual flow-duration curve. For each reach, SIAM calculates the local sediment budget for the bed load material, transporting bedload material equal to the sediment transport capacity and all wash load (material remaining in suspension) to the next downstream cross-section. SIAM implicitly assumes that the system is capacity-limited rather than supply-limited.

We divided the SIAM model of the Jordan River into four sediment reaches, based on flow changes and morphologic similarity (Below Graves, 13.6 – 17.5 km from the river mouth; Below Old State, 7.7 – 13.6 km; Below Webster, 2.6 – 7.7 km; and Below Deer Confluence, 0.0 – 2.6 km). We added a fifth sediment reach, using the most upstream cross-section of the HEC-RAS model, to act as a sediment supply reach. The sediment supply reach produces material equal to its transport capacity and serves as a source of incoming bedload material for our study reaches. We excluded the supply reach itself from our sediment analysis. We ran the SIAM model using flow-duration curves based on the averages from our thirty-year LHM runs for each land use scenario. We used the average sediment yield from LHM cells adjacent to the river as sediment inputs for each reach. We ran the SIAM model with the Meyer-Peter Müller sediment transport formula and a sediment specific gravity of 2.65.

3. Results and Discussion

3.1 Field Measurements

The flow measured at Graves Crossing during the sediment sampling was 4.76 m^3/s and 5.31 m^3/s at Webster Bridge. The five suspended sediment samples collected at Graves Crossing had concentrations ranging from 7.5 to 17.7 mg/l, with a mean of 11.9 mg/l (or 4.9 tonnes/day). Four suspended sediment samples were analyzed from Webster Bridge, ranging from 4.7 to 10.0 mg/l, with a mean of 7.7 mg/l (or 3.6 tonnes/day). We estimated bedload from our measurements as 0.9 tonnes/day at Graves Crossing and 1.6 tonnes/day at Webster Bridge for these flows.

The sieve analysis of the bed material samples indicated that there was little longitudinal variability in the gradations (Figure 2.4). We decided to model the bed gradation using the average of the three bed material sampling locations in our model domain (Graves Crossing, Old State, and Webster Bridge).

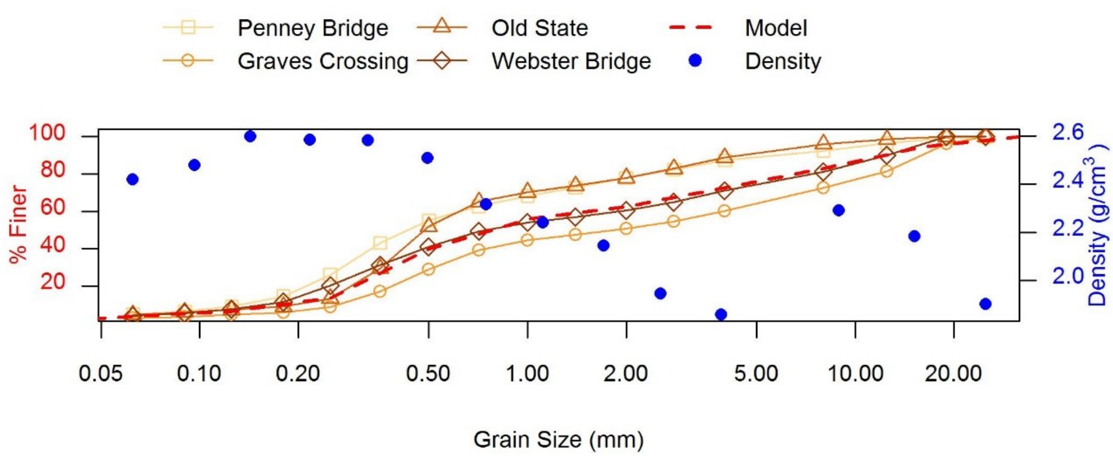

Figure 2.4. The bed material gradations collected at different locations along the Jordan River were similar. We used the average bed gradataion from the three downstream locations for modeling. The density of the bed material varied by size class, with particles larger than 0.5 mm being significantly less dense than silica (2.65 g/cm^3).

The bed material density estimates revealed that some size classes of the bed material deviated substantially from the silica density assumption (ρ = 2.65 g/cm^3) used in most sediment transport. In the Jordan River, medium sands and smaller particles have similar densities to silica. Larger particles, particularly gravel-sized and larger particles, however, were less dense, with some less than 1.9 g/cm^3. These larger particles appear to be carbonate concretions (Figure 2.5) that can be easily broken by hand. It is possible that the friable nature of these concretions biased the bed gradations as some of the particles may have broken down into smaller sizes while being sieved.

Figure 2.5. Photo of a low-density (ρ = 1.9 – 2.3 g/cm^3) concretion that makes up many of the large particles on the bed of the Jordan River.

The large, low-density particles are prevalent throughout the Jordan River. Some of these particles are cobble-sized (> 64 mm in diameter). Particles of this size with typical silica densities (2.65 g/cm^3) can form an effective armor layer that reduces bed degradation. It is not clear from our observations if the lighter material found in the Jordan acts as an effective armor layer.

3.3. LHM Flow Results

The effects of land use change increased in magnitude in a downstream direction, as expected for a gaining stream like the Jordan (Figure 2.6). Logging in the Jordan River watershed increased the median in-channel flows by 13-18%, according to our simulations. This is towards the low end of impacts of logging on streamflow reported for other watersheds (Lewis et al., 2001; Moore and Wondzell, 2005). A devastating, widespread fire similar to those that occurred elsewhere in Michigan after logging likely would have increased the median flows by 57-78% above pre-settlement conditions. This is within ranges reported for the first year after a fire (Moody and Martin, 2001b; Scott, 1993). The regrowth of much of the forested area has led to current flow conditions that are similar to pre-settlement (+3%).

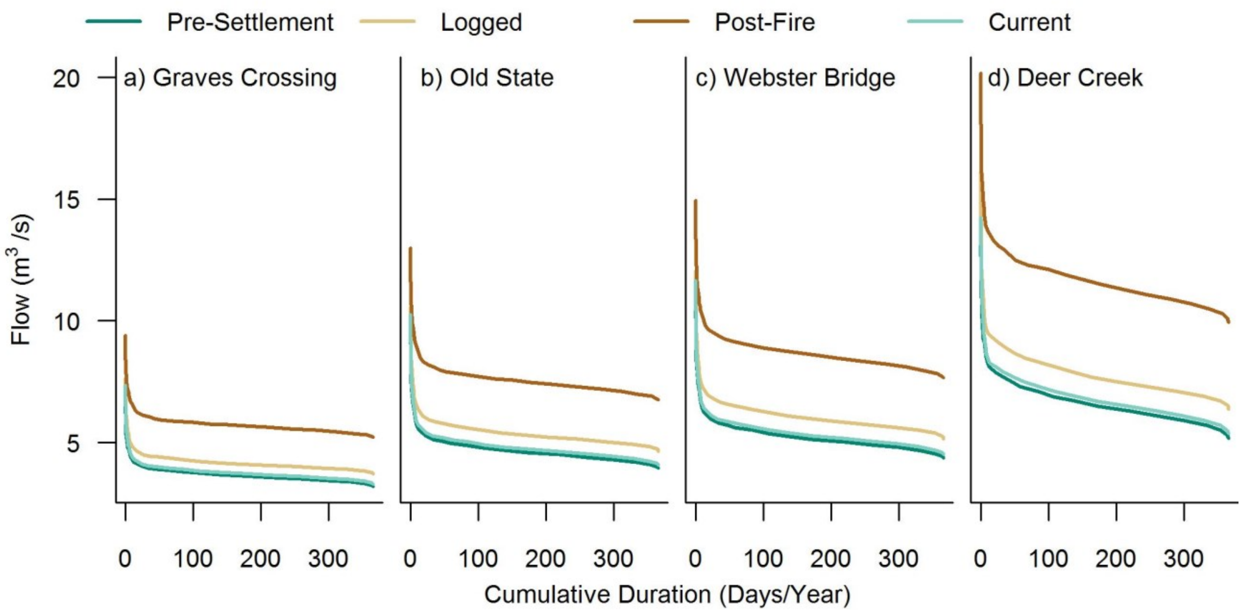

Figure 2.6. Flow duration curves for the four flow change points in the model domain; these illustrate the effects of changing land use on hydrology in the Jordan River.

3.4 Sediment Transport Capacity

The Sediment Transport Capacity hydraulic design tool in HEC-RAS has six different sediment transport functions, but only Ackers-White and Meyer-Peter Müller are based on data similar to the measured Jordan River bed material gradations and flows. We ran the calculator using both selected transport functions for each land use scenario and found that Meyer-Peter Müller produced results closer to our measured values for the same flows. The validation of the sediment transport capacity tool for the Jordan River is described in the Appendix.

The sediment transport capacity for the current land use is almost indistinguishable from the Pre-Settlement case because the flows are so similar. The mean sediment transport capacity for each land use scenario is shown in Figure 2.7, while the transport capacity associated with the 10% and 90% probability of exceedance flows can be seen in the Appendix (Figure S2.5 and Figure S2.6). The transport capacity generally increases more than flow due to the non-linear relationships between flow, shear stress, and sediment transport.

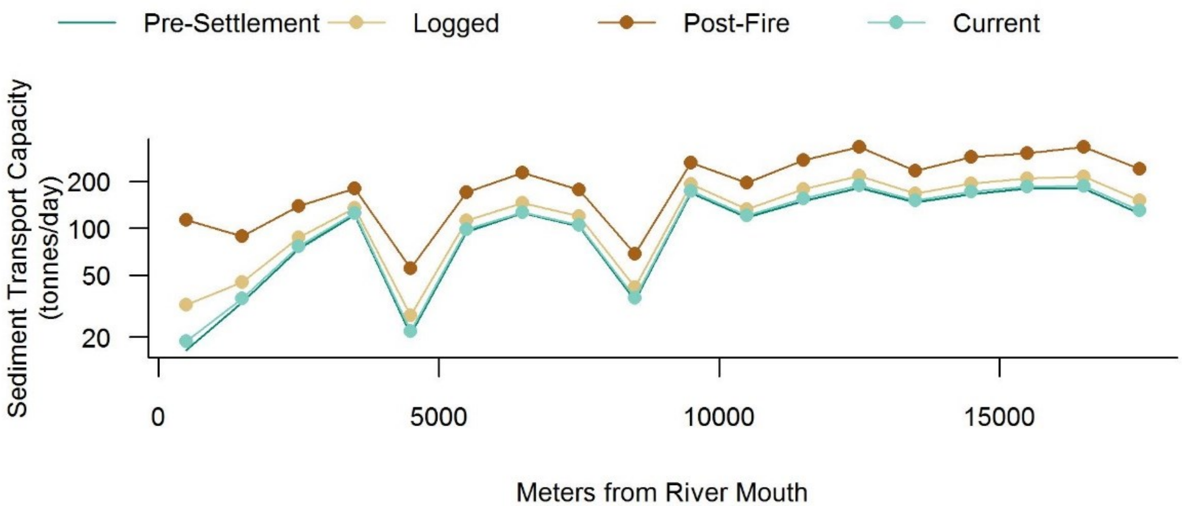

Figure 2.7. The post-fire sediment transport capacity is much higher than for the other land use scenarios. The values shown here were calculated using the Meyer-Peter Müller transport function for the median flow and averaged for each kilometer of the Jordan River. The two dips in capacity, near 4500m and 8500m, are caused by decreases in the slope of the energy grade line associated with downstream constrictions in channel width.

The logging scenario caused a noticeable increase in sediment transport capacity along the entire river, particularly at the downstream end. The modeled sediment transport capacities are 10 to 34% greater than pre-settlement except for the downstream end, where they are 95% greater. In the northern Great Lakes, other researchers have estimated post-logging sediment yields of 2 to 10 times the pre-settlement forested conditions on decadal time scales (Alighalehbabakhani et al., 2017a; Fitzpatrick and Knox, 2000), but it is difficult to directly compare modeled sediment yield at a watershed outlet to sediment transport capacity. Sediment effects at the watershed outlet can lag behind the streamflow effects by more than a decade as the sediment is alternately stored and transported along the channel (Lewis et al., 2001; Swank et al., 2001).

Flows from the Post-Fire scenario resulted in sediment transport capacities at least 48% greater than in the Pre-Settlement case. In some locations, such as the downstream end of the model or the dip in transport capacity around 4500m (Figure 2.7), the post-fire sediment transport capacity was more than double that of the pre-settlement scenario. While these increases are large, they are dwarfed by the 1-2 order of magnitude increases measured in the literature for mountainous areas (Johansen et al., 2001; Karamesouti et al., 2016; Shakesby and Doerr, 2006). Beaty (1994) observed bedload transport increases of 3-20 times the pre-fire rates near the Great Lakes, in western Ontario. A likely reason that these observed increases in sediment export are so much higher than our sediment transport capacity results is that many watersheds, especially in mountainous areas, are supply-rather than transport-limited in the absence of wildfires (Moody and Martin, 2001a).

Both the logging and post-fire scenarios produced disproportionately large sediment transport capacity increases in the downstream 1-2 km of the river. This is because the downstream model boundary condition is a constant elevation, the average level of Lake Charlevoix. The level of Lake Charlevoix fluctuates both seasonally and on an intrannual basis with the level of Lake Michigan. Over the last century, Lake Michigan water levels exhibited a range of more than 1.9 m, with an average annual range of 0.3 m. If the elevated transport rates we simulated for a fixed lake level moved material at enhanced rates for an extended period of time, they would likely produce a delta extending both into the lake and upstream. This delta would reduce the downstream slope and associated sediment transport capacity.

3.5 SIAM

The annual local sediment balance for each reach was calculated by SIAM for all of the land use scenarios. Figure 2.8 shows these sediment balances, as well as the proportions of each grain size that make up the balance. The most upstream reach (Below Graves Crossing) is slightly degradational for all of the land use scenarios except for Post-Fire. However, the local balances in this reach are all less than 2% of the pre-settlement transport capacity and it is reasonable to assume that they represent dynamic equilibrium.

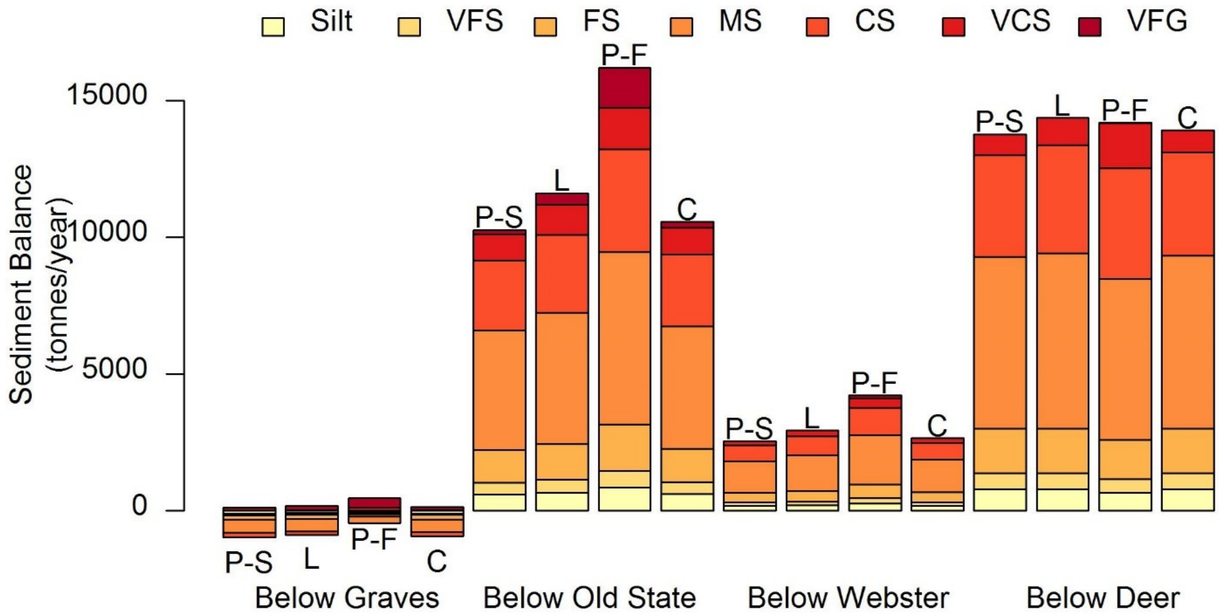

Figure 2.8. SIAM calculated the annual local sediment balance by reach for the Post-Settlement (PS), Logged (L), Post-Fire (P-F), and Current (C) land use scenarios. In addition to the total sediment balance for each scenario, the balance was calculated for the silt, very fine sand (VFS), fine sand (FS), medium sand (MS), coarse sand (CS), very coarse sand (VCS), and very fine gravel (VFG) size classes.

Sediment transport capacity declines in a downstream direction (Figure 2.7) as the slope of the river decreases. This causes the remaining reaches to all have depositional sediment balances. Land use change away from the pre-settlement condition results in increased deposition of sediment, even though more material is exported from each reach. The reach below Old State exhibits the largest increases in aggradation due to the post-fire scenario, as the sediment eroded from the steeper reach upstream begins to settle out. The most downstream reach, below the confluence with Deer Creek, is strongly controlled by the backwater from Lake Charlevoix, resulting in low energy grade line slopes and a consistently depositional sediment balance across all of the land use scenarios. The reach below Deer Creek is also unique because it is the only one where the post-fire scenario has a slightly lower sediment balance than the logged scenario, although the difference is less than 2%. The higher flows in the post-fire scenario result in greater proportions of coarse and very coarse sand in the sediment balances.

The SIAM results highlight the potential for complex watershed responses to disturbance. The Below Old State reach, for example, is likely to have a much greater initial response to a watershed-wide fire than the other reaches (Figure 2.8). This behavior is similar to observations of in-channel sediment storage and complex response in other watersheds (Benda et al., 2003; Lewis et al., 2001; Swank et al., 2001). Legleiter et al. (2003) specifically call out the need to look at the complex spatial distribution of stream response for management purposes, a task we have shown can be aided by SIAM.

4. Conclusions

Land use change affects streamflow and sediment transport in rivers. In the case of the Jordan River Watershed, these changes mostly reinforced trends that existed before European settlement. The most upstream sediment reach that we included in our models remained in dynamic equilibrium for all of the land use scenarios, transporting enough bed material to deposit in each of the downstream reaches. The complete logging of the Jordan River watershed resulted in sediment transport capacities that were 10 to 34% greater than pre-settlement capacities, while the post-fire scenario had modeled capacities 48 to 166% greater than pre-settlement. If the altered land use persisted, these changes would alter the morphology of the river, producing feedbacks that could propagate throughout the watershed. Current land use has only slightly increased the sediment transport capacity of the Jordan River slightly above the pre-settlement conditions.

The reach-based sediment budgets from SIAM demonstrate significantly different sediment responses to disturbance. While the upstream sediment reach remains in dynamic equilibrium across our land use scenarios, the three downstream reaches show varying levels of response. In most reaches, the post-fire scenario would result in the greatest levels of aggradation, demonstrating the complex responses that are possible when a watershed is disturbed.

Changing downstream water levels, multiple sediment densities of the bed materials, and potential armoring effects of the bed concretions are additional complicating factors that may significantly affect the sediment dynamics of the Jordan River and should be explored further in future work.

Acknowledgements

This chapter will be submitted for publication, co-authored by Anthony Kendall, Sherry Martin, Jim Selegean, and David Hyndman. We thank Blaze Budd for helping collect and analyze sediment samples and flows and Lon Cooper and Briana Jasinski for helping collect bathymetric survey data. Funding was provided by the Friends of the Jordan and the U.S. Army Corps of Engineers Great Lakes Tributary Modeling Program. Any opinions, findings, and conclusions or recommendations expressed in this material are those of the authors and do not necessarily reflect the views of USACE or the Friends of the Jordan.

APPENDIX

Data Collection

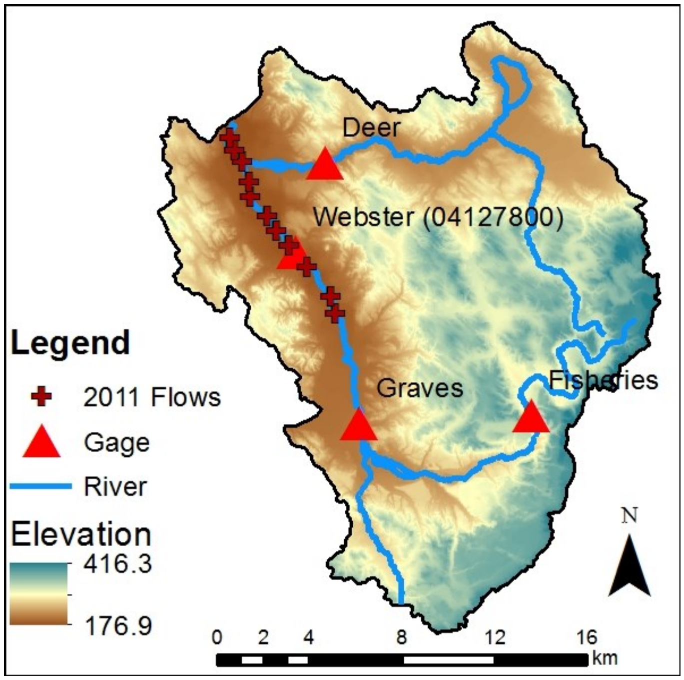

Figure S2.1. We used a Sontek ADCP to collect flow and bathymetry data at 11 sites on the Jordan River in 2011.

Bathymetric Adjustments

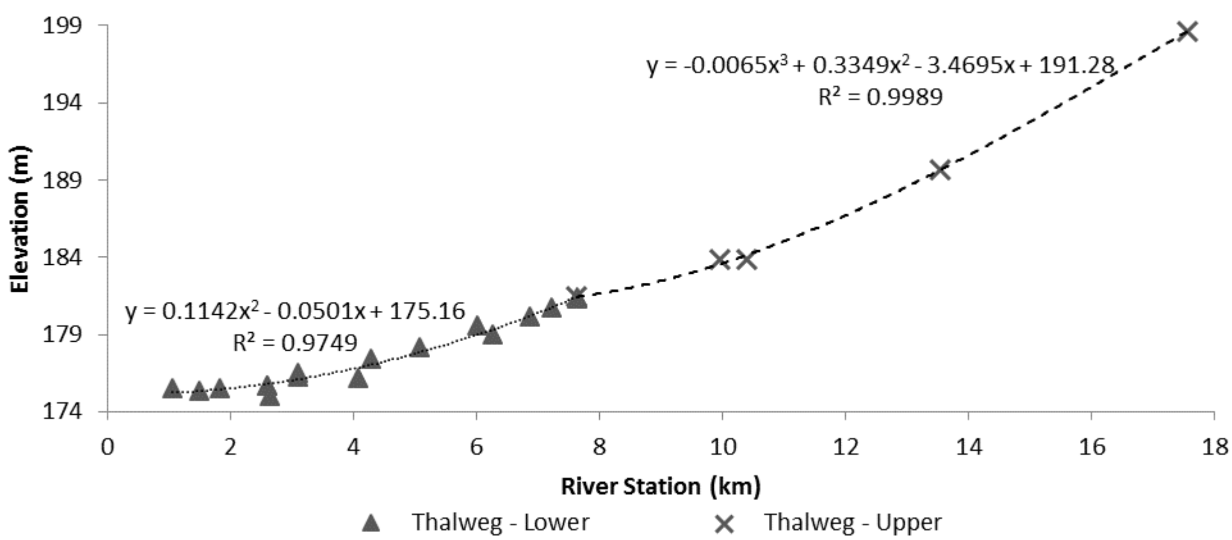

Figure S2.2. Two regression lines were fit to the surveyed thalweg elevations along the modeled portion of the Jordan River, with the break between the lines at Webster Bridge.

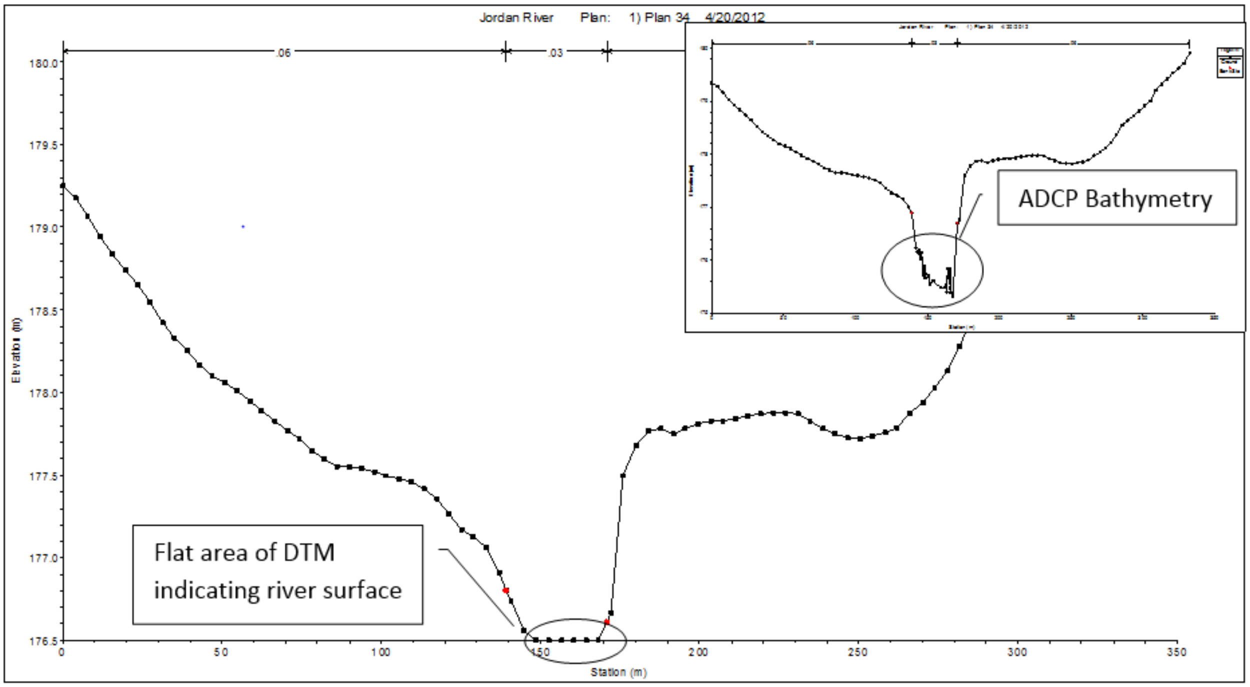

Figure S2.3. Cross-sections extracted from the DTM often contained a flat area indicating the water surface of the river. We combined this data with bathymetry collected using ADCP (inset figure) for use in the HEC-RAS model.

Hydraulic and Sediment Transport Model Validation

During calibration, we set the in-channel roughness values to 0.045 for river stations 17557.9 to 3097.9, just upstream of the confluence with Deer Creek. We reduced the roughness values for the remaining cross-sections to 0.035. Outside the banks, we set the roughness values to 0.12, representing medium to dense summer brush. These adjustments resulted in a reasonable fit of the stage data at the Webster Bridge gage with an r^2 of 0.97 and a Nash-Sutcliffe Efficiency of 0.96 (Figure S2.4).

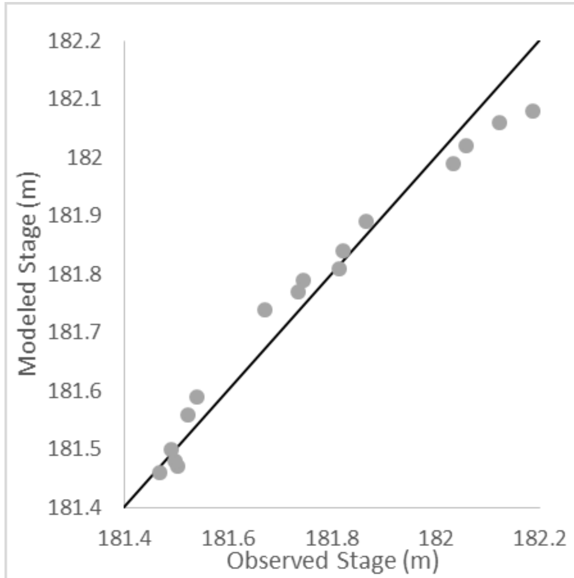

Figure S2.4. The steady-state calibration for the USGS Gage at Webster Bridge (#04127800) showed a reasonable agreement.

We validated the sediment transport capacity model using our sampling events from 2014 and the standard density assumption (ρ=2.65 g/cm^3). At Graves Crossing, we measured a total load of 5.8 tonnes/day. The sediment transport capacity tool predicted 205.1 tonnes/day (Meyer-Peter Müller) to 627.1 tonnes/day (Ackers-White) and an average capacity over the next kilometer downstream of 286.7 and 631.2 tonnes/day for Meyer-Peter Müller and Ackers-White, respectively. At Webster Bridge, we measured a total load of 5.2 tonnes/day while the model predicted 159.7 (Meyer-Peter Müller) to 342.6 (Ackers-White) tonnes/day. Within a kilometer of Webster Bridge, the estimated average transport is 71.4 and 147.4 tonnes/day for Meyer-Peter Müller and Ackers-White, respectively. The predicted sediment transport capacities are 1-2 orders of magnitude larger than what we measured, although it is possible this is a numerical modeling artifact of the procedure we used to estimate the longitudinal elevations for the hydraulic model. Graves Crossing is at the upstream cross-section of the model and Webster Bridge is at the junction of the two thalweg elevation curves, placing both of these points in areas where the model has high slopes. Given the uncertainties inherent in sediment measurement and modeling, particularly with a limited set of samples, it is difficult to draw strong conclusions from this validation. It is likely that collecting a more detailed set of surveyed thalweg elevations into the model would improve the predictions. For the purposes of this study, we opted to focus on differences from the pre-settlement case rather than the actual sediment transport numbers predicted by the model.

Sediment Transport Capacity

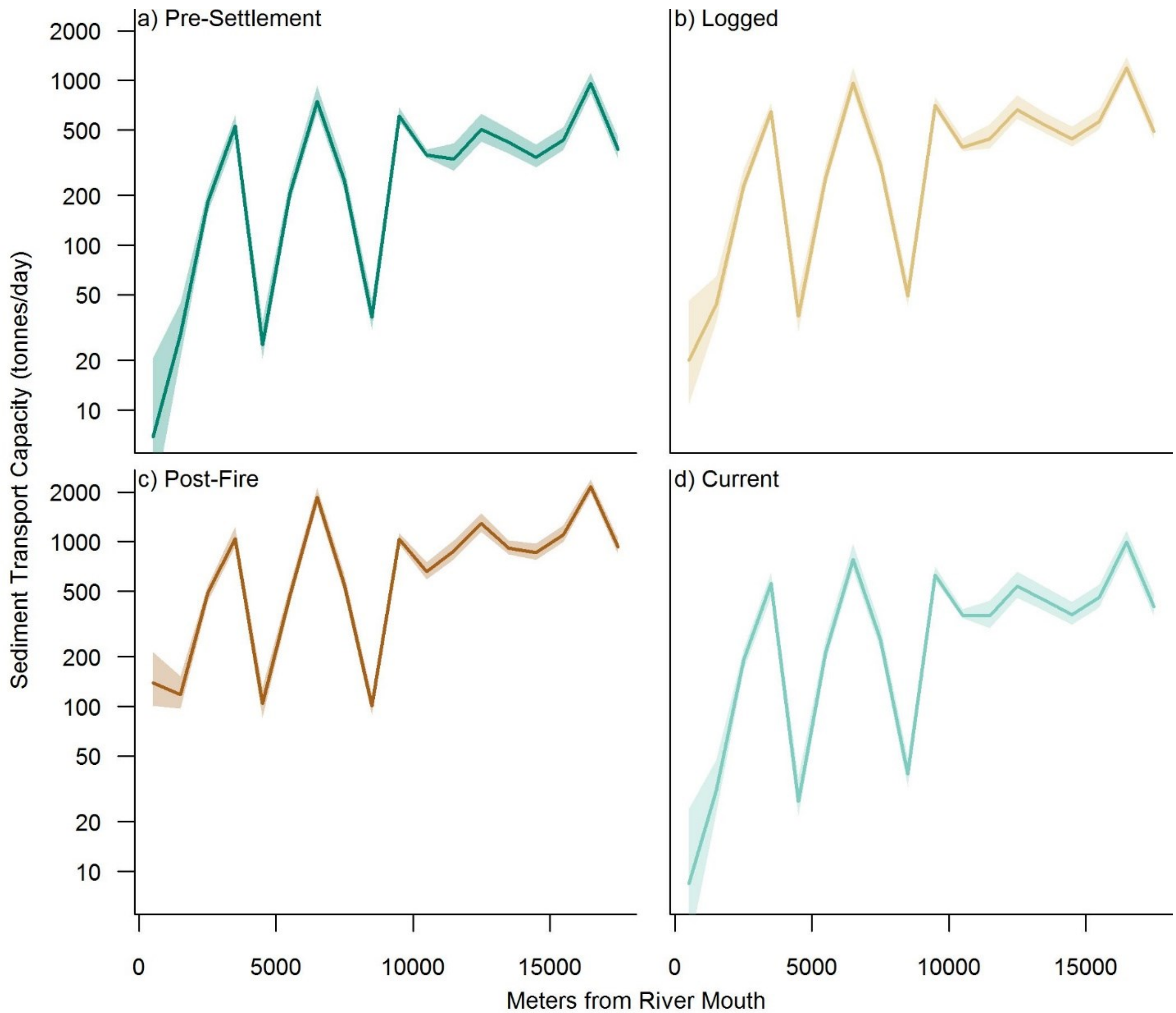

Figure S2.5. These plots show the sediment transport capacity calculated using the Ackers-White transport function and averaged for each kilometer of river. The solid lines indicate the results for the 50% exceedance flow. The difference between the sediment transport capacity at the 10% and 90% exceedance flows, indicated by the shaded polygons, is much smaller than the longitudinal variation.

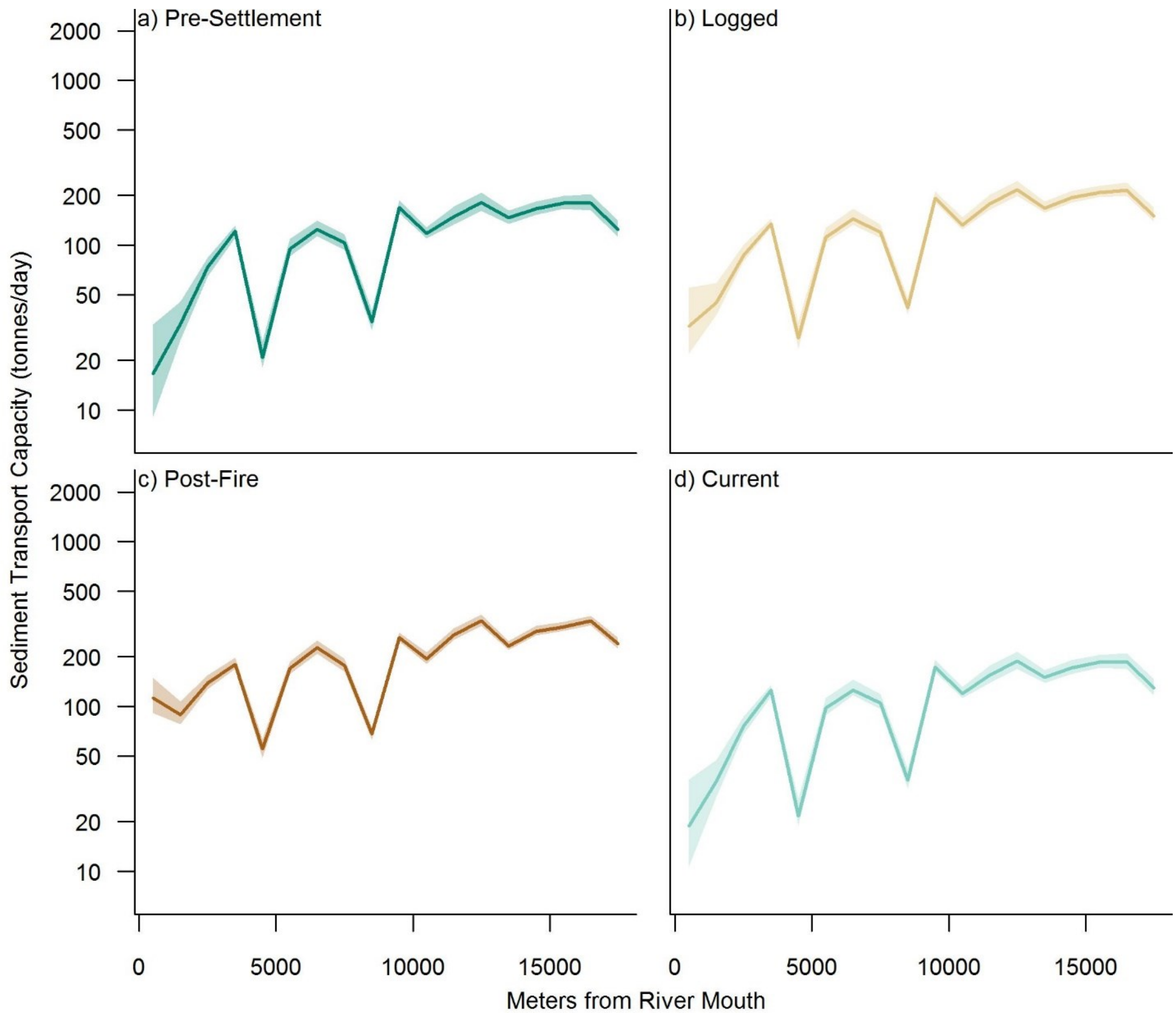

Figure S2.6. The plots below show the sediment transport capacity calculated using the Meyer-Peter Müller transport function and averaged for each kilometer of river. The solid lines indicate the transport capacity at the 50% exceedance flow while the shaded polygons represent the transport capacity for the 10% to 90% exceedance flow range.

CHAPTER 3:
IMPACTS OF PROJECTED CLIMATE CHANGE ON SEDIMENT YIELD AND DREDGING COSTS

Abstract

Changes in climate may significantly affect how sediment moves through watersheds into harbors and channels that are dredged for navigation or flood control. Here we applied a hydrologic model driven by a large suite of climate change scenarios to simulate both historical and future sediment yield and transport in two large, adjacent watersheds in the Great Lakes region. Using historical dredging expenditure data from the US Army Corps of Engineers (USACE) we then developed a pair of statistical models that link sediment discharge from each river to dredging costs at the watershed outlet. While both watersheds show similar slight decreases in streamflow and sediment yield in the near-term, by mid-century they diverge substantially. Dredging costs are projected to change in opposite directions for these two watersheds; we estimate that future dredging costs will decline in the St. Joseph River by 8-16% by mid-century but increase by 1-6% in the Maumee River. Our results show that the impacts of climate change on sediment yield and dredging may vary significantly by watershed even within a region, and that agricultural practices will play a large role in determining future streamflow and sediment loads. We also show that there are large variations in responses across climate projections that cause significant uncertainty in sediment and dredging projections.

1. Introduction

Changes in climate have the potential to significantly alter the movement of sediment through watersheds and directly affect dredging needs in rivers and harbors. There are over sixty-three commercial harbors in the Great Lakes and over 600 miles of navigation channel maintained by the U.S. Army Corps of Engineers (USACE). In 2014, an estimated 132 million tons of commodities were transported to and from U.S. ports located on the waterways of the Great Lakes system (USACE, 2014). Many of the harbors are located at the outlets of rivers that can convey large amounts of sediment, necessitating periodic dredging to maintain the navigation channels. In spite of the importance of this system, previous studies have not examined the potential impacts of projected future climate changes on both sediment yield (sediment eroded from the landscape and delivered to the river) and the dredging requirements in this region.

Current climate change projections generally show increasing temperatures and precipitation in the Great Lakes region of the United States, although the magnitude and seasonality of these changes depends on the emissions scenario and climate model (Hayhoe et al., 2010; IPCC, 2014; Pryor et al., 2013). Precipitation is expected to increase in the winter and spring, but decline in the summer; temperatures are projected to increase more in the winter during the early part of the century, with changes in summer temperatures catching up by mid-century (Hayhoe et al., 2010). The Third National Climate Assessment found that extreme rainfall and flooding events, and their associated erosion, are on an upward trend in the Midwest, including Indiana, Michigan, and Ohio (Pryor et al., 2014).

Numerous studies have examined the potential implications of climate change on streamflow and sediment yield (e.g., Mukundan et al., 2013; Park et al., 2011; Serpa et al., 2015). In the Upper Midwest and Great Lakes regions, O'Neal et al. (2005) found that variability in soil loss would increase due to changes in crops. Two separate studies looked at climate change effects on northern Illinois watersheds and found that streamflows would decrease, based on the projected climate change scenarios (Cherkauer and Sinha, 2010; Chien et al., 2013). Several Soil and Water Assessment Tool (SWAT) models of the Maumee River have examined the potential effects of climate change scenarios. For example, Bosch et al. (2014) modeled four watersheds that drain to Lake Erie and projected that flow and sediment yield would increase, based on climate projections from two emissions scenarios and three General Circulation Models (GCMs). In contrast, a more narrowly focused study on the Maumee that utilized three GCMs and a single emissions scenario found that annual average flow and sediment loads will decrease by mid-century (2045 to 2055), although there was significant variability in the monthly sediment loads (Verma et al., 2015). As part of a nationwide study of 20 watersheds with SWAT simulations, Johnson et al. (2015) found that five of their six climate change scenarios would likely increase flow and sediment delivery in the Maumee by mid-century (2041 to 2070).

Dredging quantities are imperfectly correlated to sediment discharge (the sediment delivered to the mouth of the river) since they depend on downstream water levels (for example, Lake Michigan levels varied 1.9 m over the last 30 years), the location where the sediment settles out relative to the navigation channels, and on the amount of funding available to conduct the dredging operations. Some studies that discuss dredging in the context of climate change do so through the lens of rising water levels (Schwartz et al., 2004; Smith, 1991) rather than looking at changes in delivery of sediment from rivers. Schwarz et al. (2004) used both future projections and an arbitrary scenario of Great Lakes water levels to estimate increased dredging costs at Goderich, Ontario, on Lake Huron, but did not consider the possibility of changing riverine sediment input to the harbor. Other authors consider the dredging as either one component of the overall sediment budget (Morang et al., 2013; Templeton and Jay, 2013) or as a causative effect of increased sediment delivery (Zhang et al., 2010). We are not aware of any studies that directly link projected future riverine sediment delivery to changes in dredging needs.

Here we used SWAT models of two large US watersheds draining into the Great Lakes to quantify the likely effects of climate change on the streamflow, sediment yield to the river, and sediment discharge at the mouth of the river. SWAT-calculated sediment loads are then input to two statistical sediment dredging models to estimate historical dredging costs for each system. We then drive these linked models with both historical climate and future climate simulations based on downscaled scenarios from the 5th Coupled Model Intercomparison Project (CMIP5) for both “Contemporary” (~2011-2030) and “Mid-Century” (2031-2050) periods. We run the whole suite of 234 climate models ensemble members included in the CMIP5 dataset to better understand how climate forecast uncertainties will propagate through the paired SWAT sediment transport and statistical dredging models. We discuss results for Representative Carbon Pathways (RCPs) 6.0 and 8.5, while results for the remaining RCPs (2.6 and 4.5) are in the

Supporting Information. These results provide both a more comprehensive view of how climate may impact sediment yield differentially in these neighboring watersheds and a first quantification of how dredging costs may respond to climate changes.

2. Methods

2.1. Study Domain

Two large, adjacent watersheds in the southern Great Lakes were selected for this study: the St. Joseph River and the Maumee River (Figure 3.1). We chose these two watersheds because of their size, proximity to each other, and dredging requirements at the river mouths in the Great Lakes. The St. Joseph River watershed covers parts of northern Indiana and southwestern Michigan and generally flows northwest into Lake Michigan at St. Joseph, MI. According to the 2006 National Land Cover Database (NLCD) (Fry et al., 2013), this 12,138 km^2 watershed consists of 49.3% agricultural row crops, 23.8% forest, 13.0% urban, and 12.2% pasture. The average annual flow at the USGS gage at Niles, MI (#04101500) between 1990 and 2009 was 113.6 cms. Long-term sediment data was not available for the St. Joseph River. The USACE dredges the harbor at St. Joseph, MI.

The Maumee River watershed is located in northeastern Indiana, southeastern Michigan, and northwestern Ohio. The main channel flows northeast to Toledo, OH and Lake Erie. This 17,015 km^2 watershed is more heavily agricultural and significantly less forested than the St. Joseph, consisting of 74.7% agricultural row crops, 10.8% urban, 8.2% forest, and 5.2% pasture. The average annual flow of the Maumee River in Waterville, OH (USGS gage 04193500) between 1990 and 2009 was 172.6 cms. The average annual suspended sediment load at this site between 1990 and 2003 was 1.2 million tonnes. The USACE performs dredging operations at both a Maumee River and a Maumee Bay site.

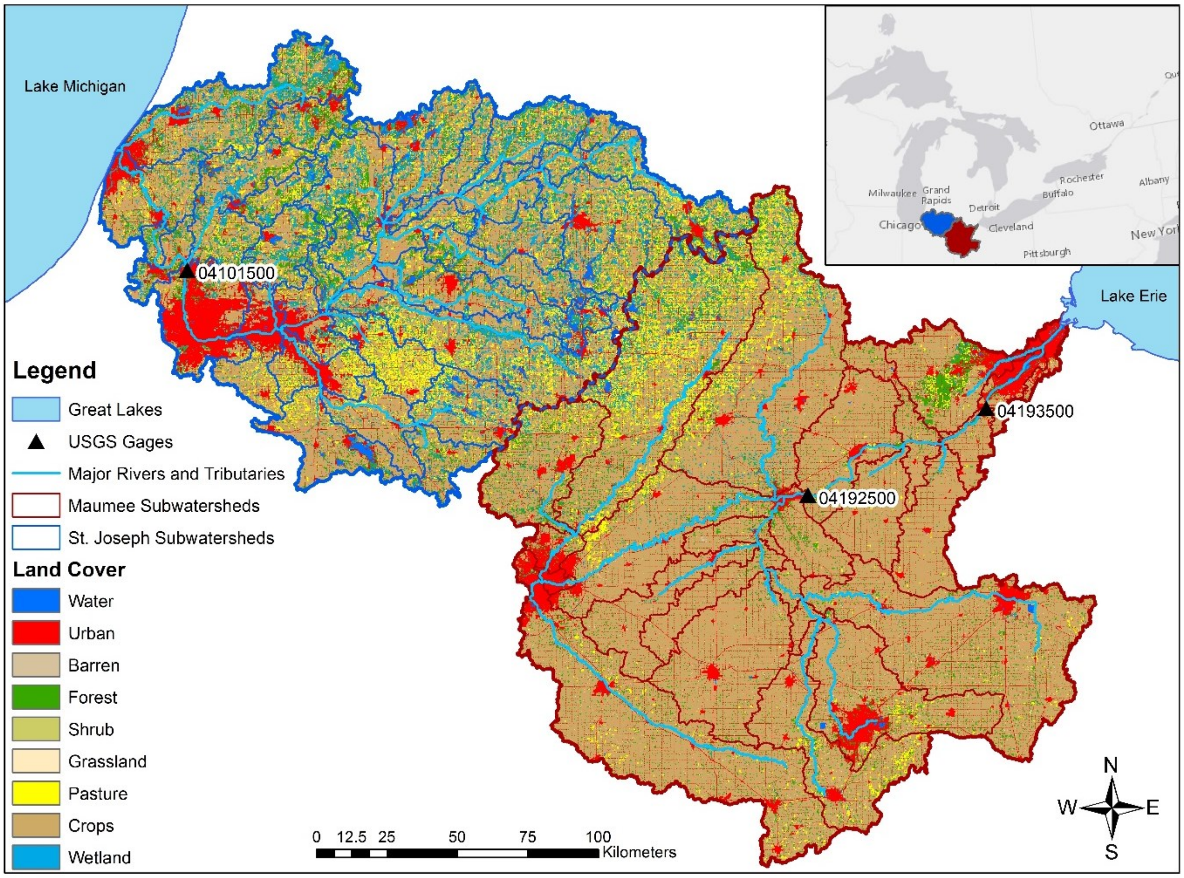

Figure 3.1. Map of the St. Joseph and Maumee River watersheds, subwatersheds, and their 2006 land use/land cover.

2.2 SWAT Model Development and Calibration

The Soil and Water Assessment Tool (SWAT) is a semi-distributed, lumped parameter hydrologic model developed by researchers at the U.S. Department of Agriculture's Agricultural Research Service (USDA-ARS) (Arnold et al., 2012; Neitsch et al., 2011). It is often used for sediment yield studies (Alighalehbabakhani et al., 2017b; Gassman et al., 2014; Krysanova and White, 2015) and is increasingly used to examine climate change impacts (Chaplot, 2007; Chien et al., 2013; Ficklin et al., 2009; Johnson et al., 2015). SWAT models split their domain into subwatersheds and then subset these into Hydrologic Response Units (HRUs). HRUs are the basic computational units of a SWAT model, which represent all of the area within a subwatershed with similar soils, slopes, and land uses.

We developed SWAT models independently for each watershed using the

ArcSWAT 2012.10.0.7 plugin for ArcGIS, and used SWAT 2012 rev. 622. Digital elevation models with a resolution of 1 arc-second were obtained from the National Elevation Dataset and used to delineate the watersheds. The 2006 National Landcover Dataset was used to determine land use/land cover types and we used the default crop and harvest management parameters from ArcSWAT. Soil types and soil hydraulic properties were determined using the SSURGO database from the Natural Resources Conservation Service. Information on dams in the watersheds was obtained from the National Inventory of Dams maintained by the U.S. Army Corps of Engineers and those we deemed significant because of size or location were included in the models. We selected dams with storage greater than 1,233,000 m^3 for inclusion in the models. We also included the St. Joseph River Dam, in Fort Wayne, IN, which only has a storage of 1,078,000 m^3 while draining over 16% of the Maumee basin. These datasets were all imported into ArcSWAT and used to determine watersheds, subwatersheds for modeling purposes (shown in Figure 3.1), and HRUs. The St. Joseph SWAT model consisted of 32 subbasins and 278 HRUs, along with 17 dams. The Maumee SWAT model had 24 subbasins, 307 HRUs, and 5 dams.

The United States Department of Agriculture's Agricultural Research Service (ARS) provides weather data, in SWAT format, for all counties across the US. The daily data covers January 1950-December 2009, with the exception of January 2002. January 2002 was filled using SWAT's weather generation routines that create typical weather time series for the location and time period. We included 2002 in our simulations, but to avoid biasing further analyses due to the weather generation routine excluded January 2002 from goodness-of-fit calculations, and excluded the entire 2002 year from the downscaling bias analyses.

After initial set up of the models in ArcSWAT, we calibrated them using the SWAT Calibration and Uncertainty Programs (SWAT-CUP) tool (Abbaspour, 2015). We ran both models from 1980 through 2009, using a daily time step, with at least a five year spin-up period. Monthly outputs from the models were used for all comparisons. We began our calibration by using the Sequential Uncertainty Fitting version 2 algorithm

(SUFI2) in SWAT-CUP to determine the sensitivity of the parameters in the SWAT models, based on the full allowable range of each parameter. We then focused our efforts in succeeding calibration iterations on those parameters that had the most significant effect on the model outputs. As a final step in the model parameterization, we tested the removal of each calibration parameter to arrive at a parsimonious set of calibration parameters.

The St. Joseph River model was calibrated to the streamflow at the USGS gage at Niles, MI (#04101500). The model was run from 1985 to 2009, with 1990-1999 used for calibration and 2000-2009 for validation. Sediment discharge was then calibrated and validated for the same periods using a streamflow:sediment discharge curve for the harbor in St. Joseph, MI. This curve was developed for a previous U.S. Army Corps of Engineers study of the St. Joseph River watershed (USACE, 2007).

We calibrated the Maumee River model by first matching the hydrology using the USGS gages at Waterville, OH (#04193500) and Defiance, OH (#04192500). The model was run from 1980 to 2003, with 1991-1999 used for calibration to match up with the period used for the St. Joseph model. The validation period was split between October 1985 to December 1990 and January 2000 to September 2003, based on the availability of USGS sediment discharge data. We calibrated and validated the simulated sediment discharge to data from the USGS Gage at Waterville, OH (#04193500) using periods matching the streamflow.

2.3 Dredging Cost Estimation

The U.S. Army Corps of Engineers provided us with dredging quantities for St. Joseph Harbor, the lower Maumee River, and the Maumee Bay (M. Mahoney, personal communication, 20 September 2013). We created two models for dredging costs: 1) a linear regression, fit to historical dredging data and simulated modeled sediment fluxes, and; 2) a simpler 1:1 correlation between simulated sediment discharge and dredging costs (or percentage change in each). Our use of two models provides an estimate of cost model structural uncertainty, and allows us to evaluate a range of possible outcomes. To fit each model, dredging data from 1989-2009 was used for St. Joseph Harbor and 1990-

2009 for the Maumee River and Maumee Bay dredging sites.

We created linear regression models between the annual dredging costs, converted to 2009 dollars using the U.S. Bureau of Labor Statistics Consumer Price Index data, and the modeled sediment discharge from the SWAT models run using the historic gage data. To evaluate possible time-lagged responses between sediment discharge and dredging, regressions were tested using simulated sediment results from the same calendar year as the dredging; the same water year as the dredging; the prior calendar and water years; and one and two year (calendar and water year) moving averages of sediment discharge. As there are two dredging sites in the Maumee Watershed, in the river itself and in the bay at its mouth, we examined regressions to the Maumee River and Bay dredging sites both separately and as a combined amount. We also added long-term average monthly water levels of Lakes Michigan and Erie to the regressions for the St. Joseph and Maumee dredging sites respectively.

2.4 Climate Model Scenarios

The analyses presented in the main paper utilized the World Climate Research Programme's (WCRP's) Coupled Model Intercomparison Project phase 5 (CMIP5; (Taylor et al., 2012) multi-model dataset. We acquired bias-corrected, spatially downscaled versions of these datasets from a publicly available archive created by the United States Bureau of Reclamation and others (Brekke et al., 2013). The temperature and precipitation data in this archive are available at a monthly time step and a spatial resolution of 1/8°. This data needed to be further disaggregated for use with the SWAT models, which use daily data at a single weather gage location for each sub-basin. We utilized all 234 CMIP5 model projections available from the archive. The CMIP5 dataset consists of multiple Representative Carbon Pathways (RCPs), run across a large number of individual models. To consider a larger ensemble, additional analyses were run with 112 CMIP3 scenarios (Meehl et al., 2007) and the results are included in the Supporting Information for this paper.

For brevity, analysis here is limited to CMIP5 RCP 6.0 (Masui et al., 2011); 37 projections) and RCP 8.5 (Riahi et al., 2011); 71 projections), which represent a plausible range of CO_2 emissions given no additional conservation efforts. These RCPs are particularly relevant given the 2011 – 2050 simulation period of this study. RCP 6.0 is most similar to the older B2 Special Report on Emissions Scenarios (SRES; (Nakicenovic and Swart, 2000), while RCP8.5 is similar to SRES A2/A1F1 (IPCC, 2014). Results for the other climate change scenarios are presented in the Supporting Information.

Two forecast periods were run: 2011 – 2030, hereafter called the Contemporary period, and; 2031 – 2050, called the Mid-Century period. SWAT model outputs for each period are individually averaged and presented below as both climate ensemble medians and ranges, as stated in figures and tables.

We matched individual, observed gage locations used by the SWAT models with the closest spatial grid cell for the downloaded climate data. These climate datasets were then spatially disaggregated from the grid cells to the individual gages and temporally disaggregated for 1980 to 2050 using the methodology from Maurer and Hidalgo (2008) and Wood et al. (2004) based on the ARS weather data described previously. This procedure involved randomly selecting months from the historical data to serve as a template for temporal distribution. Temperatures at each gage location were adjusted using a monthly additive factor to match the average temperature for each month of the GCM results. The precipitation data were adjusted using a monthly multiplier to match the total monthly precipitation for each month in the GCM results while maintaining the proportion of monthly rainfall across individual days. The same sequence of reference months was used to downscale each of the climate change scenarios.

To evaluate remaining bias in the climate simulations, we compared the downscaled precipitation and temperature data with the historical gage data. Bias was calculated by comparing the distribution of annual average temperature and total annual precipitation for the downscaled climate scenarios with that of the historical gage data from 1988-2008, excluding 2002. The SWAT models were then run using the historical gage data for 1985-2009, and for each climate model scenario for 1985-2050. To explicitly examine how biases in downscaled climate would propagate through the SWAT model streamflow and sediment discharge predictions, we compared the 1988-2008 (again excluding 2002) period for each scenario run to the same period run using gage data.

3. Results and Discussion

3.1. Model Calibration and Validation

Results for the calibration and validation of the SWAT models are shown in Figure 3.2 and Figure 3.3, with goodness-of-fit statistics summarized in Table 3-1. Hydrologic calibration and validation of monthly outputs for the St. Joseph River model were both good, with Nash-Sutcliffe efficiencies of 0.78 for calibration and 0.72 for validation. The sediment discharge calibration and validation for the St. Joseph model resulted in biases of -3.2% and +10.5%, respectively, which are both considered very good, based on the percent bias criterion of Moriasi et al. (2007).

The calibration of the Maumee River model had nearly identical goodness-of-fit statistics for monthly flows at both stream gage sites. The calibration Nash-Sutcliffe efficiency was 0.79 at Waterville, OH and 0.80 at Defiance, OH (see Figure 3.1 for locations). Validation Nash-Sutcliffe efficiencies were 0.79 at Waterville and 0.82 at Defiance. Sediment discharge at Waterville produced a very good percent bias both for the calibration period (+4.6%) and the validation period (+2.5%).

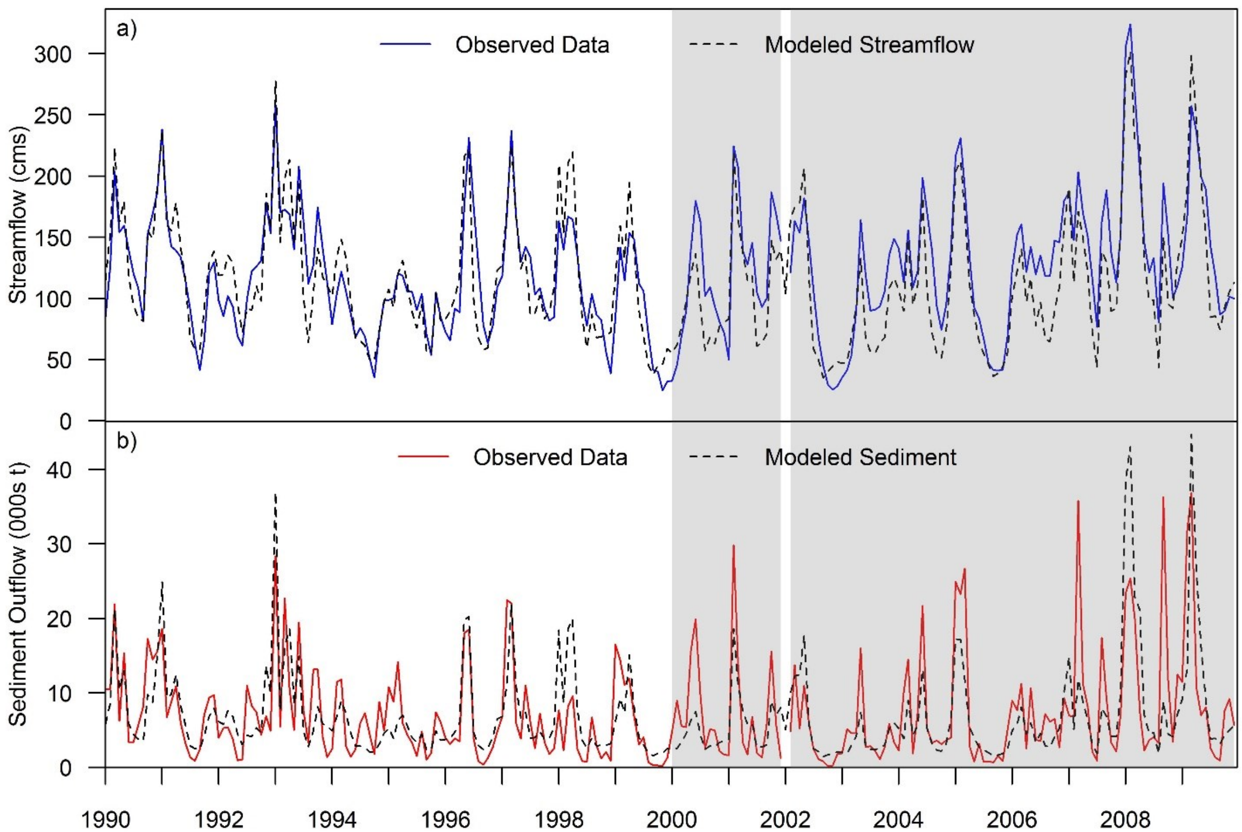

Figure 3.2. Calibration and validation of St. Joseph River SWAT model for (a) monthly streamflow and (b) monthly sediment discharge. The validation months are indicated by the grey shaded boxes. The gap in the validation period for January 2002 is due to missing weather data.

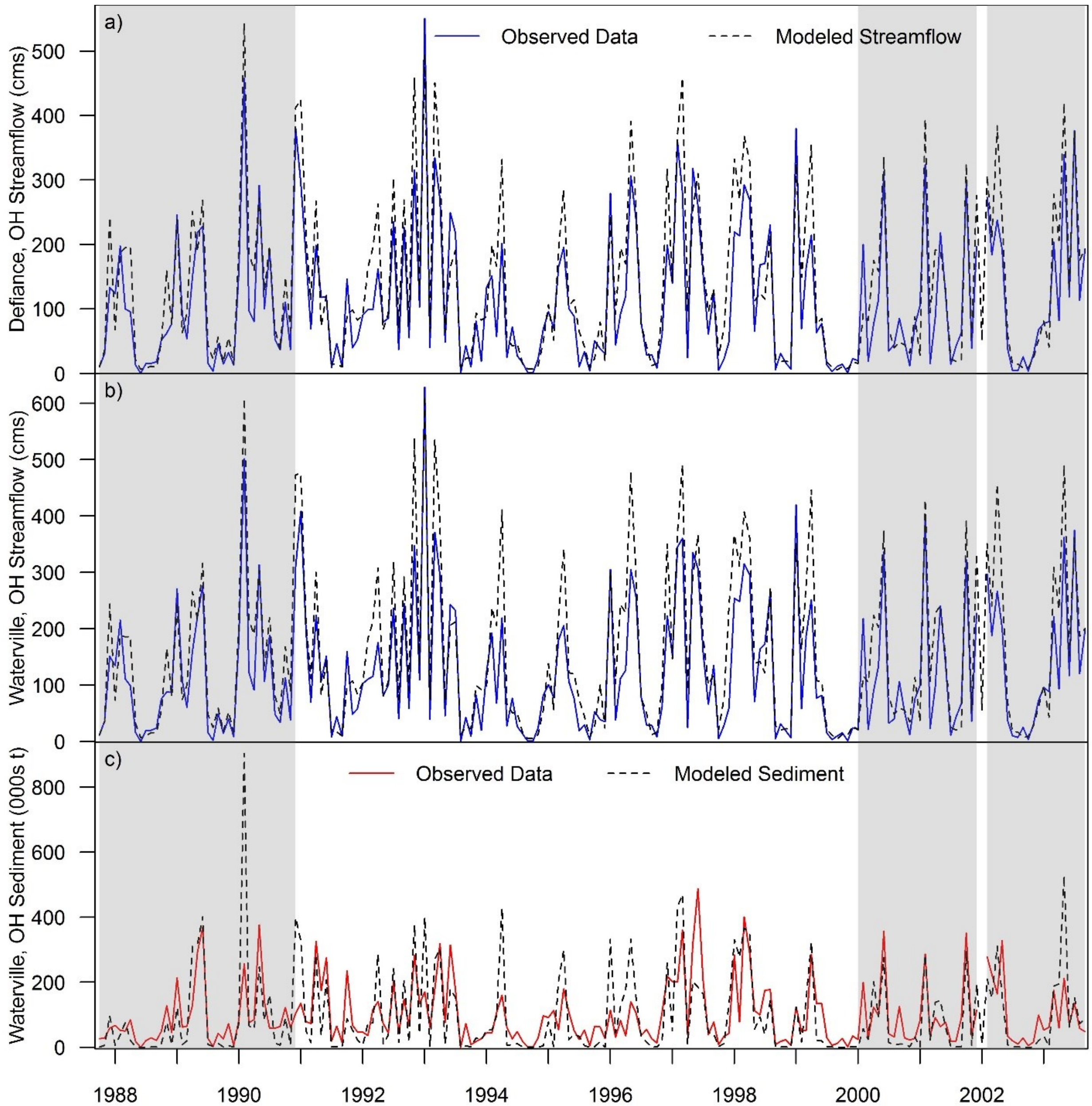

Figure 3.3. Calibration and validation of Maumee River SWAT model for (a) monthly streamflow at Defiance, OH and (b) at Waterville, OH, and (c) monthly sediment discharge at Waterville, OH. The validation months are indicated by the grey shaded boxes and were selected to maintain a common calibration period with the St. Joseph model while maximizing the use of available sediment data. The gap in the validation period for January 2002 is due to missing weather data.

Table 3-1. Summary of Calibration and Validation Statistics: R^2, Nash-Sutcliffe Efficiency (NSE), and % Bias. Note that January 2002 was excluded from the goodness-of-fit calculations due to missing weather data for that month.

			Calibration	Validation
St. Joseph River at Niles, MI		Calendar Years	1990-1999	2000-2009
	Flow	R^2	0.78	0.83
		NSE	0.78	0.72
	Sediment	R^2	0.59	0.47
		NSE	0.52	0.29
		% Bias	-3.2%	+10.5%
Maumee River at Waterville, OH		Water Years	1991-1999	Oct 1987-Dec 1990, Jan 2000-Sep 2003
	Flow	R^2	0.86	0.86
		NSE	0.79	0.79
	Sediment	R^2	0.53	0.49
		NSE	0.52	0.48
		% Bias	+4.6%	+2.5%
Maumee River at Defiance, OH	Flow	R^2	0.84	0.86
		NSE	0.80	0.82

3.2 Downscaled Climate Model Bias

We looked at Probability Density Functions (PDFs) of the mean annual temperatures and annual precipitation from both the downscaled climate model historical runs and observed station data (Figure S3.1 in the Supporting Information) in order to determine if they represented the same distribution as the observed data. The overlap and similarities between the PDFs of the observed data and those of the downscaled climate data indicates that they likely represent the same distribution. When interpreting Figure S3.1, it is important to understand that the bias correction performed on the climate model data by Brekke et al. (2013) utilized a temperature and precipitation dataset that was scaled to match long-term (1961-1990) average statistics (Maurer et al., 2002). The downscaled climate model temperatures have a mean annual bias of +0.02 °C and a standard deviation of 0.01 °C for both RCP 6.0 and 8.5, relative to the gage observations. The precipitation values for RCP 6.0 and 8.5 have mean annual biases of -49.5 mm/yr (-5.1% of mean observed precipitation) and -48.9 mm/yr (-5.0%), respectively. The standard deviation of the precipitation values is 25.0 and 29.0 mm/yr for RCP 6.0 and 8.5 respectively. It is also important to note that the sample sizes for the two RCPs discussed are different, as there were 37 RCP 6.0 scenarios and 71 RCP 8.5 scenarios available from the archive.

Biases in the downscaled climate inputs have the potential to propagate into the SWAT model outputs. Figure 3.4 shows the PDFs of the simulated historical streamflow and sediment discharge at the mouth of each river. Generally, the PDFs all follow similar patterns to the observed data. Potential differences may exist due to the small sample size of the observations. Streamflow and sediment discharge for the St. Joseph River have a slight high bias, while sediment discharge for the Maumee River has a slight low bias. The Maumee streamflow PDFs for the RCP 6.0 and 8.5 scenarios reasonably match the observed PDF. In order to limit the potential influence of this on our analysis, we used anomalies (differences between projected and historical time periods from the same data set) for the remaining analysis. Results for CMIP3 scenarios and additional CMIP5 RCP scenarios are summarized in the Supporting Information of this paper.

The biases in SWAT model outputs, when using the downscaled projections to simulate the historical time period, are most likely due to the biases in the downscaled and disaggregated CMIP precipitation and temperature data. This may be attributed to a combination of the spatial and temporal disaggregation processes used and the climate models themselves.

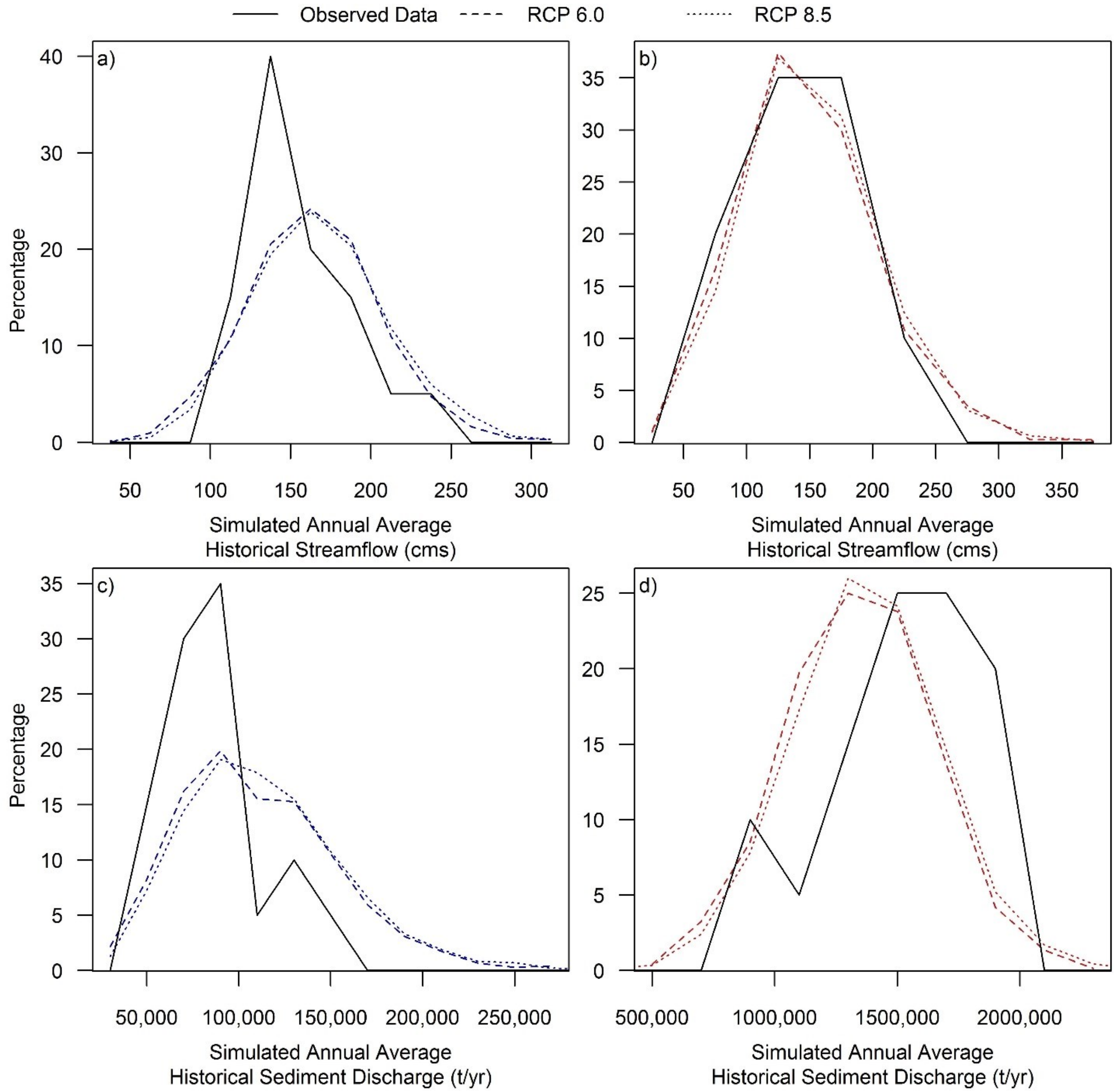

Figure 3.4. Probability density functions of: a) annual average streamflow for the St. Joseph River, b) annual average streamflow for the Maumee River, c) annual average sediment discharge for the St. Joseph River, and d) annual average sediment discharge for the Maumee River. All PDFs are for the historical period (1988-2001, 2003-2008), simulated using observed climate data and downscaled climate data.

3.3 Dredging Model Results

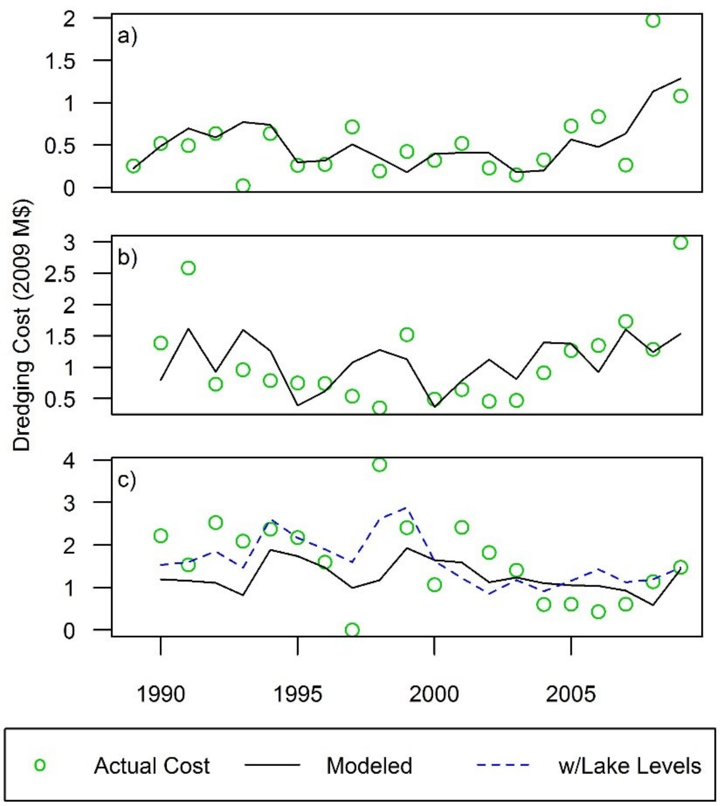

Figure 3.5. Actual and modeled historical costs using multiple linear regression for: a) St. Joseph Harbor, b) Maumee Bay, and c) Maumee River. The Maumee River modeled historical costs are shown both with and without including Lake Erie levels in the multiple linear regression.

The actual annual dredging expenditures and the modeled costs are shown in Figure 3.5.

Table 3-2 shows the fit and parameters for the best linear model of dredging costs at each location, where $Q_{S,\,WY}$ is the sediment discharge for the water year of interest, $Q_{S,\,WY\text{-}1}$ is the sediment discharge for the preceding water year, $Q_{S,\,CY\text{-}1}$ is the sediment discharge for the preceding calendar year, and $D_{S,\,WY}$ is the deposition in the downstream reach of the Maumee River for the current water year. The estimate of St. Joseph Harbor dredging costs had an R^2 of 0.48. The cost of dredging the two sites associated with the Maumee River were estimated as the sum of the Maumee Bay (R^2=0.30) and Maumee River (R^2=0.15) costs.

Table 3-2. Dredging cost linear models for each dredging location

Dredging Location	Model R^2	Equation: Intercept, b (\$)		Slope, m (\$)		Predictor Variables
St. Joseph Harbor	0.48	-693,700	+	14.30	*	$\left(Q_{S,WY} + Q_{S,WY-1}\right)/2$
Maumee Bay	0.30	-859,800	+	1.26	*	$Q_{S,CY-1}$
Maumee River	0.15	3,519,000	+	16.88	*	$D_{S,WY}$

The multiple linear regressions including water levels showed no significant improvement over the simple linear regression for either the St. Joseph Harbor or the Maumee Bay dredging sites. Inclusion of Lake Erie water levels did improve the model fit for the Maumee River site (R^2=0.38). This improved estimate is shown as the dashed blue line in Figure 3.5c. While climate change will affect future lake levels, it is unclear what the effect will be and we opted not to include it in our estimates of future dredging.

3.4 Effects of Climate Change on Streamflow, Sediment Yield, Sediment Discharge, and Dredging

The SWAT results are reported for three relevant outputs: streamflow at the river mouth, sediment yield from the entire watershed to the river, and sediment discharge at the river mouth. The SWAT outputs for the Contemporary (scenario years 2011-2030) and Mid-Century (scenario years 2031-2050) climate change scenarios are summarized Table S3.1 and Table S3.2, respectively.

The median streamflow values from the summary tables show small differences from the current climate. In contrast, the box plots in Figure 3.6 illustrate that the changes in median monthly streamflow are small relative to the variability across climate scenarios for the Contemporary period. This is also true for the St. Joseph River in the Mid-Century period. However, the Mid-Century Maumee streamflows have a median increase of 6.1 cms for the RCP 6.0 scenarios and 3.9 cms for the RCP 8.5 scenarios.

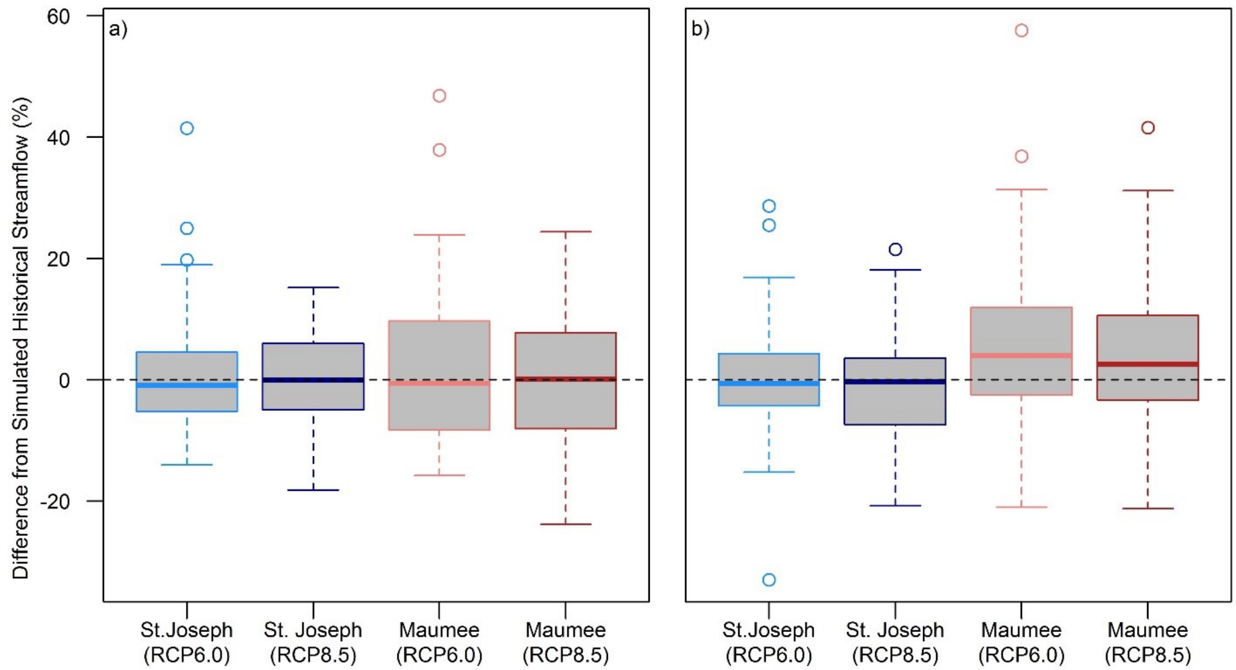

Figure 3.6. Differences in modeled streamflow between current (1989-2008), and both Contemporary (a, 2011-2030) and Mid-Century (b, 2031-2050) CMIP5 scenarios.

Median sediment yield estimates for both the St. Joseph and Maumee appear to decrease slightly in the Contemporary scenarios, as seen in Figure 3.7. Sediment yields in the St. Joseph watershed continue to decrease during the Mid-Century scenarios. In contrast, there is a slight increase in the Mid-Century sediment yields for the Maumee River under both RCP 6.0 and 8.5 scenarios.

Sediment discharge follows the same patterns as the sediment yield (Figure 3.7). The most significant difference is that over 75% of RCP 6.0 scenarios show an increase in sediment discharge for the Maumee relative to the current values. The percentage changes in the sediment discharge for the Maumee are similar to the simulated changes in streamflow. The sediment discharge changes in the St. Joseph, however more closely resemble the changes in sediment yield. There is a large amount of variability in these results and, with the exception of the Maumee RCP 6.0 sediment discharge, at least 25% of the scenarios fall on the opposite side of the no change line.

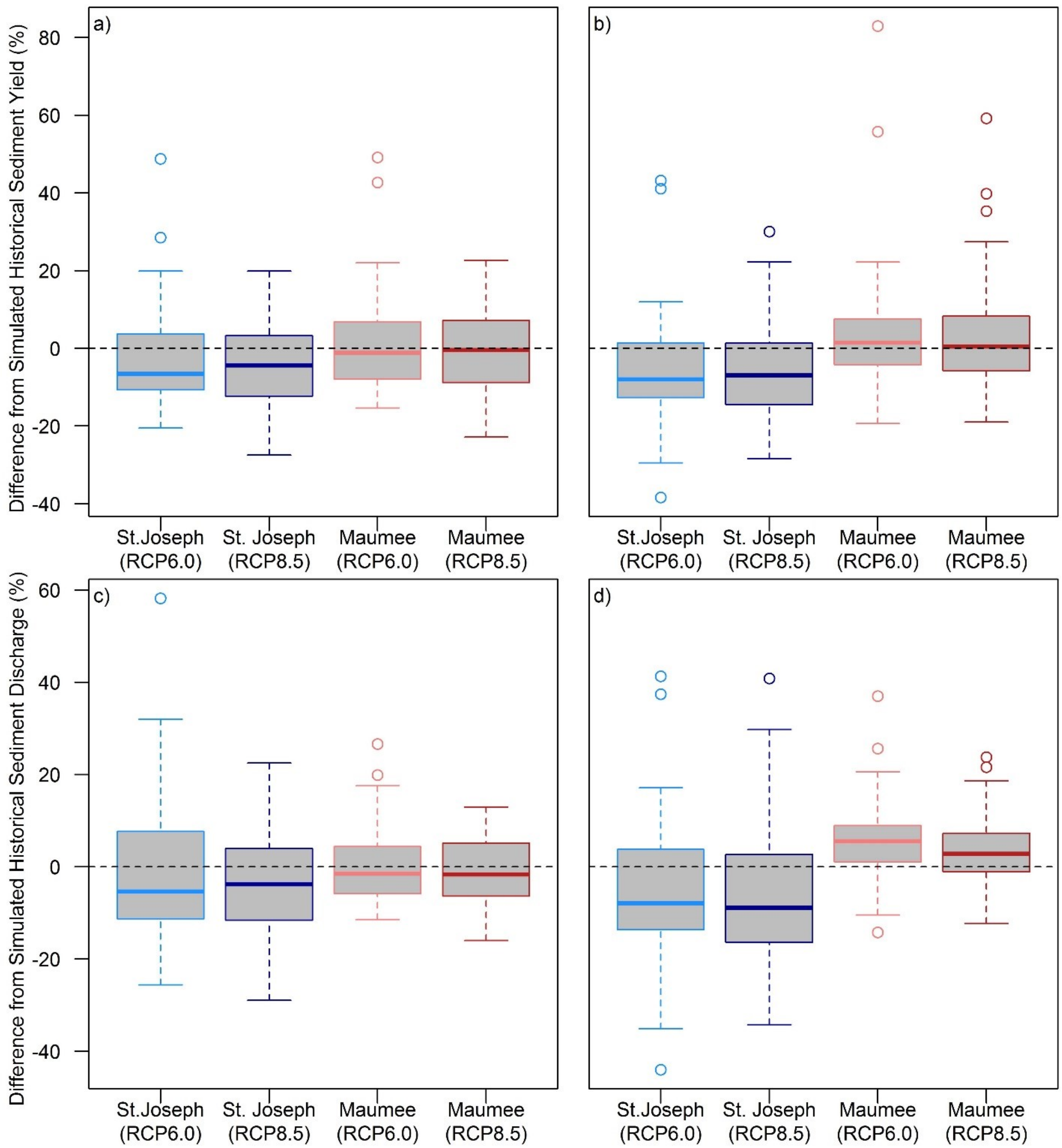

Figure 3.7. The top row shows differences in modeled sediment yield between historical (1989-2008) and both Contemporary (a, 2011-2030) and Mid-Century (b, 2031-2050) CMIP5 scenarios. The bottom row presents the differences in modeled sediment discharge between historical and Contemporary (c) and Mid-Century (d) CMIP5 scenarios.

Several other studies have examined climate change in the Maumee River, although they used the CMIP3 climate scenarios and had differences in methodologies and study periods. Results from both Johnson et al. (2015) and Cherkauer and Sinha

(2010) suggested little change in the average flows by mid-century, while Bosch (2014) projected a 6-18% increase in flow; these results are within the middle two quartiles of those presented here. Verma et al. (2015) projected a reduction in flow of 8.5%, which would be in the lowest quartile of our results. The sediment results from these studies are similar to those projected for streamflows, with Johnson et al. (2015) projecting very small (0.6%) increases in TSS, Bosch et al. (2014) projecting larger increases of 8-32%, and Verma et al. (2015) projecting decreases of 10.4%. With the exception of the high estimate of 32% from Bosch et al., these estimates are within the range of our results, with the results from Johnson et al. (2015) being closest to our median.

The responses of the two adjacent watersheds are similar, with the exception of the Mid-Century period in which median streamflow, sediment yield, and sediment discharge all start to increase in the Maumee River watershed, while they continue to decline in the St. Joseph River watershed. A deeper investigation of model outputs revealed that this difference is due to the much greater proportion of agricultural land in the Maumee (Figure 3.1). Sediment yield from agricultural land can be significantly affected by the cover practices used, with low or no-till practices and cover crops significantly reducing the soil erosion. This also implies that the timing of large precipitation events that coincide with periods of bare ground can produce a large proportion of the annual sediment yield. The effects of climate change will depend on the coincident timing of these precipitation events and conditions, also suggesting that management will be important to mitigate the effects of climate change on sediment yield in agricultural watersheds.

The higher temperatures in the Mid-Century scenarios lead to simulated faster crop growth, producing earlier and larger harvests. This increase in agricultural production can be seen in Figure 3.8, which shows the change in harvested yield per hectare. A similar increase in future crop yield due to longer growing seasons has been identified as a potential effect of climate change (Pryor et al., 2014). In the model, once a crop is harvested, the land lays fallow, with little to no transpiration, until the next growing season. This allows small increases in the modeled sediment yield (due to erosion from the bare earth) as well as increased runoff that translates into increased streamflow and sediment discharge. This model phenomenon, as evidenced by a shift in evapotranspiration earlier in the year, was also noted by Ficklin et al. (2009) for a SWAT model of a highly agricultural watershed in California. This example shows the importance of looking closely at both the model results and the underlying processes.

It is possible that this phenomenon would be more limited in the real world. If crops are harvested early enough, farmers may plant a second crop, increasing evapotranspiration and offsetting the effects on sediment and streamflow. Alternatively, they may start to plant longer season crops that benefit from the increased temperatures. Both possibilities would also likely be accompanied by the use of additional fertilizers and possibly increased irrigation from groundwater.

Whatever the outcome of future management decisions, these results point to the sensitivity of sediment yield and discharge to agricultural management. Research is needed to quantify the likely effects of climate changes and to translate scientific results into potential policies to adapt to a changing climate. While hydrologists and atmospheric scientists are prepared to discuss the physical aspects of the water cycle, agricultural specialists and social scientists can better predict how farmers will respond to the changing climatic conditions.

Recent (1989-2009) dredging of St. Joseph Harbor averaged $517k per year (in 2009 dollars). Relative to modeled historical dredging costs, median estimates using the regression equation decline 5-13% in the Contemporary scenario and 14-16% in the Mid-Century time period (Table 3-2, Figure 3.9). The upper quartiles ranged from +6-12% in the Contemporary and +2-6% in the Mid-Century while the lower quartiles were -18% in the Contemporary and -25-28% in the Mid-Century. The decreases in median dredging costs estimated using the 1:1 sediment discharge:dredging cost relationship were only about half as much, 4-5% in the Contemporary and 8-9% in the Mid-Century time periods. The upper quartiles for the 1:1 cost relationship ranged from +4-8% in the Contemporary and +3-4% in the Mid-Century while the lower quartiles were -11-12% in the Contemporary and -14-16% in the Mid-Century.

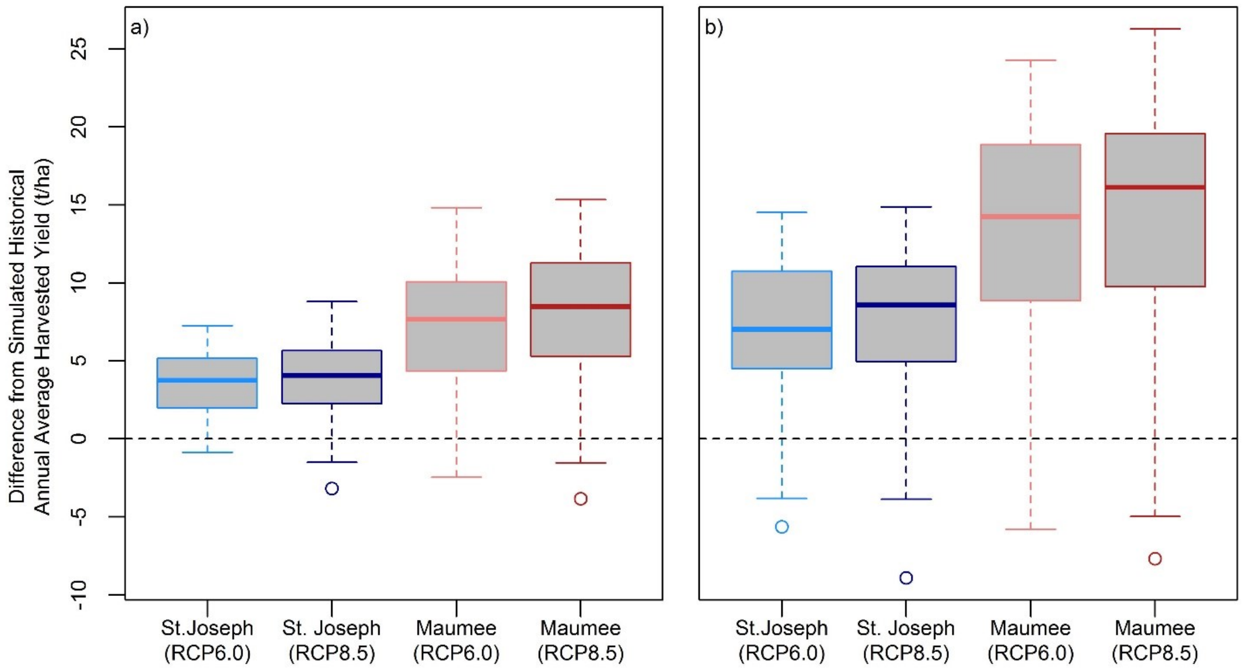

Figure 3.8. Difference in annual harvested yield per hectare estimated by the SWAT models for a) Contemporary (2011-2030) and b) Mid-Century (2031-2050) time periods. As harvested yield increases, more land is left fallow in the SWAT models, leading to increased runoff and sediment yield. Note that the values of the change in harvested yield are reflective of both area of cultivation, which is much greater in the Maumee, and increasing temperatures under climate change scenarios. In our models, once the crops were harvested, SWAT treated the land as fallow, allowing increased runoff and sediment yield.

The average dredging cost for the combination of the Maumee River and Maumee Bay sites between 1990 and 2009 was $2.7M (in 2009 $). The median estimated future dredging costs (Table S3.3, Figure 3.9) based on the regression equation estimates show an increase of 1% or less for both the Contemporary and Mid-Century scenarios, with upper quartiles of 1-2% and lower quartiles of 0%. The estimates that are based on the 1:1 sediment discharge:dredging cost relationship are more variable, with median decreases of 2% in the Contemporary and 3-6% increases in the Mid-Century time period. The upper quartiles for the 1:1 relationship are 4-5% in the Contemporary and 7-9% in the Mid-Century time periods, while the lower quartiles indicate a decrease of 6% in the Contemporary and a change of ±1% by Mid-Century.

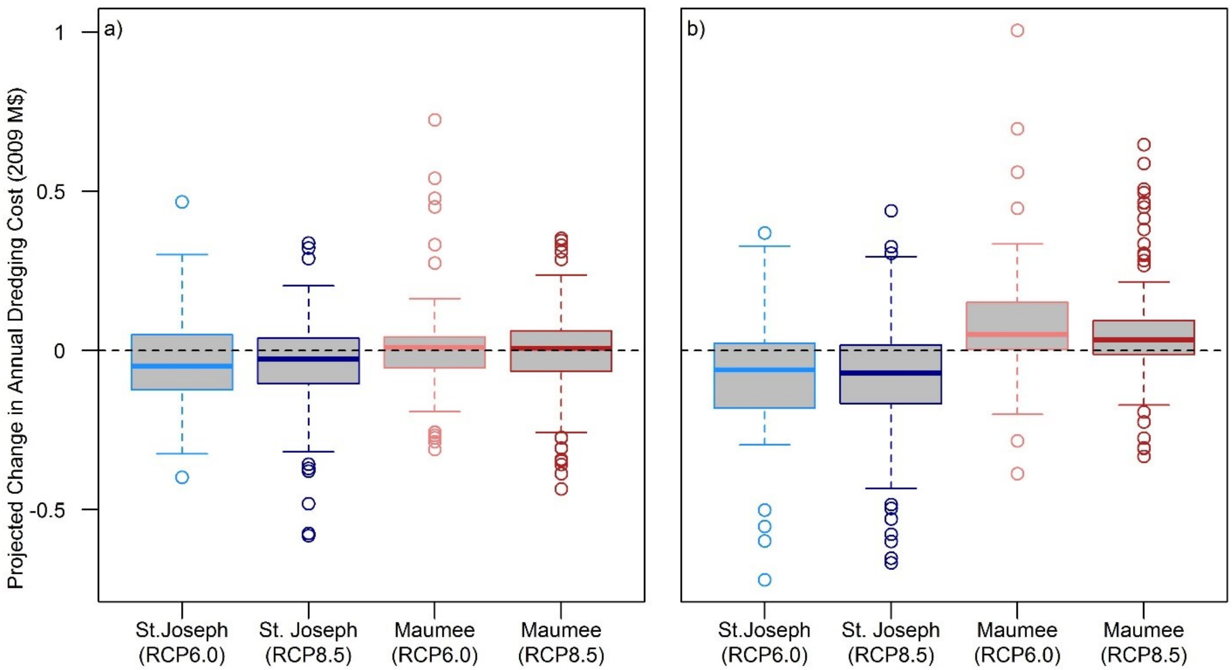

Figure 3.9. Projected changes in dredging costs for: a) Contemporary (2011-2030) and b) Mid-Century (2031-2050) scenarios, relative to historical (1989-2008) costs. Data shown includes both cost estimation methods, which are given equal weight, doubling the sample size.

The changes in dredging costs vary between the two watersheds, the modeled time periods, across the climate models, and between the two different estimates of costs. Of note is that, for the St. Joseph River, the regression equation estimates show greater changes and variability than the 1:1 sediment discharge:dredging cost relationship, while the opposite is true for the Maumee. This difference in response between the two approaches to estimating the future dredging costs indicates the potential importance of examining multiple approaches when using empirical models.

The historical dredging was not driven solely by the amount of sediment being delivered by the river. The areas dredged are coastal harbors on the Great Lakes and are affected by longshore transport of sediment, short time period seiche events (over hours to days), and variations in lake levels on seasonal, annual, and decadal time scales (Gronewold and Stow, 2014; Quinn, 2002). In particular, our modeling shows that the Maumee River site dredging appears to be driven by lake level variations on Lake Erie (Figure 3.5c). Dredged volumes are also affected by the limited budget available to the U.S. Army Corps of Engineers in any given year; there is a backlog of dredging need across the Great Lakes (USACE, 2015).

4. Conclusions

We modeled future conditions in two large watersheds, the Maumee and St. Joseph Rivers, using 108 different sets of climate change inputs representing a plausible range of CO_2 emissions. In general, the median results suggest small decreases in streamflow in both watersheds, with similar decreases in sediment delivery to the river mouths. The exception to this is the Mid-Century scenario (2031-2050) for the Maumee River Watershed, where its managed agricultural landscapes are likely to drive the sediment and streamflow response of the watershed. This implies that the response of farmers to the changing climate will significantly impact the streamflow and sediment yield in agricultural areas.

There is a large amount of variation in the climate change model projections that drive similarly large variations in the predicted sediment yield and sediment discharge response. Even though averages across climate model ensembles tend to show little change, the variance is large. Of note, the differences between RCP 6.0 and RCP 8.5 scenarios are smaller than the variation across models within each scenario. The responses will also vary between watersheds depending on the dominance of agricultural lands, farming practices, soil types, and other factors.

We also estimated dredging costs using two methods and, in general, they decrease slightly at St. Joseph, MI (~ 4-8% median decrease in the Contemporary, 8-18% median decrease in the Mid-Century). The Maumee dredging costs are likely to remain near the current range in the Contemporary, but are projected to increase slightly in the Mid-Century period (median increase of 1-6% in the Mid-Century). This will depend on the responses of farmers in the watershed to climate change. The model variance also indicates a significant uncertainty in outcomes.

This study focused on the aggregated effects of a large number of downscaled climate scenarios but only a single sediment modeling framework using SWAT. Our understanding of the potential impacts of climate change could benefit by extending this research to include other sediment models and to examine the differences and variability within the CMIP5 projections. There is also a need to explore the likely responses of farmers to lengthening growing seasons and the impacts of climate-induced changes in agricultural and management practices on the sediment regime of watersheds.

Supporting Information

Interested readers may view additional model results in the Appendix accompanying this chapter. Figure S3.1 shows the PDFs of observed and downscaled temperature and precipitation. Figure S3.2 shows the PDFs of mean annual temperature and precipitation for both the CMIP3 and CMIP5 scenarios. We have provided the results for all of the CMIP3 scenarios modeled and the A1b scenarios as Figure S3.3 to Figure S3.7. CMIP5 results for all RCPs combined, as well as for RCPs 2.6 and 4.5 are presented in Figure S3.8 to Figure S3.12. Table S3.1 and report the SWAT model outputs for the Contemporary and Mid-Century periods, respectively. Table S3.3 reports the estimated change in dredging costs.

Acknowledgements

This chapter was co-authored by Anthony Kendall and David Hyndman and previously published in *Hydrological Processes* (Dahl et al., 2018). Portions of this work were funded by a U.S. Army Corps of Engineers (USACE) Institute of Water Resources (IWR) Responses to Climate Change Pilot Project, USDA NIFA Water CAP grant 2015-68007-23133, and a Food Energy and Water supplement to the KBS LTER project, NSF grant #1637653. Any opinions, findings, conclusions, or recommendations expressed in this material are those of the authors and do not necessarily reflect the views of the National Science Foundation or the USDA National Institute of Food and Agriculture.

We acknowledge the World Climate Research Programme's Working Group on Coupled Modelling, which is responsible for CMIP, and we thank the climate modeling groups for producing and making available their model output. For CMIP the U.S. Department of Energy's Program for Climate Model Diagnosis and Intercomparison provides coordinating support and led development of software infrastructure in

partnership with the Global Organization for Earth System Science Portals.

APPENDIX

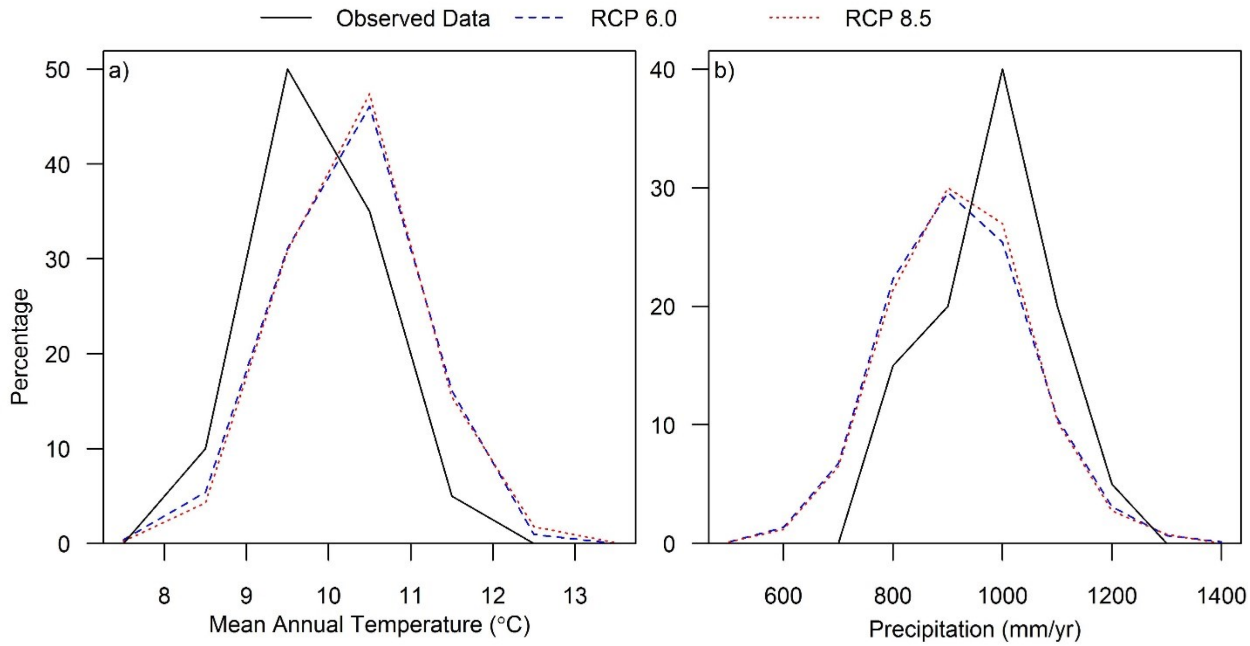

Figure S3.1. Probability Density Functions for the historical period (1988-2001, 2003-2008) of observed and downscaled a) mean annual temperature and b) annual precipitation. Note that in panel b the RCP 6.0 and 8.5 lines are identical.

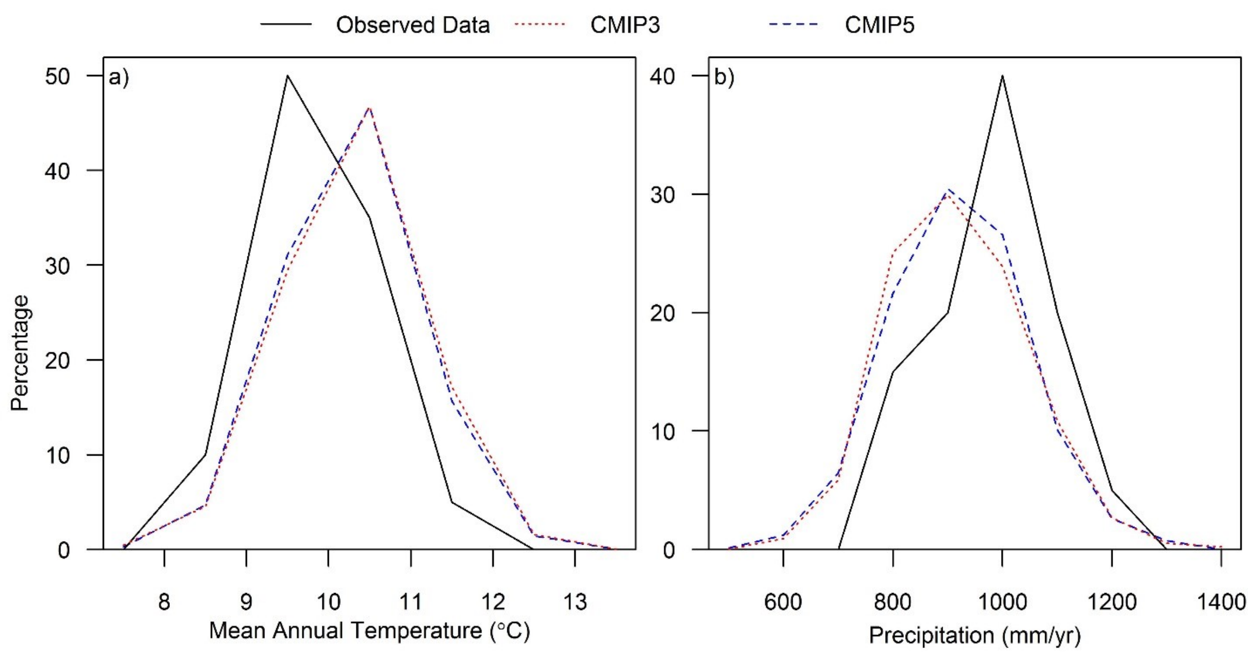

Figure S3.2. Probability Density Functions of observed and downscaled a) mean annual temperature and b) annual precipitation for all CMIP3 and CMIP5 projections.

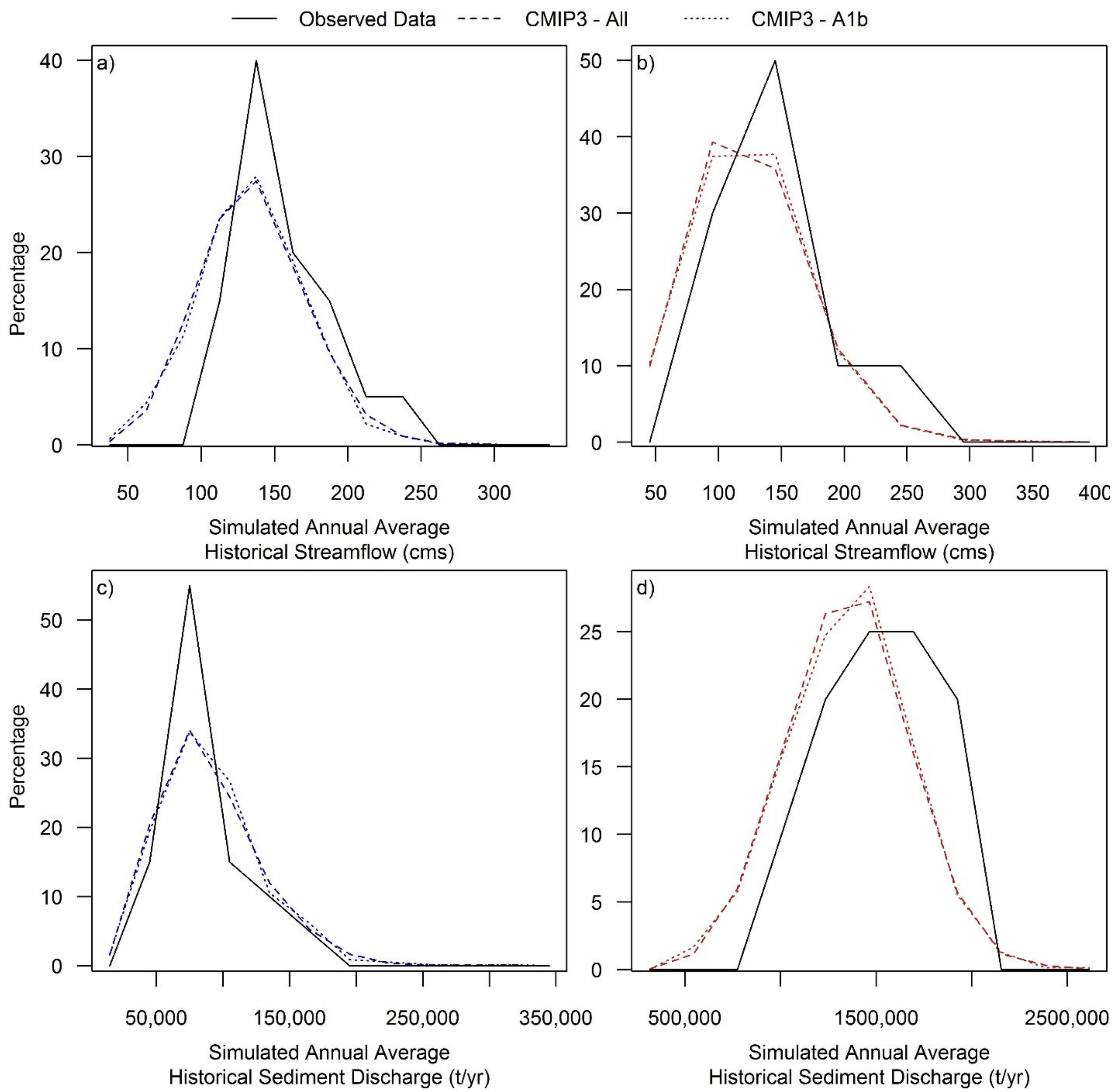

Figure S3.3. Probability density functions for the historical period (1988-2001, 2003-2008) simulated using observed climate data and downscaled climate data from CMIP3: a) annual average streamflow for the St. Joseph River, b) annual average streamflow for the Maumee River, c) annual average sediment discharge for the St. Joseph River, and d) annual average sediment discharge for the Maumee River.

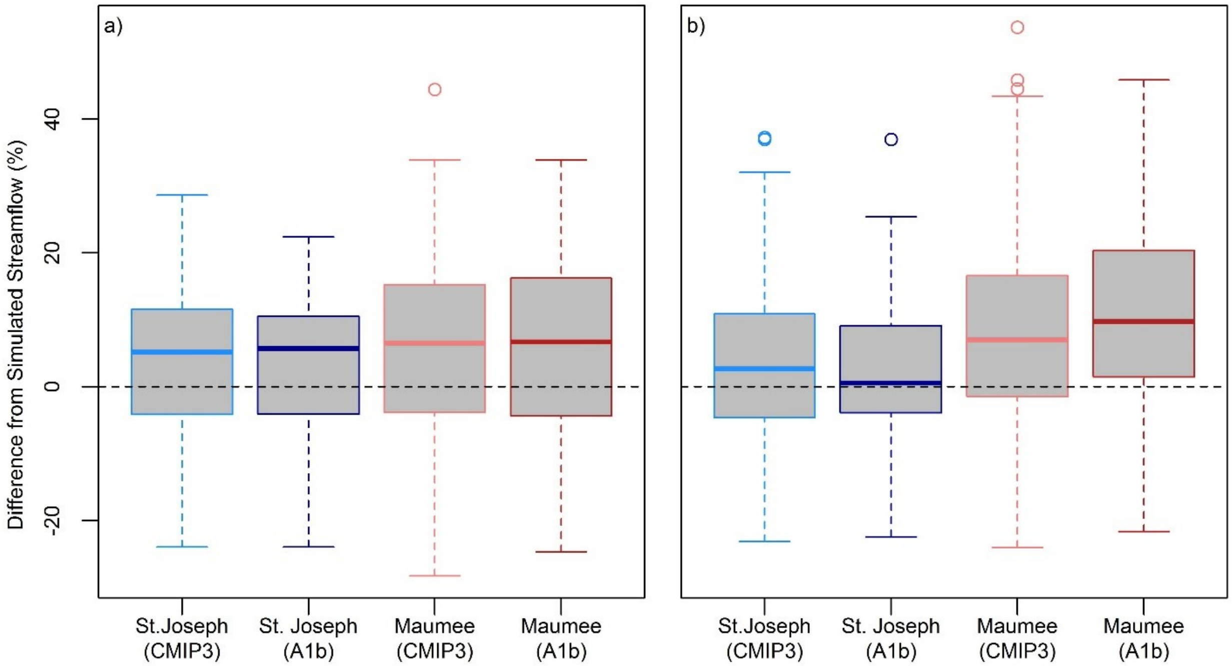

Figure S3.4. Differences in modeled streamflow between current (1989-2008), and both Contemporary (a, 2011-2030) and Mid-Century (b, 2031-2050) CMIP3 scenarios. CMIP3 indicates all downscaled CMIP3 scenarios while A1b are only those scenarios that used the A1b emissions scenario.

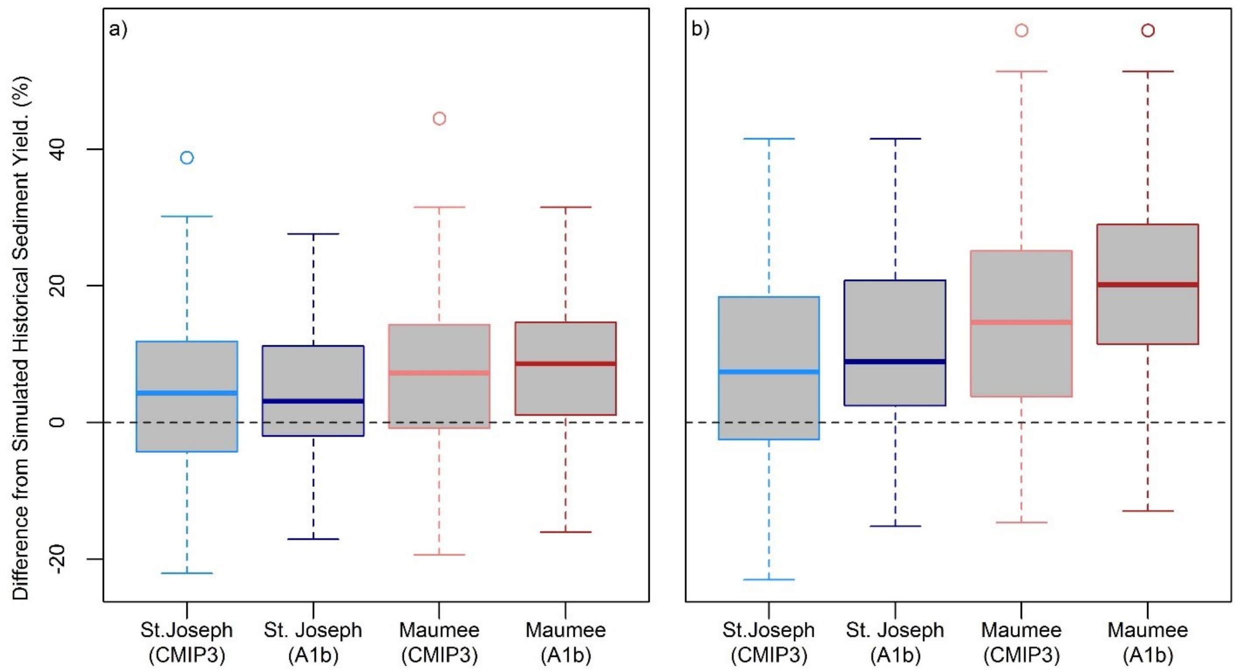

Figure S3.5. Differences in modeled sediment yield between current (1989-2008), and both Contemporary (a, 2011-2030) and Mid-Century (b, 2031-2050) CMIP3 scenarios. CMIP3 indicates all downscaled CMIP3 scenarios while A1b are only those scenarios that used the A1b emissions scenario.

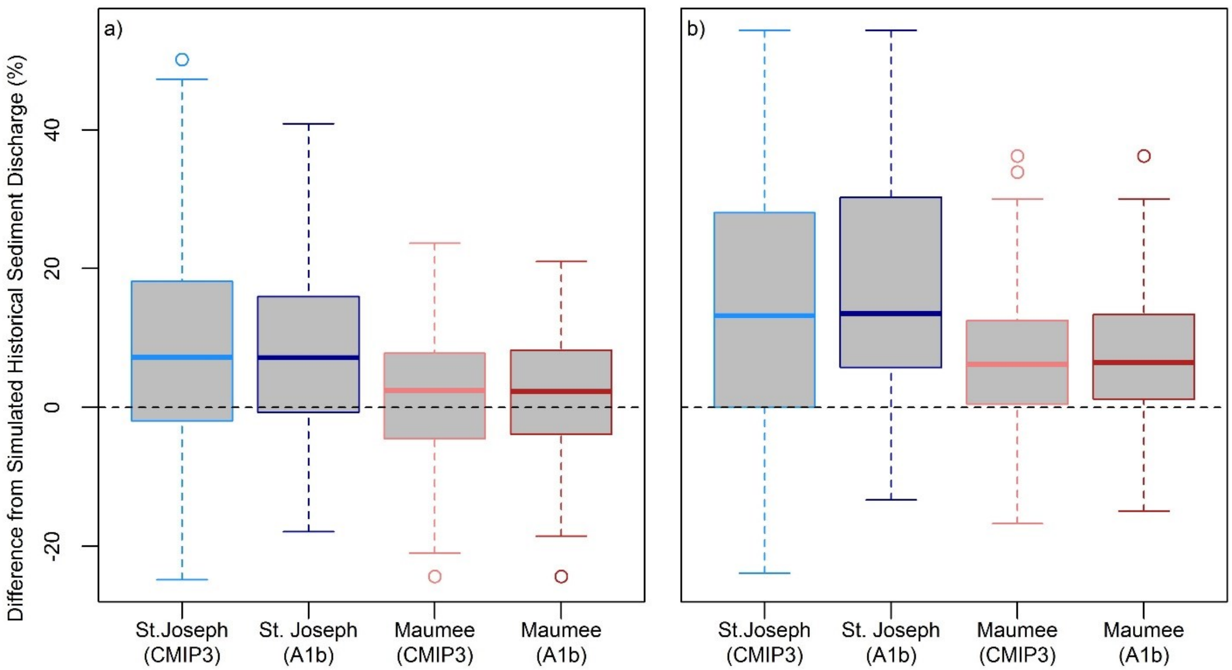

Figure S3.6. Differences in modeled sediment discharge between current (1989-2008), and both Contemporary (a, 2011-2030) and Mid-Century (b, 2031-2050) CMIP3 scenarios. CMIP3 indicates all downscaled CMIP3 scenarios while A1b are only those scenarios that used the A1b emissions scenario.

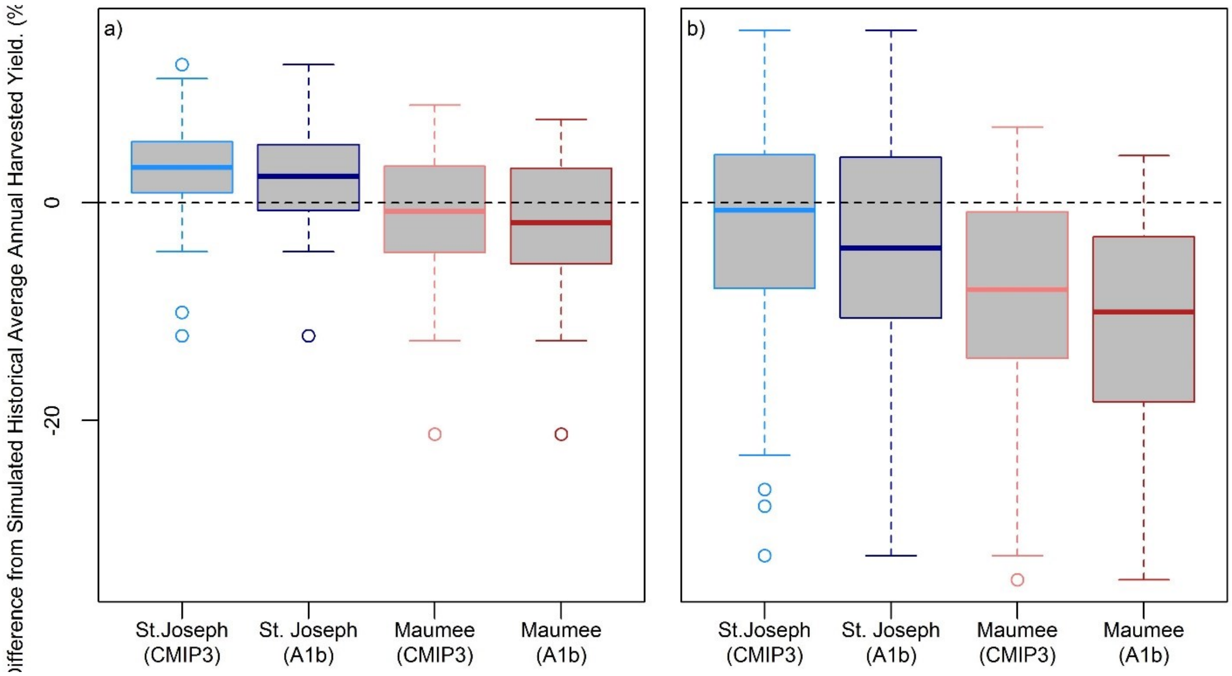

Figure S3.7. Difference in annual harvested yield per hectare estimated by the SWAT models for a) Contemporary (2011-2030) and b) Mid-Century (2031-2050) CMIP3 scenarios. CMIP3 indicates all downscaled CMIP3 scenarios while A1b are only those scenarios that used the A1b emissions scenario.

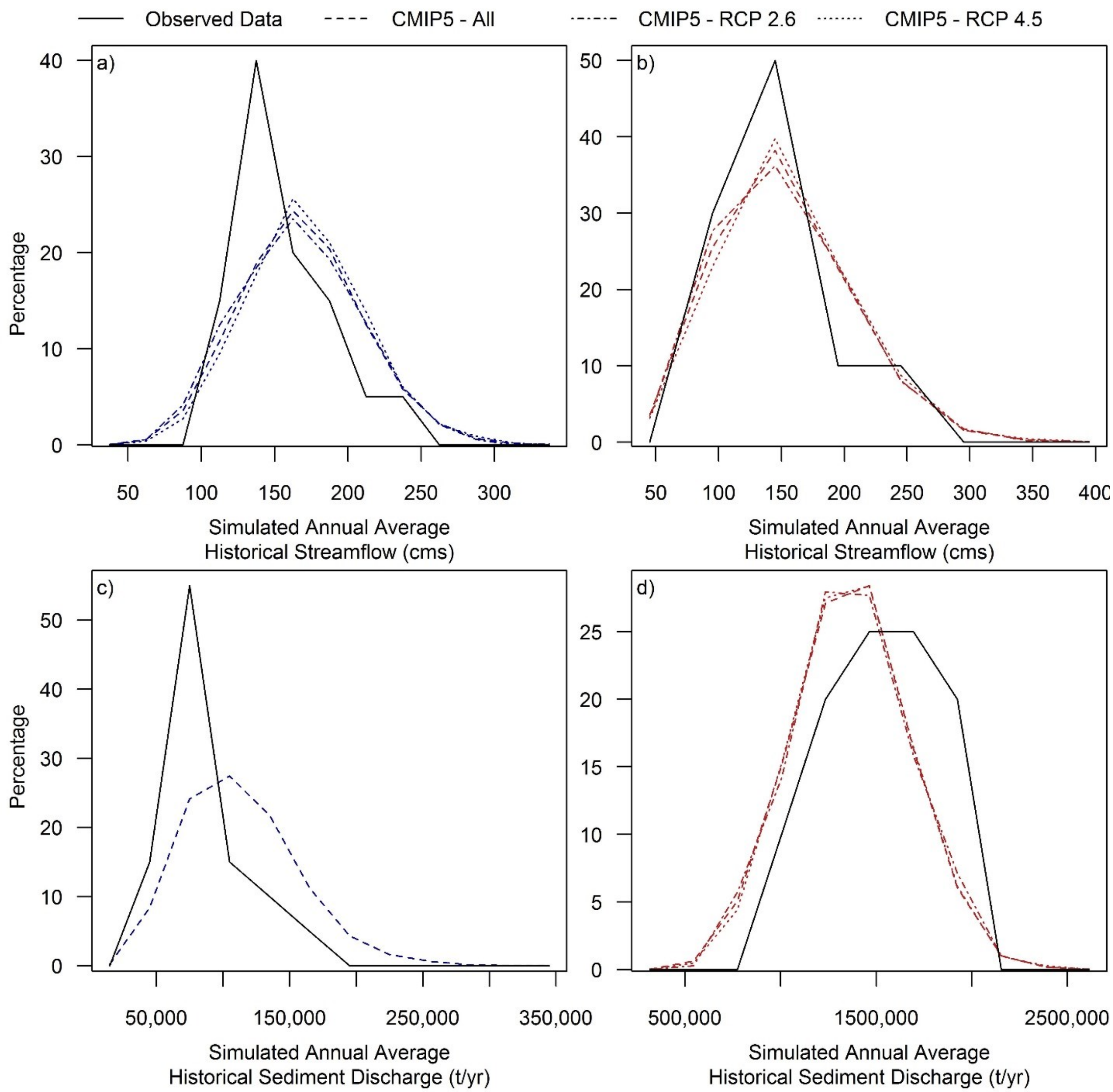

Figure S3.8. Probability density functions for the historical period (1988-2001, 2003-2008) simulated using observed climate data and downscaled climate data from CMIP5: a) annual average streamflow for the St. Joseph River, b) annual average streamflow for the Maumee River, c) annual average sediment discharge for the St. Joseph River, and d) annual average sediment discharge for the Maumee River.

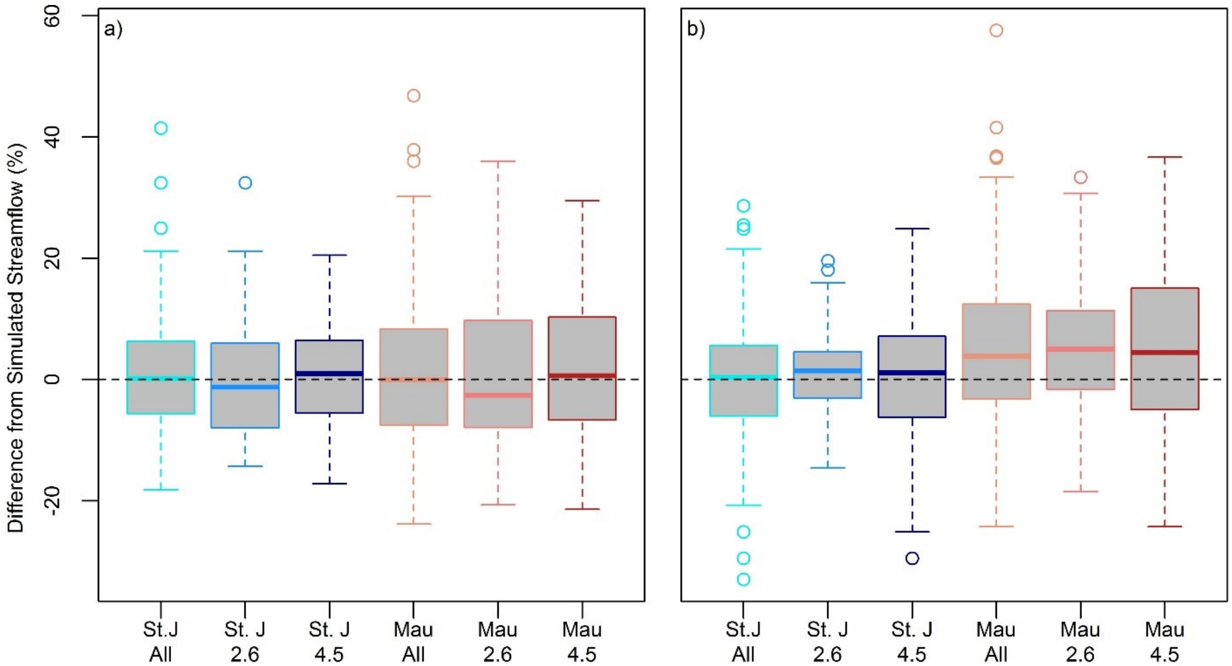

Figure S3.9. Differences in modeled streamflow between current (1989-2008), and both Contemporary (a, 2011-2030) and Mid-Century (b, 2031-2050) CMIP5 scenarios. CMIP5 indicates all downscaled CMIP5 scenarios. 2.6 and 4.5 indicate the RCP 2.6 and 4.5 emissions pathways, respectively.

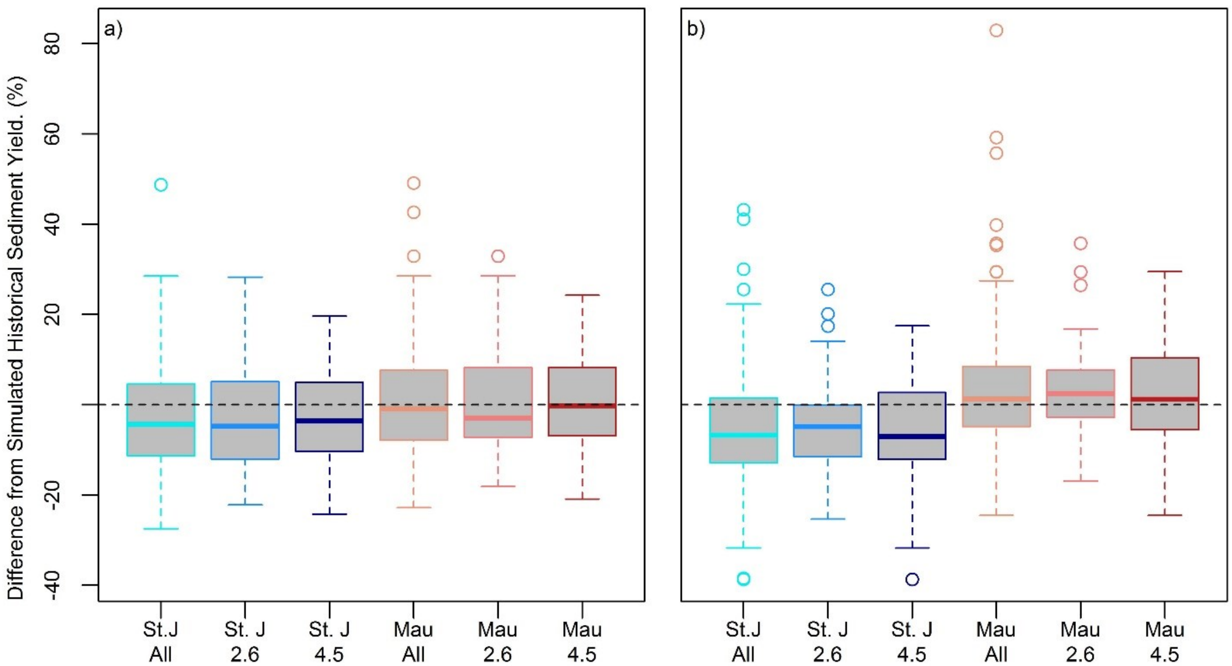

Figure S3.10. Differences in modeled sediment yield between current (1989-2008), and both Contemporary (a, 2011-2030) and Mid-Century (b, 2031-2050) CMIP5 scenarios. CMIP5 indicates all downscaled CMIP5 scenarios. 2.6 and 4.5 indicate the RCP 2.6 and 4.5 emissions pathways, respectively.

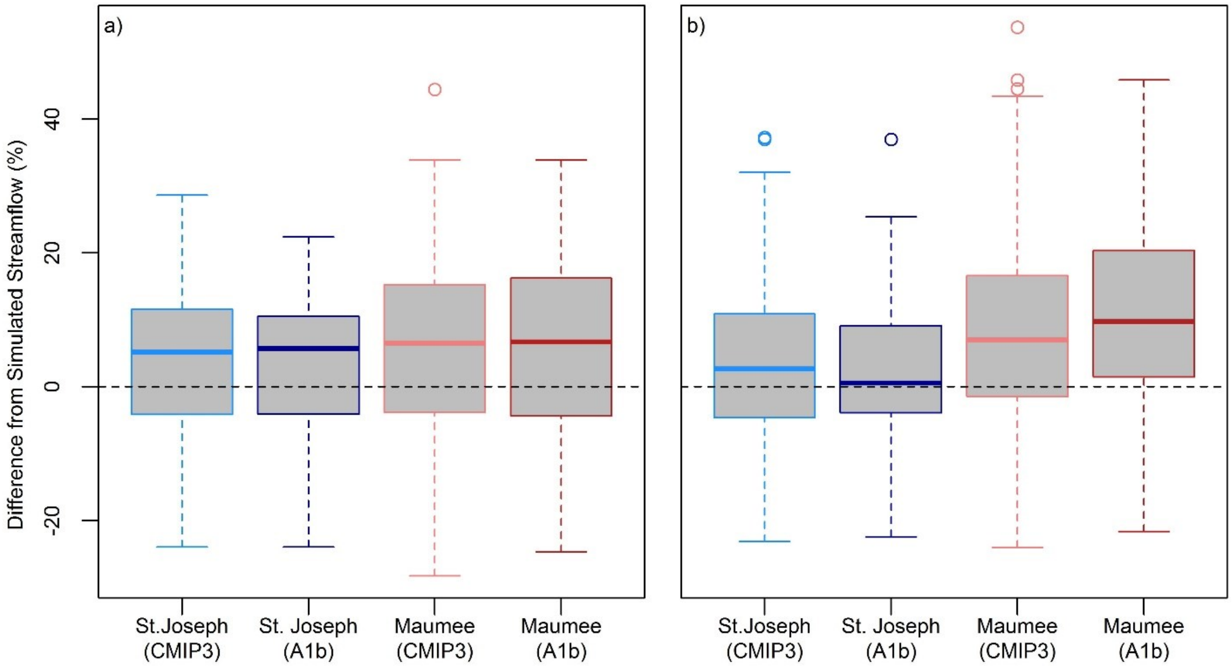

Figure S3.11. Differences in modeled sediment discharge between current (1989-2008), and both Contemporary (a, 2011-2030) and Mid-Century (b, 2031-2050) CMIP5 scenarios. CMIP5 indicates all downscaled CMIP5 scenarios. 2.6 and 4.5 indicate the RCP 2.6 and 4.5 emissions pathways, respectively.

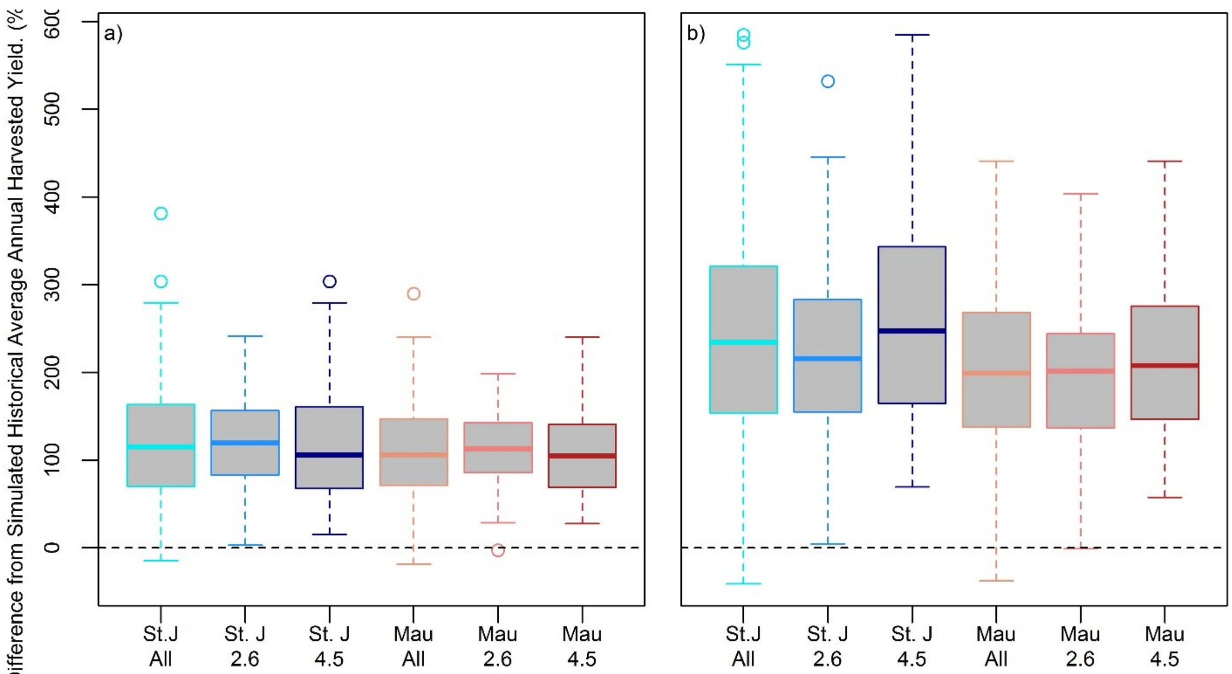

Figure S3.12. Difference in annual harvested yield per hectare estimated by the SWAT models for a) Contemporary (2011-2030) and b) Mid-Century (2031-2050) CMIP5 scenarios. CMIP5 indicates all downscaled CMIP5 scenarios. 2.6 and 4.5 indicate the RCP 2.6 and 4.5 emissions pathways, respectively.

Table S3.1. SWAT model outputs for the Contemporary period (Scenario Years 2011-2030), reported as change from modeled historical (1989-2008) averages.

		St. Joseph		Maumee	
		RCP 6.0	RCP 8.5	RCP 6.0	RCP 8.5
Streamflow (cms)	Lower Quartile	-9.1	-8.6	-11.6	-12.5
	Median	-1.6	-0.1	-0.9	0.2
	Upper Quartile	7.5	9.2	14.2	10.3
Sediment Yield (10^5t/yr)	Lower Quartile	-24.03	-30.02	-88.67	-100.47
	Median	-14.83	-10.17	-13.36	-4.25
	Upper Quartile	8.07	6.13	72.63	77.97
Sediment Discharge (10^5t/yr)	Lower Quartile	-2.55	-3.08	-16.02	-18.77
	Median	-1.39	-0.92	-4.56	-4.80
	Upper Quartile	1.50	0.95	11.86	13.75

Table S3.2. SWAT model outputs for the Mid-Century period (Scenario Years 2031-2050), reported as change from modeled historical averages.

		St. Joseph		Maumee	
		RCP 6.0	RCP 8.5	RCP 6.0	RCP 8.5
Streamflow (cms)	Lower Quartile	-7.6	-13.0	-4.0	-5.3
	Median	-1.1	-0.5	6.1	3.9
	Upper Quartile	6.8	6.3	17.0	16.0
Sediment Yield (10^5t/yr)	Lower Quartile	-27.41	-35.62	-49.10	-64.23
	Median	-16.84	-16.35	16.31	5.45
	Upper Quartile	2.96	3.07	76.54	88.07
Sediment Discharge (10^5t/yr)	Lower Quartile	-3.05	-4.35	2.92	-3.03
	Median	-2.04	-2.13	15.03	7.96
	Upper Quartile	0.78	0.65	23.63	20.07

Table S3.3. Projected median annual dredging cost changes in $000s relative to dredging costs simulated using downscaled CMIP5 historical climate data for 1989-2008. 1:1 Sediment OutflowDischarge:Dredging Cost method is based on 1989-2009.

			Regression		1:1 Sediment Discharge (Based on 1989-2009)	
			Contemporary	Mid-Century	Contemporary	Mid-Century
		Years	2011-2030	2031-2050	2011-2030	2031-2050
St. Joseph Dredging Costs	RCP 6.0	Upper Quartile	95	60	40	19
		Median	-120	-131	-28	-41
		Lower Quartile	-173	-241	-59	-71
	RCP 8.5	Upper Quartile	53	20	20	14
		Median	-50	-159	-20	-46
		Lower Quartile	-187	-297	-60	-85
Maumee Dredging Costs	RCP 6.0	Upper Quartile	33	52	119	242
		Median	11	28	-42	150
		Lower Quartile	-11	3	-159	29
	RCP 8.5	Upper Quartile	43	49	138	198
		Median	14	25	-45	75
		Lower Quartile	-10	-2	-174	-28

CHAPTER 4:
CLIMATE AND HYDROLOGIC ENSEMBLING LEAD TO DIFFERING STREAMFLOW AND SEDIMENT YIELD PREDICTIONS

Abstract

Climate change is leading to alterations of the hydrologic cycle and sediment movement within watersheds, but there are large amounts of uncertainty about the details and impacts of these changes in the future. To reduce this uncertainty, many researchers create ensembles by averaging together the projected temperature and precipitation from multiple global climate model (GCM) ensemble members before running these as forcing inputs through hydrologic and sediment yield models. There is little research on whether these ensembled climate scenarios produce hydrologic model results to those that are representative of the hydrologic results based on individual climate ensemble members. We created multiple sets of ensembled climate inputs for hydrologic and sediment yield models for a pair of adjacent watersheds that drain to the Great Lakes, based on both Representative Concentration Pathway (RCP) 4.5 and RCP 8.5. We then compared the hydrologic and sediment results of a model forced by these ensembled climate scenarios with those hydrologic ensembles created by running the individual climate ensemble members through the same hydrologic models. We found that in all cases the results are significantly different at the 5% confidence level and the ensembled climate scenarios can lead to systematic negative biases in streamflow and sediment yield.

We also looked at three different subset hydrologic ensembles: all 10 CMIP5 ensemble members from the CSIRO mk3.6 model; a Representative ensemble with high, moderate and low precipitation predictions; and a Best Fit ensemble based on GCM performance relative to historic climate. We found that the subset ensembles covered a large portion of the range of outputs for the whole set while producing mean annual streamflow, sediment yield, and sediment discharge results that are within 12.2% of the full hydrologic ensemble results.

1. Introduction

Changes in climate, particularly precipitation and temperature, can cause a wide range of impacts to our environment. Streamflow and sediment movement are particularly susceptible to changes in both magnitude and timing of precipitation. They are also affected by differences in temperature, although less directly. These changes to streamflow and sediment movement through a watershed in turn impact infrastructure, agriculture, and ecosystems.

Many researchers have looked at the potential impacts of climate change on streamflow and sediment, but most limit their modeling efforts to a handful of climate scenarios (e.g., Cherkauer and Sinha, 2010; Johnson et al., 2015; O'Neal et al., 2005; Park et al., 2011; Serpa et al., 2015; Verma et al., 2015). This can be problematic because research has shown there can be a significant difference in streamflows, sediment yield from the landscape, and sediment discharge across climate model ensemble members, even when they are driven by the same forcing conditions (Dahl et al., 2018). One approach to reduce this variability while still minimizing the number of simulations required is to create an ensemble of the climate inputs (Praskievicz, 2016; Shrestha et al., 2012; van Liew et al., 2012), with the implicit assumption that the mean behavior across models is representative of the most likely future conditions.

Ensembled climate inputs are typically created by averaging the precipitation and temperature for a given point in time and space across multiple climate ensemble members. This single ensembled climate is then run through a hydrologic model to produce a future streamflow and sediment discharge prediction (Figure 4.1). It is not clear from the literature whether the streamflow and sediment transport resulting from a single, ensembled climate are the same as if all of the component climate ensemble members were run through the hydrologic model and used to create an ensembled hydrology.

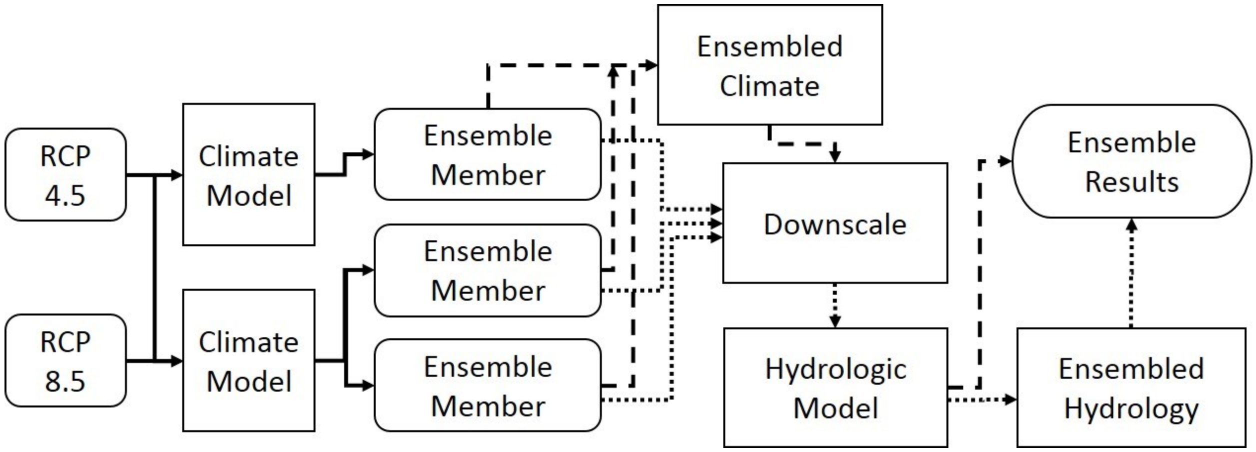

Figure 4.1. In this paper, we focus on two RCPs (4.5 and 8.5). Each of these RCPs was run through multiple climate models, with each climate model having one or more ensemble members provided to the CMIP5. We define ensembled climate scenarios as being an average of selected climate model ensemble members before they are downscaled and run through a hydrologic model (dashed lines). Ensembled hydrology scenarios are ones where the individual climate ensemble members are downscaled and run through the hydrologic model separately before being averaged together (dotted lines).

To directly address this question, we modeled two large, adjacent watersheds in the Great Lakes region using the Soil and Water Assessment Tool (SWAT). We ran these models using both individually downscaled climate model outputs and ensembles of these outputs. We then compared the streamflow, sediment yield, and sediment transport results to determine whether a single climate ensemble run or a subset of the climate ensemble members can be used to accurately represent the climate model effects of all of the available ensemble members.

2. Methods

2.1. Site Description

The Maumee and St. Joseph River watersheds span the lower portion of Michigan, stretching from Lake Erie to Lake Michigan (Figure 4.2). The Maumee watershed covers 17,015 km^2 and is primarily agricultural (74.7% row crops and 5.2% pasture), according to the 2006 National Land Cover Database (Fry et al., 2013). It drains portions of northeastern Indiana, southwestern Michigan, and northwestern Ohio to Lake Erie at Toledo, OH. The mainstem of the Maumee River has United States Geological Survey

(USGS) flow gages at Defiance, OH (#04192500) and further downstream at Waterville, OH (#04193500). The flow at Waterville averaged 172.6 m^3/s between 1990 and 2009 while the average annual suspended sediment load was 1.2 million tonnes between 1990 and 2003.

The St. Joseph River watershed abuts the northwestern edge of the Maumee watershed and extends westward to its outlet at St. Joseph, MI on Lake Michigan. The St. Joseph watershed is smaller (12,138 km^2) and has a lower proportion of agriculture (49.3% row crops, 12.2% pasture) than the Maumee, but more than twice as much forest (23.8% versus 8.2%). The USGS gage at Niles, MI (#04101500) reported average flows of 113.6 m^3/s between 1990 and 2009. There is no long-term sediment gaging at Niles, but a sediment-discharge relationship was developed by the USACE (2007).

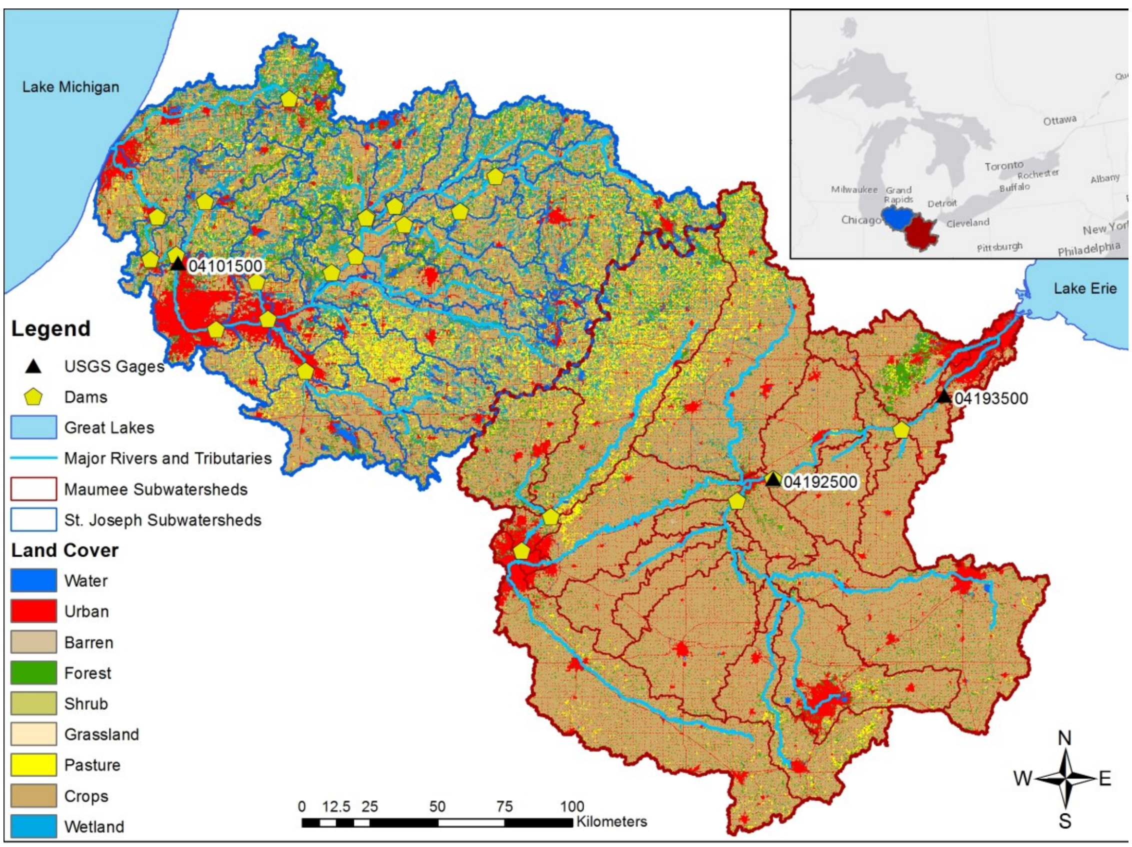

Figure 4.2. The Maumee and St. Joseph River watersheds constitute a contiguous block of land between Lake Erie and Lake Michigan, covering portions of Michigan, Ohio, and Indiana (modified from Dahl et al. (2018)).

2.2. Soil and Water Assessment Tool (SWAT) Models

We used individual SWAT models for each watershed based on 1 arc-second resolution elevation data from the National Elevation Dataset, land use/land cover from the 2006 National Land Cover Database, and soil data from the Natural Resources Conservation Service's Soil Survey Geographic database. Information on dams included in the models was obtained from the National Inventory of Dams maintained by the U.S. Army Corps of Engineers. The development and calibration of these models is more fully described in Dahl et al. (2018). We ran the models using downscaled climate model data for 2010-2099 and used the first 5 years as a warmup period, excluding it from our analysis.

2.3. Climate Data and Downscaling

The Fifth Coupled Model Intercomparison Project (CMIP5; (Taylor et al., 2012)) resulted in at least 234 ensemble members from 37 different climate models. We selected Representative Concentration Pathways (RCP) 4.5 (Masui et al., 2011) and 8.5 (Riahi et al., 2011) because they were both required by the CMIP5 experimental design and therefore had the largest numbers of available ensemble members. We retrieved bias-corrected, statistically downscaled versions of the CMIP5 climate model ensemble members from a dataset created by the United States Bureau of Reclamation and others (Brekke et al., 2013). The archive of downscaled CMIP5 model runs contains 70 complete runs of both RCP 4.5 and 8.5 with precipitation and temperature available on a monthly-basis for the North American Land Data Assimilation (NLDAS) grid. We eliminated seven of the climate ensemble members (access1-3.1.rcp85, fgoals-s2.2.rcp85, fgoals-s2.3.rcp85, noresm1-me.1.rcp85, access1-3.1.rcp45, fgoals-s2.2.rcp45, and noresm1-me.1.rcp45) because they only had average tempertures available and one (hadgem2-es.1.rcp45) because it was missing data from December 2099.

We created four separate climate ensembles for each of the selected RCPs by averaging the precipitation and temperature for all ensemble members at each time step and grid cell. The first pair (RCP 4.5 and RCP 8.5) of climate ensembles used all of the available climate model ensemble members. We then created a pair of climate ensembles based only on the 10 ensemble members submitted from the CSIRO mk3.6 model (Jeffrey et al., 2013), because this submission had the most individual ensemble members of any model in the CMIP5. We generated a third pair of climate ensembles based on a representative subset of climate model ensemble members in an attempt to create a parsimonious representation of the full range of potential climate forcings. Finally, we created a fourth pair of climate ensembles based on the subset of climate model ensemble members that did the best job of matching the historical climate of our study region.

To select climate ensemble members representative of the full range, we first totaled the precipitation for each run both spatially (over the NLDAS grid cells centered on 40.1875°N to 42.4375°N and 86.4375°W to 83.0625°W) and temporally (from 2010 to 2099). The ensemble members were then sorted based on the total precipitation and percentiles were assigned to each run. We then selected one ensemble member each from the top and bottom 10% and three from the middle 20% of total precipitation, choosing the same ensemble member from both RCP 4.5 and RCP 8.5 whenever possible. Additionally, we chose the lowest and highest ranked ensemble members from the CSIRO-mk3-6-0 model, because this submission had the largest number of ensemble members submitted to CMIP5. The selected members of the Representative ensemble are all shown in Table 4-1.

Table 4-1. Climate ensemble members selected for use in the Representative climate ensemble.

RCP 4.5		RCP 8.5	
Ensemble Member	Precipitation %	Ensemble Member	Precipitation %
access1-0.1.rcp45	3%	access1-0.1.rcp85	3%
ccsm4.4.rcp45	45%	csiro-mk3-6-0.10.rcp85	43%
mpi-esm-lr.1.rcp45	51%	mpi-esm-lr.1.rcp85	46%
csiro-mk3-6-0.7.rcp45	55%	ccsm4.4.rcp85	47%
csiro-mk3-6-0.1.rcp45	99%	csiro-mk3-6-0.1.rcp85	93%

The Best Fit ensemble represents the set of climate ensemble members that did the best job in matching the historical climate of the study region. We determined this by summing the precipitation over the study region and averaging the temperature for each ensemble member for 1971-1999 and comparing these results to the actual numbers taken from the NLDAS dataset. We selected all climate ensemble members that were in the most representative quartile for both precipitation and temperature (Table 4-2). Similar to the observation of Knutti et al. (2010), we found that few ensemble members performed well for both temperature and precipitation, despite being bias-corrected to long-term (1961-1990) average temperature and precipitation (Brekke et al., 2013).

We downscaled all selected scenarios using the same methodology as Dahl et al. (2018), which is based on the work of other researchers (Maurer and Hidalgo, 2008; Wood et al., 2004). This method takes the bias-corrected, spatially downscaled data provided by the United States Bureau of Reclamation and disaggregates it spatially to individual gage locations and temporally to daily time steps.

Table 4-2. Climate ensemble members selected for the best fit climate ensemble were chosen based on being in the most accurate quartile for both total precipitation and average temperature over the period 1971-1999.

RCP 4.5			RCP 8.5		
Ensemble Member	Precipitation Percentile	Temperature Percentile	Ensemble Member	Precipitation Percentile	Temperature Percentile
noresm1-m.1.rcp45	6%	15%	noresm1-m.1.rcp85	6%	16%
miroc-esm-chem.1.rcp45	8%	23%	miroc-esm-chem.1.rcp85	8%	23%
hadgem2-es.2.rcp45	13%	7%	hadgem2-es.2.rcp85	11%	7%
mri-cgcm3.1.rcp45	17%	8%	mri-cgcm3.1.rcp85	15%	9%
ccsm4.2.rcp45	25%	21%	ccsm4.2.rcp85	23%	21%
			miroc5.1.rcp85	24%	10%

2.4 Statistical Analysis

We tested the differences between the hydrologic outputs of the ensembled climate and the ensembled hydrologic outputs of the individual climate ensemble members using Analysis of Covariance (ANCOVA). ANCOVA tests for differences in both the slope and y-intercept of regression lines fit to the data. We centered the years by subtracting the mean in order to minimize the effect of the large year values on the slope in the ANCOVA test. We also tested each line for monotonic trends using the Mann-Kendall test. We used a significance level of α = 0.05 for all tests.

3. Results and Discussion

3.1. Streamflow

The mean annual streamflow based on the ensembled climate for the full set of GCM outputs and that from the ensembled hydrology for the same input data are shown in Figure 4.3. This figure also shows the range of all of the individual climate ensemble members. The streamflow for the ensembled climate is significantly different from the ensembled hydrology for the Maumee and St. Joseph Rivers under both RCP 4.5 and RCP 8.5 at the 5% level of confidence. Table S4.1 provides p-values for the ANCOVA tests. These significant differences are all based on the y-intercept and not slope, indicating a constant, systematic, negative bias induced by the ensembled climate. The ensembled climate produces a mean annual streamflow that is 16.2 to 17.7 m^3/s (12.1-13.0%) lower than the ensembled hydrology for the Maumee and 7.1 to 8.2 m^3/s (5.2-6.1%) for the St. Joseph (Table 4-3).

The Maumee River streamflow from the ensembled hydrology has statistically significant upward trends for both RCP 4.5 ($p = 1.7\times10^{-3}$) and RCP 8.5 ($p = 4.78\times10^{-11}$). The ensembled climate streamflow trend is also significant for RCP 8.5 ($p = 8.9\times10^{-7}$) while the trend for RCP 4.5 is just outside of our selected significance range ($p = 0.0524$), indicating that choice of ensembling methodology can affect the detection of projected trends. None of the St. Joseph River streamflows had statistically significant streamflow trends. This disparity is likely due to the difference in land use between the two watersheds. The Maumee has a much higher proportion of agriculture and, as noted by Dahl et al. (2018), this leads to a feedback effect on streamflow under a warming climate. As the climate warms, crops mature and are harvested earlier in the year, reducing the late season transpiration and allowing greater runoff. Increasing crop yields have been noted as a potential effect of climate change previously (Pryor et al., 2014).

The difference between the negative bias of the ensembled climate relative to the ensembled hydrology is likely due to the combination of the non-linear hydrologic processes and a loss of the precipitation signal. Knutti et al. (2010) noted this effect in GCMs and showed that the distribution of precipitation in multi-model ensembles is narrower than any of the individual runs because the differences from average are not co-located in space or time. When the precipitation and temperature differences are translated through the hydrologic model, this effect can be magnified.

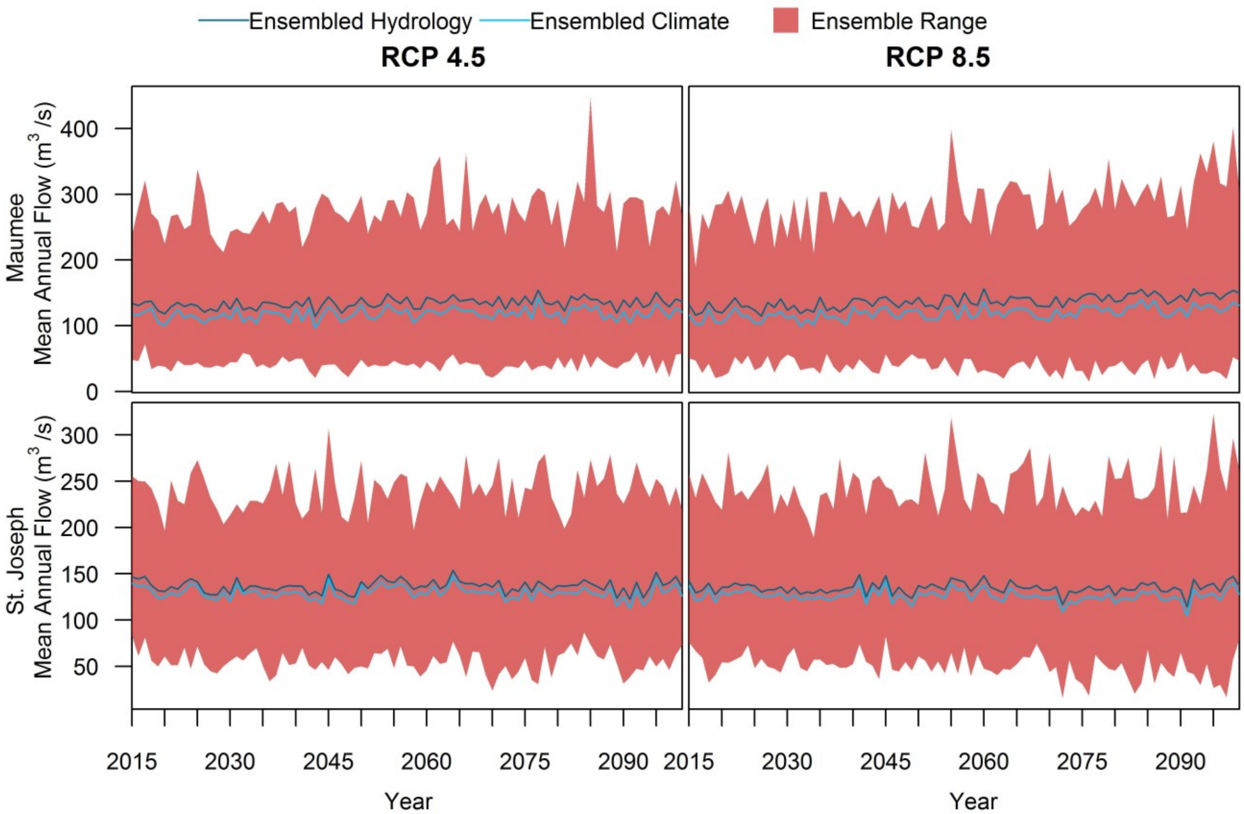

Figure 4.3. The mean annual flow of all the climate ensemble members is greater than the mean annual flow of the ensembled climate run through the same hydrologic model. This is true for both the Maumee (top) and St. Joseph Rivers (bottom) and regardless of RCP. The red shaded area represents the full range of the individual climate runs used to create the ensembled hydrology.

3.2. Sediment Yield

The annual sediment yield produced by the ensembled climate and ensembled hydrology for all GCM outputs are significantly different ($p < 0.05$) for both the St. Joseph and Maumee Rivers (Figure 4.4; Table S4.2). None of the slopes are significantly different between the two ensembling methods, indicating that the difference between the two manifests as a consistent bias, with the ensembled climate resulting in mean annual sediment yields 899,728 to 952,111 tonnes (12.4-14.0%) lower in the Maumee and 8,617 to 10,131 tonnes (10.8-11.2%) lower in the St. Joseph.

All of the ensembled sediment yields have statistically significant, upwards trends with p-values less than 2×10^{-3}. The ensembled climate results in consistently lower sediment yields than the ensembled hydrology. It is interesting to note that both watersheds show large increases in sediment yield towards the end of the century under RCP 8.5. These increases may be the result of earlier crop harvest leaving behind bare ground for longer periods of the year, an effect previously noted by Dahl et al. (2018).

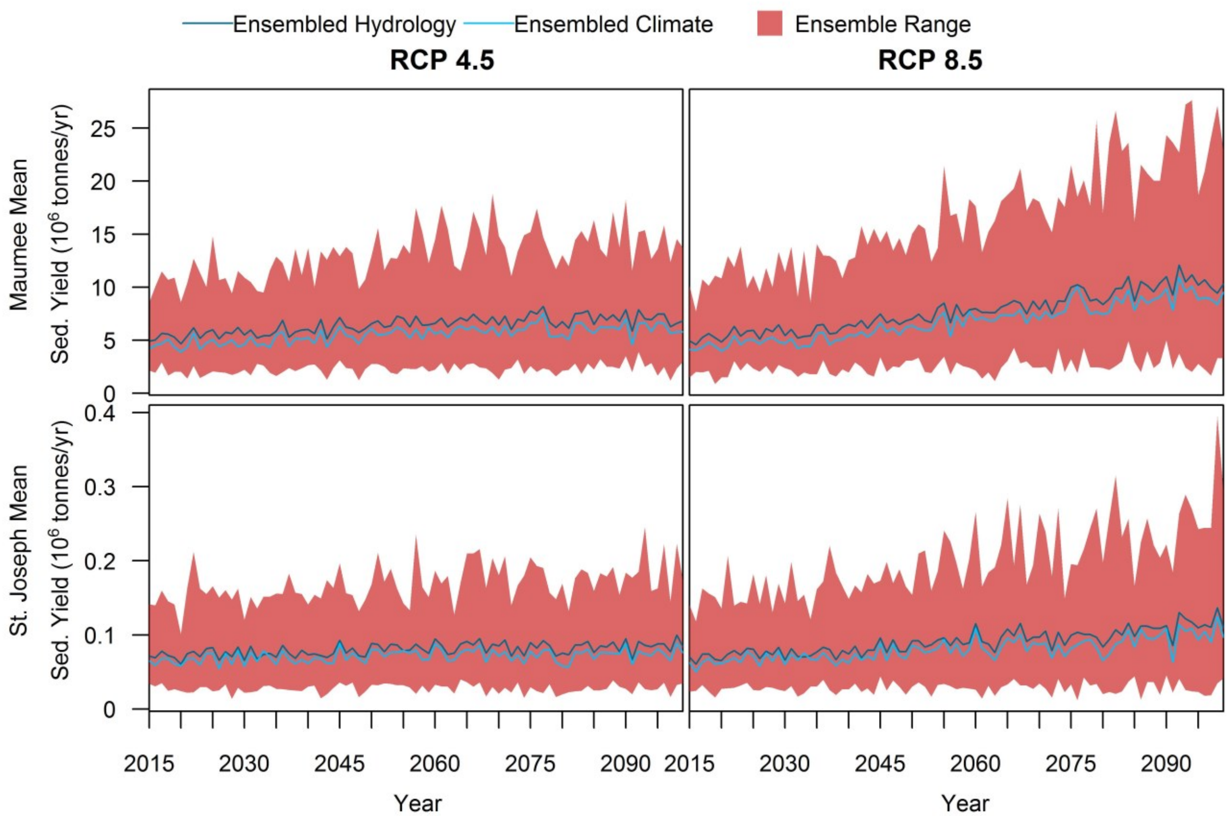

Figure 4.4. The mean amount of sediment delivered to the river each year has statistically significant differences between the ensembled climate and ensembled hydrology approaches. The red shaded area represents the full range of the individual climate runs.

3.3. Sediment Discharge

We report the sediment discharge as the amount of sediment exiting the mouth of the river (Figure 4.5). The ensembled climate and ensembled hydrology for all climate ensemble members produce statistically different sediment discharges ($p < 0.05$) for all watershed and RCP combinations, based on the intercept (Table S4.3). The total annual sediment discharge at the mouth of the St. Joseph River is 1,591 (18.7%) to 1,744 (18.7%) tonnes lower for the ensembled climate than the ensembled hydrology.

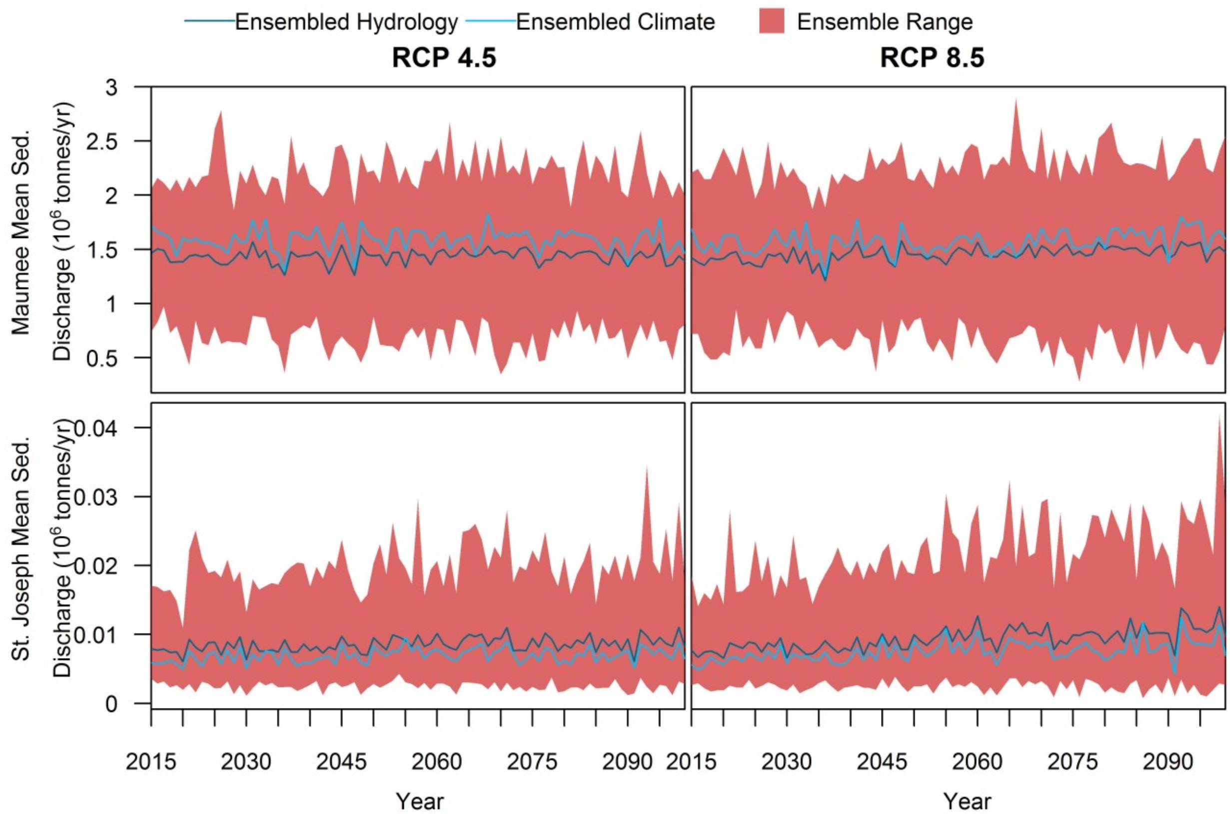

Figure 4.5. Sediment discharge differs between the climate and hydrologic ensembling methods. The direction of this difference varies between the watersheds and depends on the reservoir sediment properties.

The sediment discharge for the Maumee is the one variable we examined where the ensembled climate is greater than the ensembled hydrology. The total annual sediment discharge at the mouth of the Maumee River is 118.5 to 155.4 kilotonnes (8.1-10.8%) higher for the ensembled climate but 1.6 to 1.7 kilotonnes (18.7-18.7%) lower at the mouth of the St. Joseph River. This difference between the two watersheds is caused primarily by the reservoirs in the models and the predominant grain sizes. While all of the reservoirs in both SWAT models are treated as run-of-river, the median grain size (d_{50}) differs between the two watersheds. In the Maumee model reservoirs, the d_{50} is

0.041 mm (coarse silt) and the equilibrium sediment concentration is 1,135 mg/l. Changing these parameters to match those of the St. Joseph model reservoirs (d_{50} = 0.265 mm or fine sand; normal sediment concentration = 335 mg/l) greatly reduces the difference between the ensembled climate and ensembled hydrology results (Figure S4.1). The importance of dams for sediment movement through the Maumee watershed has been previously established. Alighalehbabakhani et al. (2017a) found that Independence dam, the second most downstream dam on the mainstem of the Maumee, had the highest sediment accumulation of the 12 dams they studied across the Great Lakes and their modeling results suggest that the Independence reservoir may already be filled with sediment.

3.4 Effect of Ensemble Member Choice

We created an ensembled climate and ensembled hydrology based on the 10 ensemble members for the CSIRO mk3.6 model (Figure 4.6). The ensembled climate and ensembled hydrology mean annual flows are significantly ($p < 0.05$) different in their y-intercepts, but not their slopes (Table S4.1). The ensembled climate is consistently lower than the ensembled hydrology with differences in the Maumee of 15 to 15.7 m^3/s (10.6-11.2%) and 6.8 to 7.2 m^3/s (4.8 to 5.2%) in the St. Joseph (Table 4-3). All of the Maumee River ensembles and the RCP 4.5 St. Joseph River ensembles have statistically significant increasing trends. The CSIRO mk3.6 ensemble results for sediment yield (Figure S4.2, Table S4.2) and sediment discharge (Figure S4.3, Table S4.3) are similar to those for the ensembles based on the entire range of available climate ensemble members.

It is interesting to note that the range of streamflows of the 10 ensemble members from the CSIRO mk3.6 model span almost the entire range of all the climate ensemble members (Figure 4.6). While all of these ensemble members are from the same global climate model, they were initialized at different times from the control run (Jeffrey et al., 2013), producing significant variability over the duration of the climate change run. Earlier work found that inter-model variability is the largest source of uncertainty in climate change ensemble members (Giorgi and Francisco, 2000a; Giorgi and Francisco, 2000b), but the wide range of streamflow and sediment results produced by the CSIRO mk3.6 ensemble members indicate that may no longer be the case for modern GCMs.

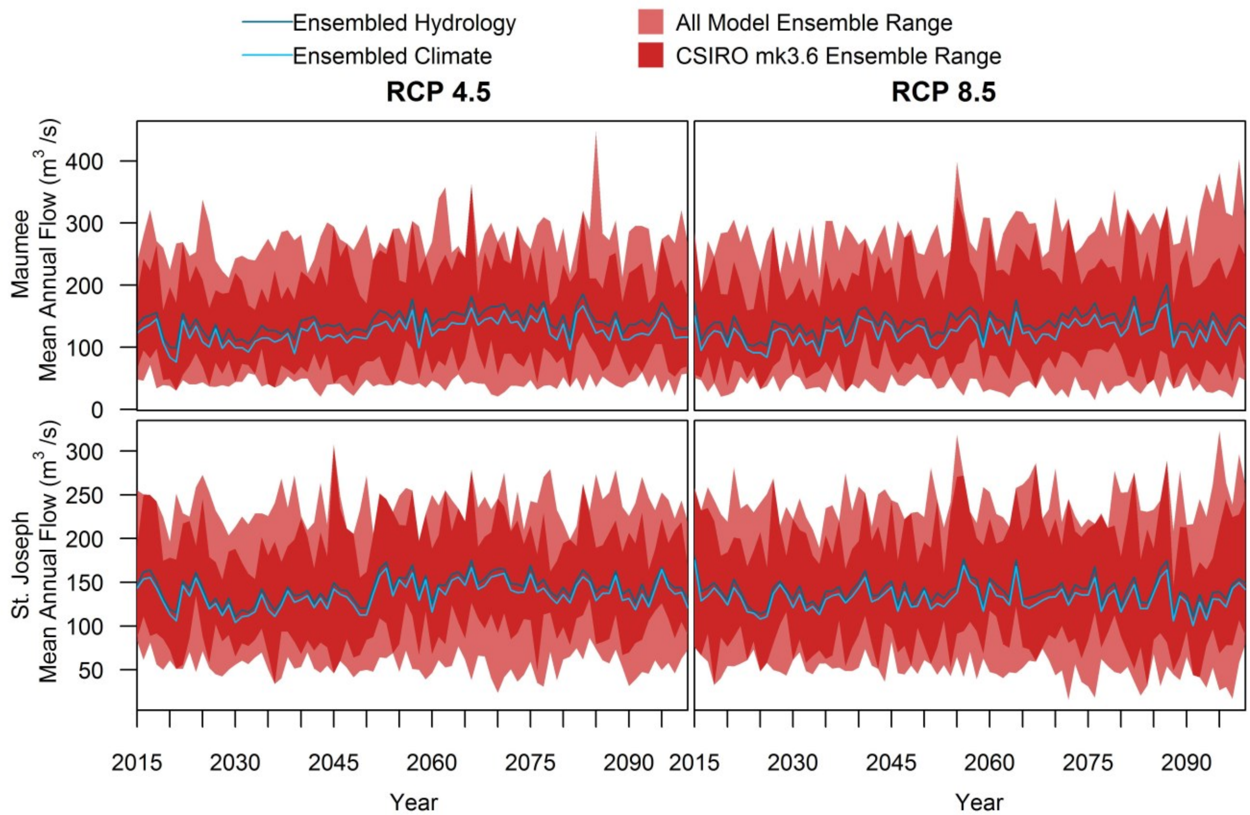

Figure 4.6. The ten ensemble member from the CSIRO mk3.6 model have almost as large a range as all of the available climate ensemble members.

The Representative ensembled climate streamflow is significantly different from the Representative ensembled hydrology across both models and RCPs (Figure 4.7, Table S4.1). This difference is due to the y-intercept and there is no statistically significant difference in slope. The ensembled climate results in streamflows that are 11.6 to 13.3 m^3/s (8.7-9.7%) lower in the Maumee and 6.4 to 6.5 m^3/s (4.75-5.0%) lower in the St. Joseph than the ensembled hydrology (Table 4-3). Both ensembling methods for the Representative climate ensemble members have statistically significant increasing trends for the Maumee River under RCP8.5. The St. Joseph River only has a statistically significant trend for the RCP 8.5 ensembled climate. Even though we selected the ensemble members to be representative, there are very different patterns of statistically significant trends between this method and the ensembles made up of the full suite of climate ensemble members. The impacts of ensembling using representative climate ensemble members on sediment yield and sediment discharge can be seen in Figure S4.4 and Figure S4.5, respectively. The ANCOVA results are available in Table S4.2 and Table S4.3.

Table 4-3. The ensembled climate streamflow is consistently biased lower than from the ensembled hydrology, regardless of the choice of ensemble members.

	RCP	Ensemble Method	Maumee Mean Annual Streamflow (m3/s)	St. Joseph Mean Annual Streamflow (m3/s)
All Members	4.5	Hydrology	134.0	136.7
		Climate	117.8	129.7
	8.5	Hydrology	136.8	134.7
		Climate	119.1	126.4
CSIRO mk3.6	4.5	Hydrology	140.9	143.2
		Climate	125.9	136.4
	8.5	Hydrology	139.9	139.8
		Climate	124.3	132.6
Representative	4.5	Hydrology	136.8	138.0
		Climate	123.5	131.6
	8.5	Hydrology	133.4	130.7
		Climate	121.8	124.2
Best Fit	4.5	Hydrology	134.7	134.8
		Climate	121.1	128.5
	8.5	Hydrology	143.2	137.5
		Climate	128.0	130.1

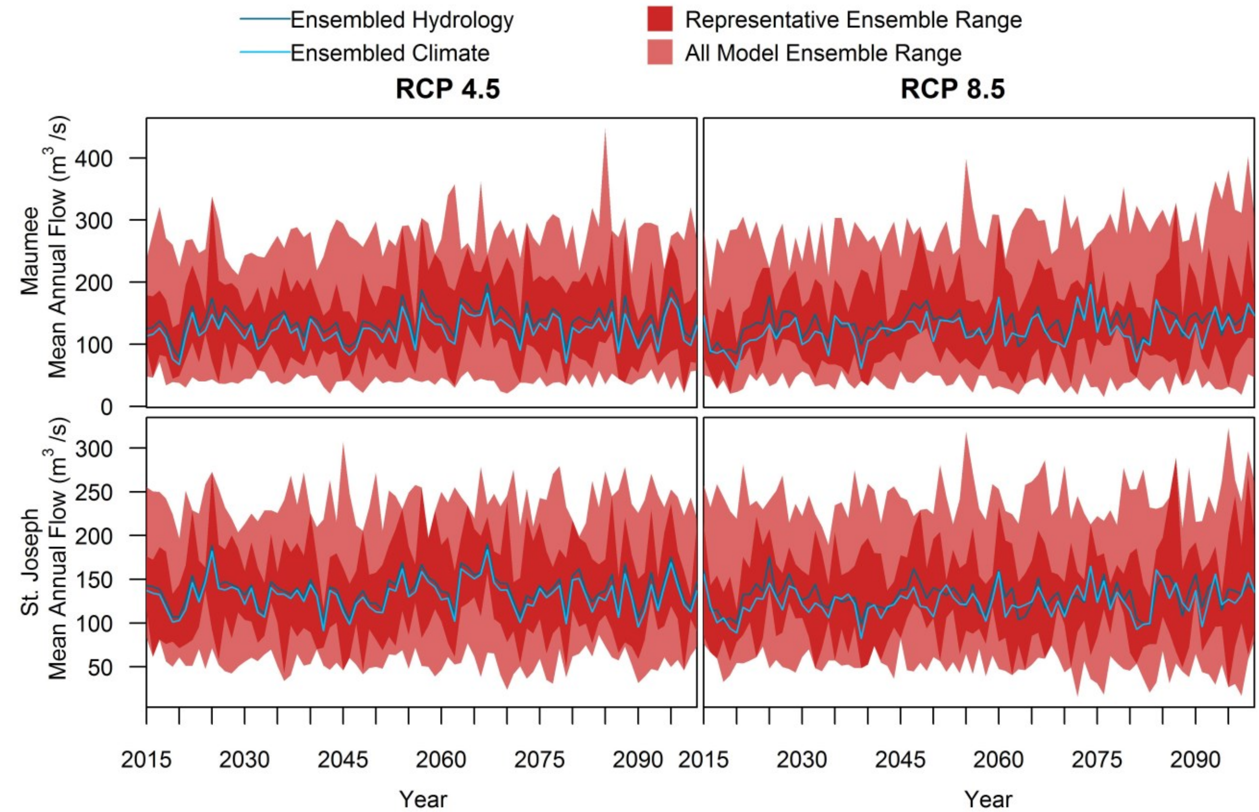

Figure 4.7. The ensemble of a small number of representative climate model ensemble members does not capture the full range of variability and suffers from the same bias between ensembled climate and ensembled hydrology.

The Best Fit ensembles behaved similarly to the Representative ensembles (Figure 4.8). Again, the streamflow associated with the ensembled climate was lower than the ensembled hydrology and significantly different in intercept but not slope (Table 4-3, Table S4.1). The ensembled climate mean annual streamflow was 13.6 to 15.3 m^3/s (10.1-10.7%) lower in the Maumee and 6.3 to 7.4 m^3/s (4.7-5.4%) lower in the St. Joseph than the streamflow for the ensembled hydrology. In spite of these ensemble members being among the best at matching the historic climate, they still account for some of the most extreme streamflow in the all model ensemble and cover a large portion of the range of results. This is not surprising because GCMs that perform well for historic climate can produce divergent outputs under future climate scenarios (Knutti et al., 2010).

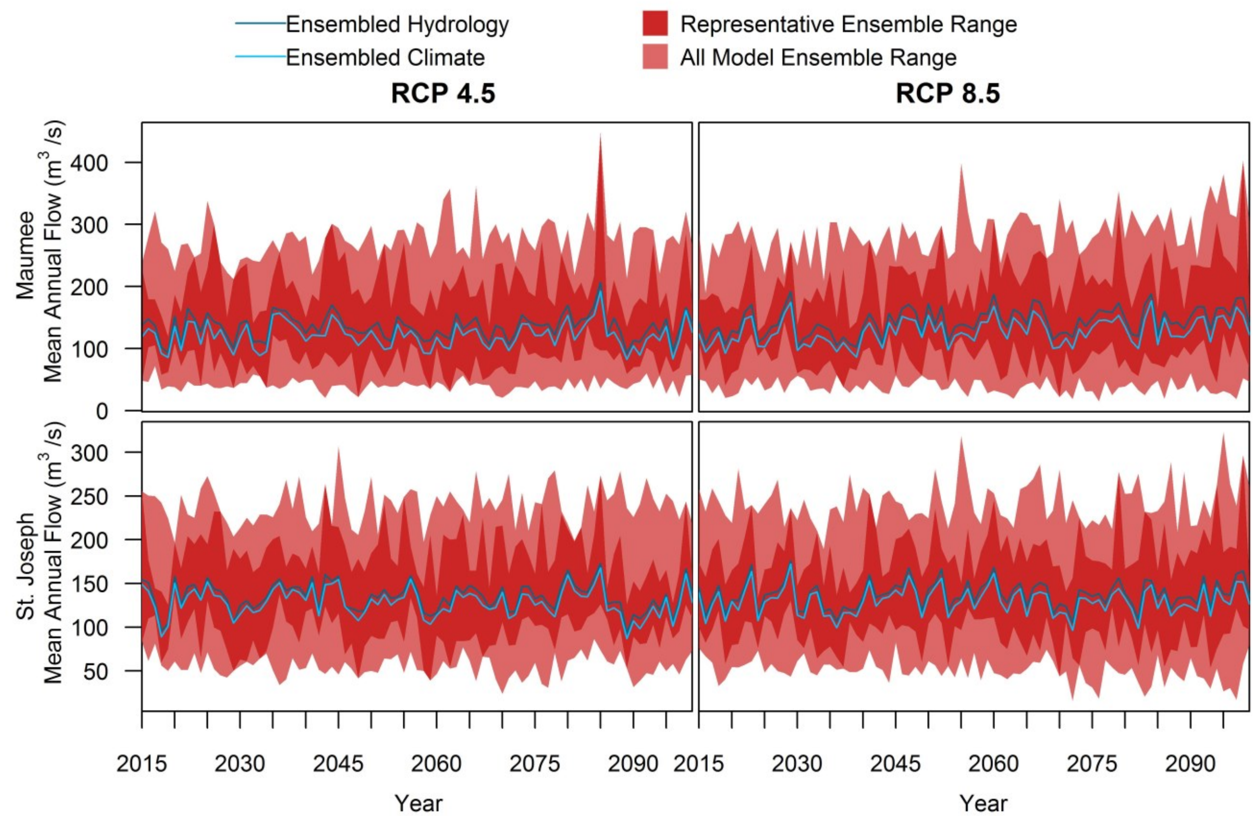

Figure 4.8. The Best Fit Ensemble, based on the climate model ensemble members that most closely match historical climate results, is still susceptible to differences between ensembled hydrology and ensembled climate.

These results clearly show that the ensembled climate and ensembled hydrology do not produce the same results. Since many studies have limited computational resources, there are likely to be questions about which, if any, of the ensemble subsets (e.g., CSIRO mk3.6, Representative, or Best Fit) should be used. When we compare the results for the three ensemble subsets presented here to the results from the full set of ensemble members, the mean streamflows are all within 5% (Table 4-4). The mean Representative ensemble streamflow, sediment yield, and sediment discharge are all within 3% of the ensembled hydrology for the full set of GCM outputs. Based on these results, we suggest that researchers looking to mimic the full range of ensemble members with a limited subset should consider something akin to our Representative ensemble where a limited subset of high, average, and low precipitation scenarios are combined.

Table 4-4. The three different subset ensembles all produce similar results to the full set of ensembles. Here we show the difference from the mean ensembled hydrology for all GCM outputs.

		Streamflow		Sediment Yield		Sediment Discharge	
	RCP	Maumee	St. Joseph	Maumee	St. Joseph	Maumee	St. Joseph
CSIRO mk3.6	4.5	+5.2%	+4.7%	+9.5%	+11.3%	+3.9%	+12.2%
	8.5	+2.3%	+3.8%	+5.0%	+7.5%	+3.4%	+7.8%
Representative	4.5	+2.1%	+1.0%	+2.1%	+2.5%	+1.9%	+1.9%
	8.5	-2.5%	-2.9%	+0.8%	+0.0%	-1.3%	-0.8%
Best Fit	4.5	+0.5%	-1.4%	+1.1%	-0.9%	+0.5%	-2.0%
	8.5	+4.7%	+2.1%	+7.0%	+2.8%	+2.3%	+3.3%

Comparing the subset ensembles to the full ensemble raises some philosophical questions about what the correct ensemble is. A common assumption in climate change studies is that climate models that predict the past well will continue to do so in the future. This is far from certain, because climate models that agree on historical conditions often diverge for future predictions (Knutti et al., 2010; Pierce et al., 2009). The Reliability Ensemble Averaging (REA) technique (Giorgi and Mearns, 2002) attempts to address this by assigning weights based on both historical accuracy and how close they are to the mean of all future model predictions. The REA method reduces the weight of outliers, implicitly assuming that they are much less likely to occur and may be the product of a flawed model. In contrast, our Representative ensemble equally weights all of the ensemble members based solely on historical accuracy. We suggest that if the purpose of a study is to look at the potential range of hydrologic and sediment impacts that may occur, a Representative ensemble is a good surrogate for the full range of climate ensemble members.

4. Conclusions

The use of an ensembled climate scenario as the input to a hydrologic model biases the result relative to the ensembled hydrologic output based on the individual climate ensemble members, producing results that are significantly different ($p < 0.05$). This is most likely due to the loss of the precipitation signal that is offset temporally and spatially in the individual ensemble members. When possible, ensembling should be done using the outputs of hydrological models rather than their inputs. Avoiding or acknowledging the potential for biasing the results will help scientists and policy makers formulate better responses to the changing climate.

It is often necessary to use an ensembled climate or a limited number of climate runs due to computational limitations or time constraints, but it is important to do so in an informed manner. In this paper we have shown that it is possible to capture a significant amount of the range of all climate ensemble members using only a limited number (5-10) of members. Selection of the ensemble members to encompass the full range of temperature and precipitation can result in a parsimonious ensemble that produces mean annual hydrologic and sediment model results similar to the full suite of potential ensemble members. The selection of the particular ensemble members deserves further study and should consider whether the goal is to achieve a consistent mean or account for the likely range of future scenarios.

Acknowledgements

This chapter was co-authored by Anthony Kendall and David Hyndman. Sherry Martin provided additional insight and feedback. Portions of this work were funded by a U.S. Army Corps of Engineers (USACE) Institute of Water Resources (IWR) Responses to Climate Change Pilot Project, USDA NIFA Water CAP grant 2015-68007-23133, and a Food Energy and Water supplement to the KBS LTER project, NSF grant #1637653. Any opinions, findings, conclusions, or recommendations expressed in this material are those of the authors and do not necessarily reflect the views of the USACE, the National Science Foundation or the USDA National Institute of Food and Agriculture.

We acknowledge the World Climate Research Programme's Working Group on Coupled Modelling, which is responsible for CMIP, and we thank the climate modeling groups for producing and making available their model output. For CMIP the U.S.

Department of Energy's Program for Climate Model Diagnosis and Intercomparison provides coordinating support and led development of software infrastructure in partnership with the Global Organization for Earth System Science Portals.

APPENDIX

Table S4.1. ANCOVA tests for streamflow show that the ensembled climate is significantly ($p < 0.05$) different from the ensembled hydrology in all cases, based on the intercept. None of the slopes are significantly different.

			Maumee		St. Joe	
		Ensemble	ANCOVA		ANCOVA	
	RCP	Method	Slope	Intercept	Slope	Intercept
All Members	4.5	Hydrology Climate	5.50E-01	5.54E-27	4.79E-01	1.64E-10
	8.5	Hydrology Climate	6.01E-02	5.35E-25	2.61E-01	5.35E-25
CSIRO mk3.6	4.5	Hydrology Climate	7.92E-01	1.31E-07	8.55E-01	2.87E-03
	8.5	Hydrology Climate	8.22E-01	5.64E-08	8.29E-01	5.64E-08
Representative	4.5	Hydrology Climate	8.73E-01	3.21E-04	8.10E-01	2.61E-02
	8.5	Hydrology Climate	5.83E-01	1.01E-03	4.16E-01	1.01E-03
Best Fit	4.5	Hydrology Climate	9.85E-01	2.56E-05	7.97E-01	1.32E-02
	8.5	Hydrology Climate	6.35E-01	3.36E-06	6.29E-01	3.36E-06

Table S4.2. ANCOVA tests on the mean annual sediment yield demonstrate that the ensembled climate is significantly ($p < 0.05$) than the ensembled hydrology in intercept but not slope, for all cases.

			Maumee		St. Joe	
		Ensemble	ANCOVA		ANCOVA	
	RCP	Method	Slope	Intercept	Slope	Intercept
All Members	4.5	Hydrology Climate	5.56E-01	7.30E-21	2.34E-01	6.02E-12
	8.5	Hydrology Climate	2.92E-01	2.19E-18	9.72E-02	2.19E-18
CSIRO mk3.6	4.5	Hydrology Climate	8.30E-01	2.21E-07	4.20E-01	9.63E-05
	8.5	Hydrology Climate	9.33E-01	2.72E-07	4.86E-01	2.72E-07
Representative	4.5	Hydrology Climate	8.31E-01	5.94E-05	7.99E-01	7.44E-03
	8.5	Hydrology Climate	5.05E-01	1.64E-03	5.90E-01	1.64E-03
Best Fit	4.5	Hydrology Climate	9.44E-01	1.39E-07	9.96E-01	9.88E-05
	8.5	Hydrology Climate	8.22E-01	9.21E-06	3.80E-01	9.21E-06

Table S4.3. ANCOVA tests on the mean total annual sediment discharge show that the ensembled climate is significantly ($p < 0.05$) different from the ensembled hydrology for all cases. This difference manifests in the intercepts but not the slopes.

			Maumee		St. Joe	
		Ensemble	ANCOVA		ANCOVA	
	RCP	Method	Slope	Intercept	Slope	Intercept
All Members	4.5	Hydrology Climate	4.27E-01	2.23E-24	5.13E-01	1.29E-19
	8.5	Hydrology Climate	6.90E-01	4.42E-17	1.25E-01	4.42E-17
CSIRO mk3.6	4.5	Hydrology Climate	8.32E-01	1.53E-10	5.36E-01	1.00E-08
	8.5	Hydrology Climate	7.70E-01	2.65E-06	7.69E-01	2.65E-06
Representative	4.5	Hydrology Climate	7.54E-01	2.07E-03	9.76E-01	1.75E-05
	8.5	Hydrology Climate	2.25E-01	9.64E-05	5.09E-01	9.64E-05
Best Fit	4.5	Hydrology Climate	3.38E-01	4.39E-05	4.26E-01	1.82E-07
	8.5	Hydrology Climate	1.05E-01	1.52E-04	4.40E-01	1.52E-04

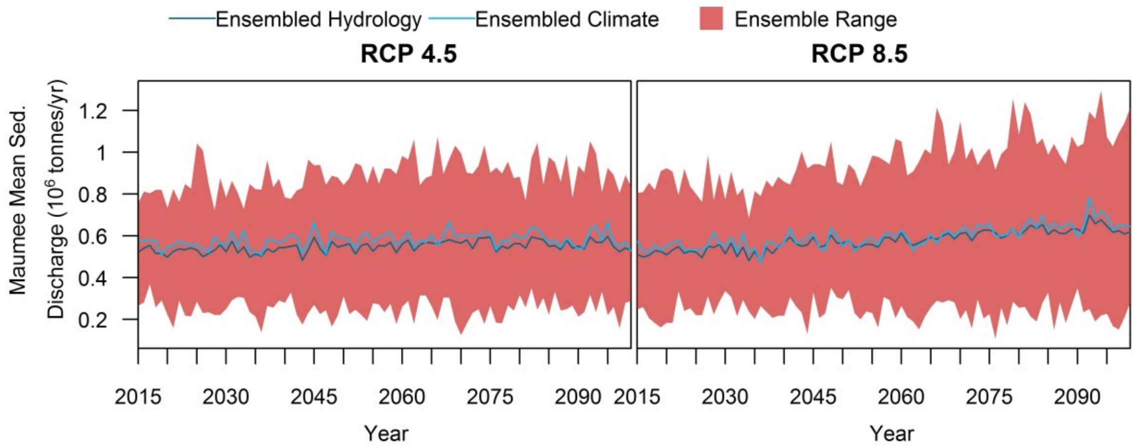

Figure S4.1. The reservoir sediment processes play an important role in sediment discharge, particularly under climate change. Increasing the reservoir sediment d_{50} and normal concentration for the Maumee model to match those used for the St. Joseph River reservoirs causes the ensembled hydrology and ensembled climate to approach each other.

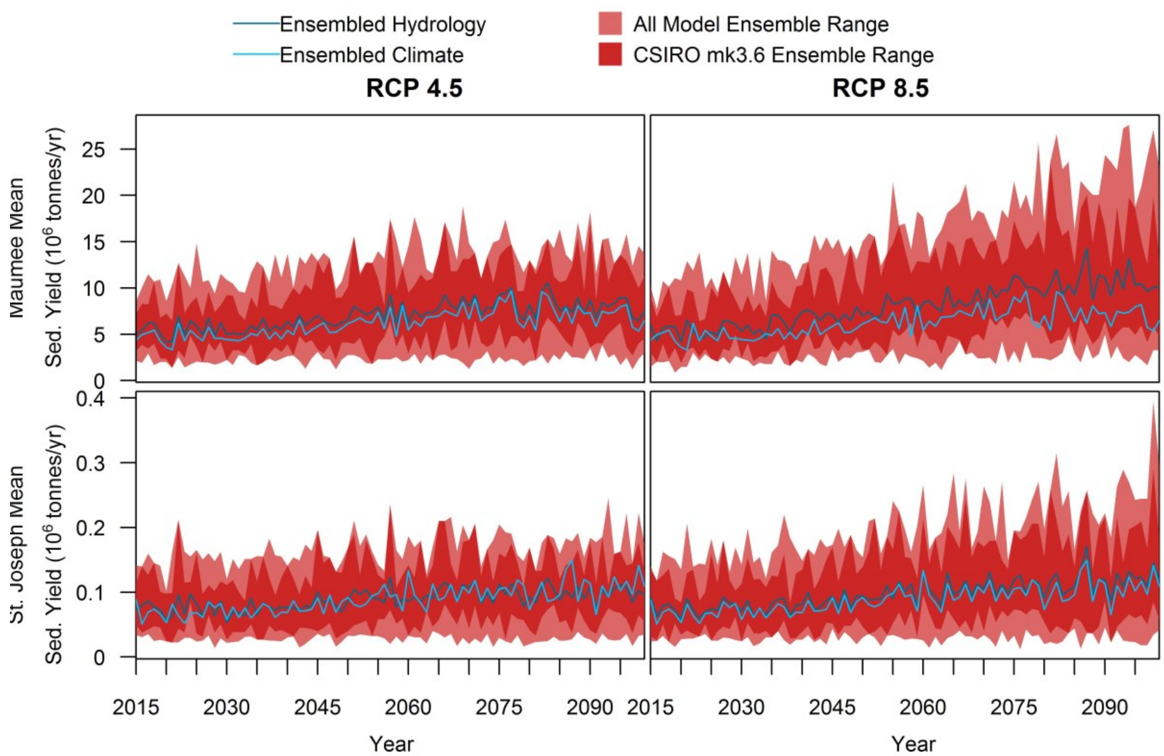

Figure S4.2. Sediment yields based on climate inputs from the CSIRO mk3.6 global climate model.

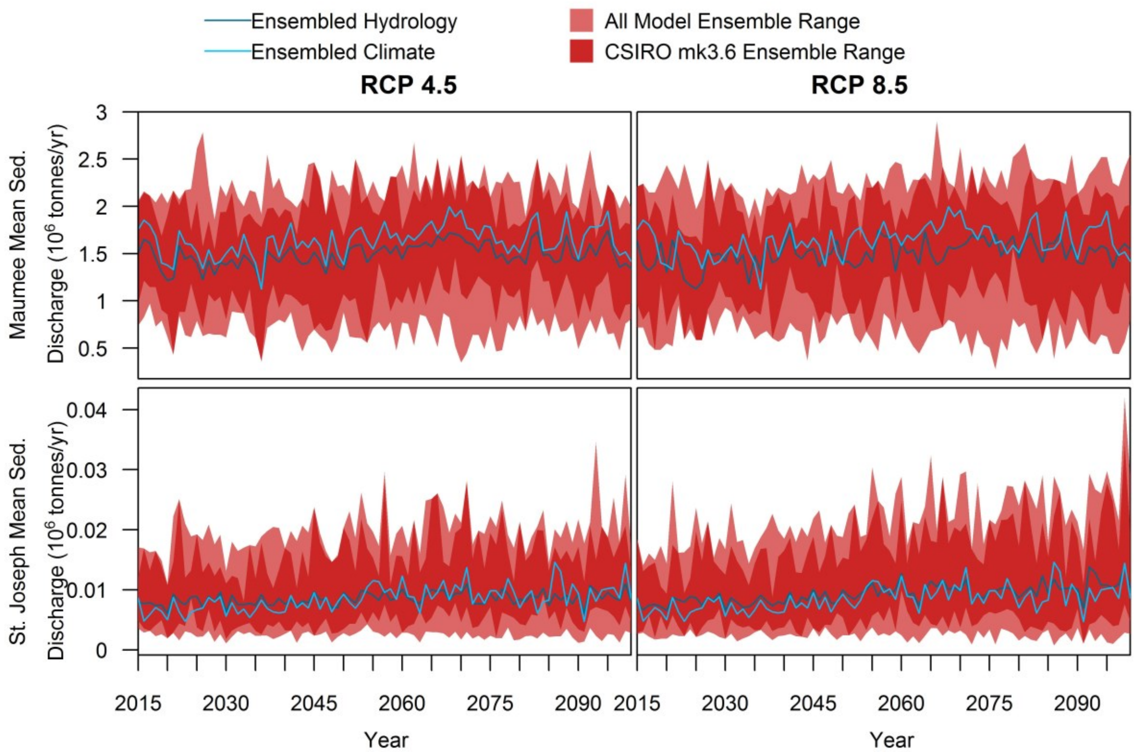

Figure S4.3. Sediment discharge based on climate inputs from the CSIRO mk3.6 global climate model.

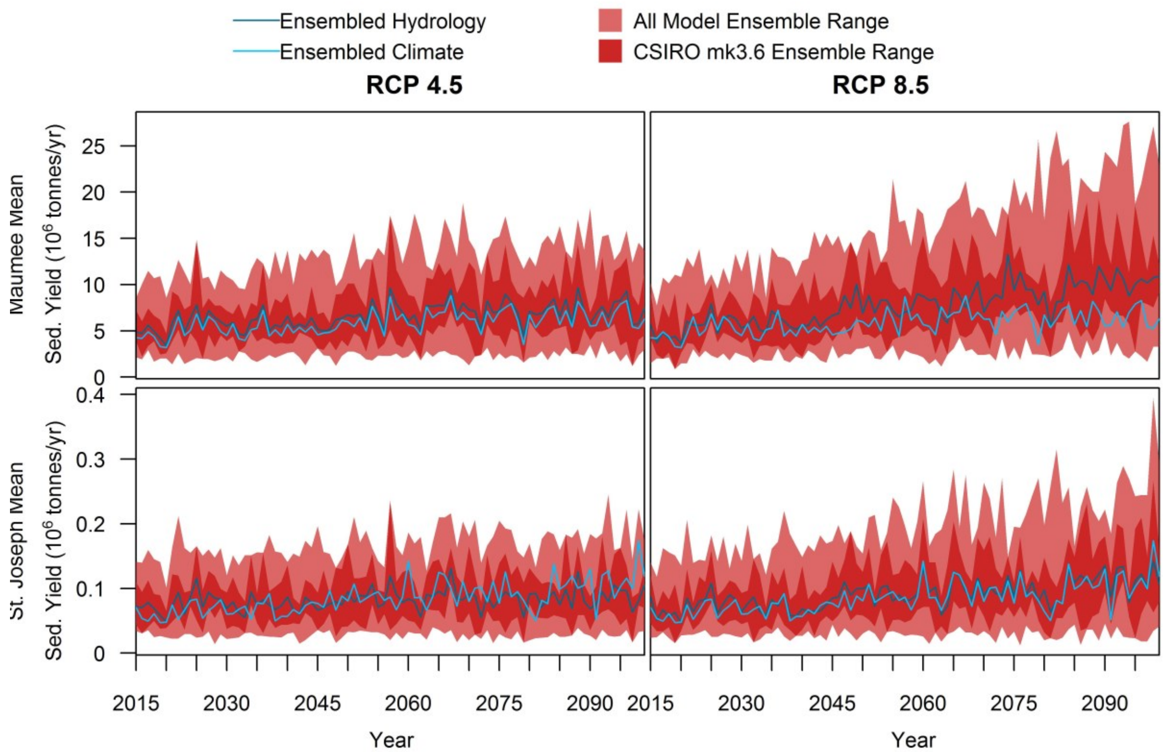

Figure S4.4. Sediment yields based on climate inputs from a representative selection of available climate ensemble members.

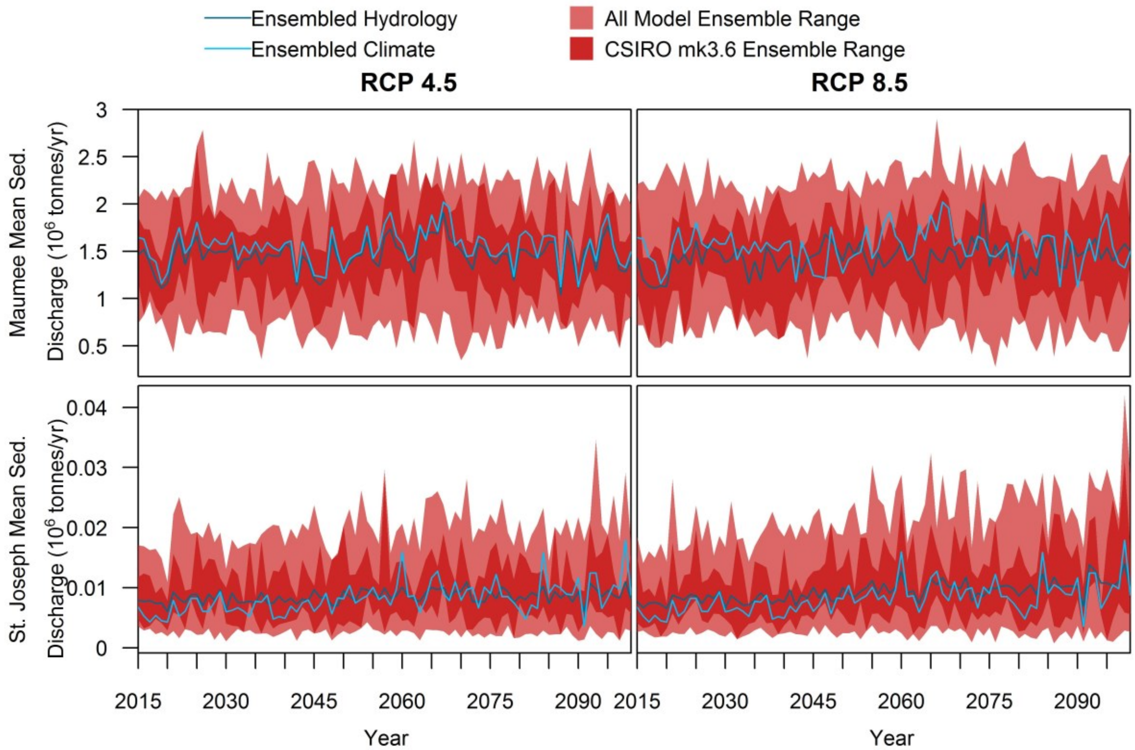

Figure S4.5. Sediment discharge based on climate inputs from a representative selection of available climate ensemble members.

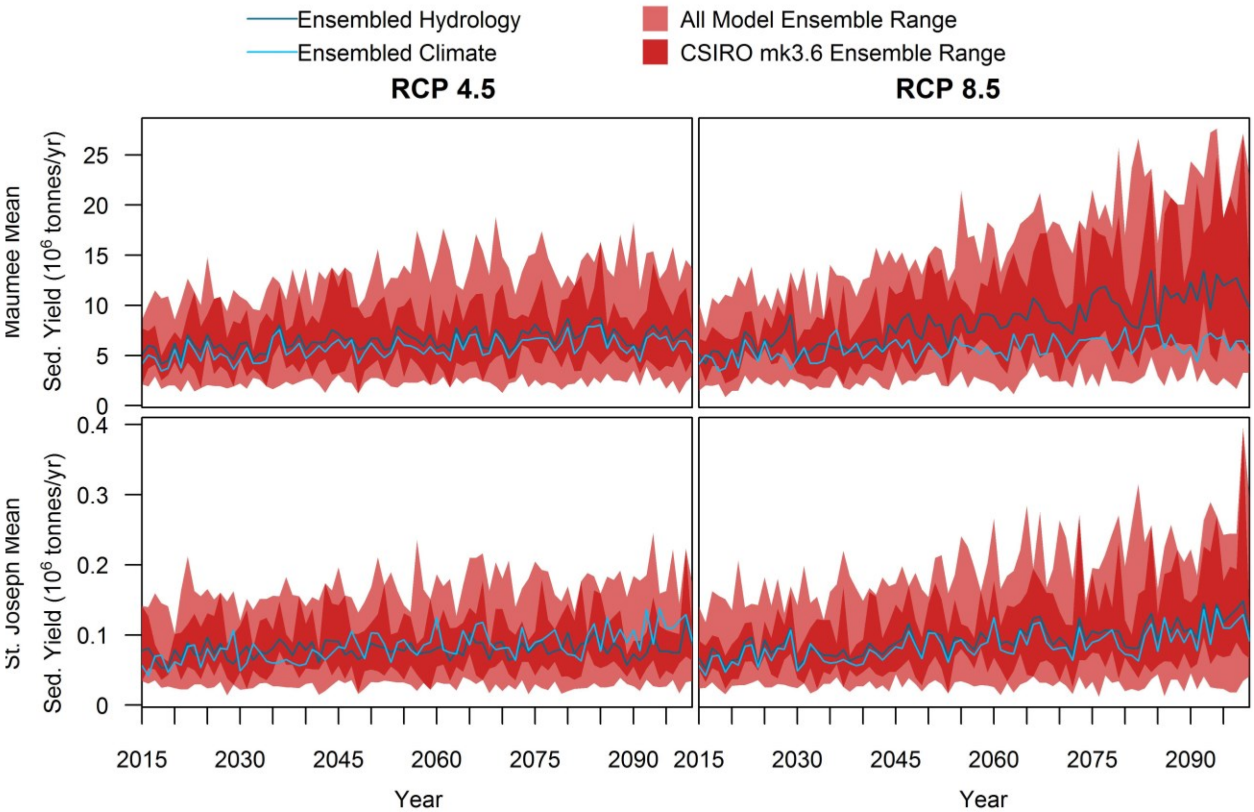

Figure S 4.6. Sediment yields based on climate inputs from the best fit climate ensemble members.

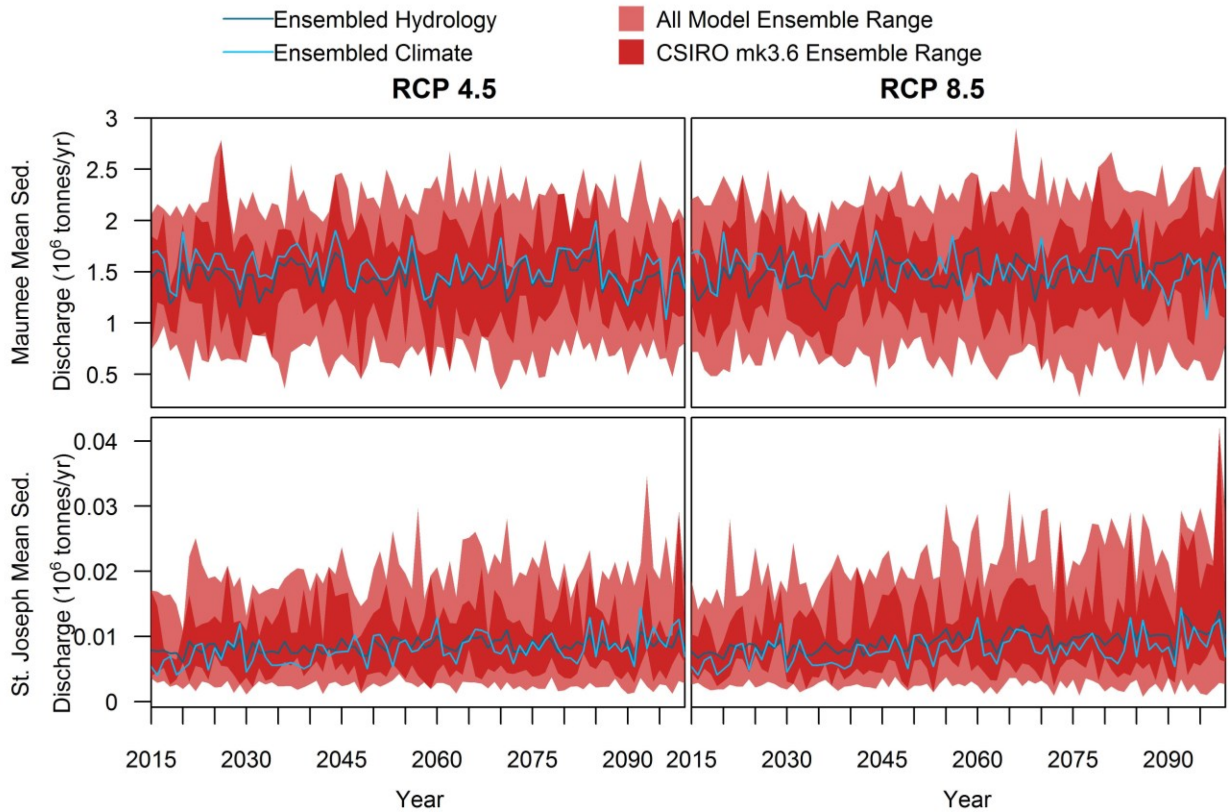

Figure S 4.7. Sediment discharge based on climate inputs from the best fit climate ensemble members.

Table S4.4. The ensembled climate sediment yield is consistently biased lower than the ensembled hydrology, regardless of the choice of ensemble members.

	RCP	Ensemble Method	Maumee Total Annual Sediment Yield (tonnes)	St. Joseph Total Annual Sediment Yield (tonnes)
All Members	4.5	Hydrology	6,434,215	80,081
		Climate	5,534,487	71,464
	8.5	Hydrology	7,699,588	90,527
		Climate	6,747,477	80,397
CSIRO mk3.6	4.5	Hydrology	7,044,665	89,116
		Climate	6,214,455	81,784
	8.5	Hydrology	8,085,969	97,351
		Climate	7,250,606	88,792
Representative	4.5	Hydrology	6,570,391	82,052
		Climate	5,865,431	76,019
	8.5	Hydrology	7,757,722	90,552
		Climate	7,113,726	85,084
Best Fit	4.5	Hydrology	6,506,819	79,372
		Climate	5,749,773	72,359
	8.5	Hydrology	8,239,787	93,046
		Climate	7,372,572	84,225

Table S4.5. The ensembled climate sediment discharge is consistently biased lower than the ensembled hydrology for the St. Joseph River, regardless of the choice of ensemble members. This difference is reversed for the Maumee River, where the ensembled hydrology produces lower annual sediment discharges than the ensembled climate.

	RCP	Ensemble Method	Maumee Total Annual Sediment Discharge (tonnes)	St. Joseph Total Annual Sediment Discharge (tonnes)
All Members	4.5	Hydrology	1,433,531	8,519
		Climate	1,588,889	6,929
	8.5	Hydrology	1,454,865	9,312
		Climate	1,573,345	7,568
CSIRO mk3.6	4.5	Hydrology	1,488,785	9,556
		Climate	1,637,137	8,095
	8.5	Hydrology	1,503,671	10,034
		Climate	1,614,038	8,499
Representative	4.5	Hydrology	1,461,130	8,685
		Climate	1,545,479	7,464
	8.5	Hydrology	1,436,010	9,239
		Climate	1,537,315	8,178
Best Fit	4.5	Hydrology	1,440,338	8,350
		Climate	1,542,808	7,133
	8.5	Hydrology	1,487,714	9,619
		Climate	1,573,732	8,046

REFERENCES

REFERENCES

Abbaspour, K.C., 2015. SWAT-CUP: SWAT Calibration and Uncertainty Programs. Eawag.

Abrams, E.M., Rue, D.J., 1988. The causes and consequences of deforestation among the prehistoric Maya. Human Ecology, 16(4): 377-395. DOI:10.1007/bf00891649

Alighalehbabakhani, F. et al., 2017a. Forecasting the remaining reservoir capacity in the Laurentian Great Lakes watershed. J. Hydrol., 555: 926-937. DOI:10.1016/j.jhydrol.2017.10.052

Alighalehbabakhani, F. et al., 2017b. Estimates of Sediment Trapping Rates for Two Reservoirs in the Lake Erie Watershed: Past and Present Scenarios. J. Hydrol., 544: 147-155. DOI:10.1016/j.jhydrol.2016.11.032

Arnold, J.G. et al., 2012. Soil and Water Assessment Tool Input/Output Documentation Version 2012, Texas Water Resources Institute, College Station, TX.

Bathurst, J.C., Iroume, A., 2014. Quantitative generalizations for catchment sediment yield following forest logging. Water Resour. Res., 50(11): 8383-8402. DOI:10.1002/2014wr015711

Beaty, K., 1994. Sediment transport in a small stream following two successive forest fires. Canadian Journal of Fisheries and Aquatic Sciences, 51(12): 2723-2733.

Benda, L., Miller, D., Bigelow, P., Andras, K., 2003. Effects of post-wildfire erosion on channel environments, Boise River, Idaho. For. Ecol. Manage., 178(1-2): 105-119. DOI:10.1016/s0378-1127(03)00056-2

Beschta, R.L., 1978. Long-term patterns of sediment production following road construction and logging in the Oregon coast range. Water Resour. Res., 14(6): 1011-1016. DOI:10.1029/WR014i006p01011

Blewett, W.L., Lusch, D.P., Schaetzl, R.J., 2009. The Physical Landscape: A Glacial Legacy. In: Schaetzl, R., Darden, J., Brandt, D. (Eds.), Michigan Geography and Geology. Pearson, pp. 249-273.

Bosch, J.M., Hewlett, J.D., 1982. A review of catchment experiments to determine the effect of vegetation changes on water yield and evapo-transpiration. J. Hydrol., 55(1-4): 3-23. DOI:10.1016/0022-1694(82)90117-2

Bosch, N.S., Evans, M.A., Scavia, D., Allan, J.D., 2014. Interacting effects of climate change and agricultural BMPs on nutrient runoff entering Lake Erie. Journal of Great Lakes Research, 40(3): 581-589. DOI:10.1016/j.jglr.2014.04.011

Bowling, L.C., Storck, P., Lettenmaier, D.P., 2000. Hydrologic effects of logging in western Washington, United States. Water Resour. Res., 36(11): 3223-3240. DOI:10.1029/2000wr900138

Brekke, L., Thrasher, B.L., Maurer, E.P., Pruitt, T., 2013. Downscaled CMIP3 and CMIP5 Climate and Hydrology Projections: Release of Downscaled CMIP5 Climate Projections, Comparison with preceding Information, and Summary of User Needs, U.S. Department of the Interior, Bureau of Reclamation.

Cerda, A., 1998. Changes in overland flow and infiltration after a rangeland fire in a Mediterranean scrubland. Hydrol. Process., 12(7): 1031-1042. DOI:10.1002/(sici)1099-1085(19980615)12:7<1031::Aid-hyp636>3.0.Co;2-v

Chaplot, V., 2007. Water and soil resources response to rising levels of atmospheric CO_2 concentration and to changes in precipitation and air temperature. J. Hydrol., 337(1-2): 159-171. DOI:10.1016/j.jhydrol.2007.01.026

Cherkauer, K.A., Sinha, T., 2010. Hydrologic impacts of projected future climate change in the Lake Michigan region. Journal of Great Lakes Research, 36: 33-50. DOI:10.1016/j.jglr.2009.11.012

Chien, H.C., Yeh, P.J.F., Knouft, J.H., 2013. Modeling the potential impacts of climate change on streamflow in agricultural watersheds of the Midwestern United States. J. Hydrol., 491: 73-88. DOI:10.1016/j.jhydrol.2013.03.026

Comer, P.J., Albert, D.A., 1998. Vegetation of Michigan Circa 1800: An Interpretation of the General Land Office Surveys. Michigan Natural Features Inventory.

Dahl, T.A., Kendall, A.D., Hyndman, D.W., 2018. Impacts of projected climate change on sediment yield and dredging costs. Hydrol. Process., 32(9): 1223-1234. DOI:doi:10.1002/hyp.11486

Dekker, L.W., Doerr, S.H., Oostindie, K., Ziogas, A.K., Ritsema, C.J., 2001. Water repellency and critical soil water content in a dune sand. Soil Science Society of America Journal, 65(6): 1667-1674. DOI:10.2136/sssaj2001.1667

Dickmann, D.I., 2009. Forests and Forestry from an Historical Perspective. In: Schaetzl, R., Darden, J., Brandt, D. (Eds.), Michigan Geography and Geology. Pearson.

Doerr, S.H., Shakesby, R.A., Walsh, R.P.D., 2000. Soil water repellency: its causes, characteristics and hydro-geomorphological significance. Earth-Science Reviews, 51(1-4): 33-65. DOI:10.1016/s0012-8252(00)00011-8

Doerr, S.H., Thomas, A.D., 2000. The role of soil moisture in controlling water repellency: new evidence from forest soils in Portugal. J. Hydrol., 231: 134-147. DOI:10.1016/s0022-1694(00)00190-6

Ebel, B.A., Rengers, F.K., Tucker, G.E., 2016. Observed and simulated hydrologic response for a first-order catchment during extreme rainfall 3 years after wildfire disturbance. Water Resour. Res., 52(12): 9367-9389. DOI:10.1002/2016wr019110

Edwards, T.K., Glysson, G.D., 1999. Field methods for measurement of fluvial sediment. Techniques of Water-Resources Investigations of the U.S. Geological Survey: , 3. U.S. Geological Survey, Reston, VA.

Ellis, E.C. et al., 2013. Used planet: A global history. Proceedings of the National Academy of Sciences of the United States of America, 110(20): 7978-7985. DOI:10.1073/pnas.1217241110

Fernandez, C., Vega, J.A., Vieira, D.C.S., 2010. Assessing soil erosion after fire and rehabilitation treatments in NW Spain: performance of RUSLE and revised Morgan-Morgan-Finney models. Land Degrad. Dev., 21(1): 58-67. DOI:10.1002/ldr.965

Ficklin, D.L., Luo, Y.Z., Luedeling, E., Zhang, M.H., 2009. Climate change sensitivity assessment of a highly agricultural watershed using SWAT. J. Hydrol., 374(1-2): 16-29. DOI:10.1016/j.jhydrol.2009.05.016

Fitzpatrick, F.A., Knox, J.C., 2000. Spatial and temporal sensitivity of hydrogeomorphic response and recovery to deforestation, agriculture, and floods. Physical Geography, 21(2): 89-108. DOI:10.1080/02723646.2000.10642701

Foster, G., Lane, L., Nowlin, J., Laflen, J., Young, R., 1980. A Model to Estimate Sediment Yield from Field-Sized Areas: Development of Model, International Institute for Applied Systems Analysis, Laxenburg, Austria.

Foster, G., Lane, L., Nowlin, J., Laflen, J., Young, R., 1981. Estimating erosion and sediment yield on field-sized areas. Transactions of the ASAE, 24(5): 1253-1262.

Frans, C., Istanbulluoglu, E., Mishra, V., Munoz-Arriola, F., Lettenmaier, D.P., 2013. Are climatic or land cover changes the dominant cause of runoff trends in the Upper Mississippi River Basin? Geophysical Research Letters, 40(6): 1104-1110. DOI:10.1002/grl.50262

Fry, J.A. et al., 2013. Completion of the 2006 National Land Cover Database for the Conterminous United States. Photogrammetric Engineering & Remote Sensing, 130: 294-304.

Gassman, P.W., Balmer, C., Siemers, M., Srinivasan, R., 2014. The SWAT Literature Database: Overview of Database Structure and Key SWAT Literature Trends, SWAT 2014 Conference. Texas Water Resources Institute, Pernambuco, Brazil.

Gentry, A.H., Lopez-Parodi, J., 1980. Deforestation and Increased Flooding of the Upper Amazon. Science, 210(4476): 1354. DOI:10.1126/science.210.4476.1354

Gibson, S.A., Little, C.D., 2006. Implementation of the sediment impact assessment model (SIAM) in HEC-RAS, 8th Federal Interagency Sedimentation Conference, Reno, NV.

Giorgi, F., Francisco, R., 2000a. Evaluating uncertainties in the prediction of regional climate change. Geophysical Research Letters, 27(9): 1295-1298. DOI:10.1029/1999gl011016

Giorgi, F., Francisco, R., 2000b. Uncertainties in regional climate change prediction: a regional analysis of ensemble simulations with the HADCM2 coupled AOGCM. Climate Dynamics, 16(2-3): 169-182. DOI:10.1007/pl00013733

Giorgi, F., Mearns, L.O., 2002. Calculation of average, uncertainty range, and reliability of regional climate changes from AOGCM simulations via the "reliability ensemble averaging"(REA) method. Journal of Climate, 15(10): 1141-1158.

Gould, G.K. et al., 2016. The effects of climate change and extreme wildfire events on runoff erosion over a mountain watershed. J. Hydrol., 536: 74-91. DOI:10.1016/j.jhydrol.2016.02.025

Gronewold, A.D., Stow, C.A., 2014. Water Loss from the Great Lakes. Science, 343(6175): 1084-1085. DOI:10.1126/science.1249978

Haines, D.A., Sando, R.W., 1969. Climatic Conditions Preceding Historicaly Great Fires in the North Central Region. In: Agriculture, U.S.D.o. (Ed.). North Central Forest Experiment Station, St. Paul, MN, pp. 23.

Hansen, M.C., Stehman, S.V., Potapov, P.V., 2010. Quantification of global gross forest cover loss. Proceedings of the National Academy of Sciences of the United States of America, 107(19): 8650-8655. DOI:10.1073/pnas.0912668107

Harbaugh, A.W., Banta, E.R., Hill, M.C., McDonald, M.G., 2000. MODFLOW-2000, The U. S. Geological Survey Modular Ground-Water Model-User Guide to Modularization Concepts and the Ground-Water Flow Process. Open-file Report. U. S. Geological Survey(92): 134.

Hay, R.L., Meriwether, M., 2004. Jordan River Assessment. Michigan Department of Natural Resources, Fisheries Division, East Lansing, MI.

Hayhoe, K., VanDorn, J., Croley Ii, T., Schlegal, N., Wuebbles, D., 2010. Regional climate change projections for Chicago and the US Great Lakes. Journal of Great Lakes Research, 36, Supplement 2: 7-21. DOI:http://dx.doi.org/10.1016/j.jglr.2010.03.012

Helvey, J.D., 1980. Effects of a North Central Washington wildfire on runoff and sediment production. JAWRA Journal of the American Water Resources Association, 16(4): 627-634. DOI:doi:10.1111/j.1752-1688.1980.tb02441.x

Hicks, B.J., Beschta, R.L., Harr, R.D., 1991. Long-Term Changes in Streamflow Following Logging in Western Oregon and Associated Fisheries Implications. Water Resour. Bull., 27(2): 217-226.

Huffman, E.L., MacDonald, L.H., Stednick, J.D., 2001. Strength and persistence of fire-induced soil hydrophobicity under ponderosa and lodgepole pine, Colorado Front Range. Hydrol. Process., 15(15): 2877-2892. DOI:doi:10.1002/hyp.379

Hyndman, D.W., Kendall, A.D., Welty, N.R.H., 2007. Evaluating Temporal and Spatial Variations in Recharge and Streamflow Using the Integrated Landscape Hydrology Model (ILHM). In: Hyndman, D.W., DayLewis, F.D., Singha, K. (Eds.), Subsurface Hydrology: Data Integration for Properties and Processes. Geophysical Monograph Series, pp. 121-141. DOI:10.1029/171gm11

IPCC, 2014. Climate Change 2014: Synthesis Report. Contribution of Working Groups I, II and III to the Fifth Assessment Report of the Intergovernmental Panel on Climate Change, IPCC, Geneva, Switzerland.

Jeffrey, S. et al., 2013. Australia's CMIP5 submission using the CSIRO Mk3. 6 model. Aust. Meteor. Oceanogr. J, 63: 1-13.

Johansen, M.P., Hakonson, T.E., Breshears, D.D., 2001. Post-fire runoff and erosion from rainfall simulation: contrasting forests with shrublands and grasslands. Hydrol. Process., 15(15): 2953-2965. DOI:10.1002/hyp.384

Johnson, T. et al., 2015. Modeling Streamflow and Water Quality Sensitivity to Climate Change and Urban Development in 20 US Watersheds. J. Am. Water Resour. Assoc., 51(5): 1321-1341. DOI:10.1111/1752-1688.12308

Kalamandeen, M. et al., 2018. Pervasive Rise of Small-scale Deforestation in Amazonia. Scientific Reports, 8. DOI:10.1038/s41598-018-19358-2

Karamesouti, M., Petropoulos, G.P., Papanikolaou, I.D., Kairis, O., Kosmas, K., 2016. Erosion rate predictions from PESERA and RUSLE at a Mediterranean site before and after a wildfire: Comparison & implications. Geoderma, 261: 44-58. DOI:10.1016/j.geoderma.2015.06.025

Kendall, A.D., 2009. Predicting the impacts of land use and climate on regional-scale hydrologic fluxes, Michigan State University, East Lansing, MI.

Klein, R.D., Lewis, J., Buffleben, M.S., 2012. Logging and turbidity in the coastal watersheds of northern California. Geomorphology, 139: 136-144. DOI:10.1016/j.geomorph.2011.10.011

Knutti, R., Furrer, R., Tebaldi, C., Cermak, J., Meehl, G.A., 2010. Challenges in Combining Projections from Multiple Climate Models. Journal of Climate, 23(10): 2739-2758. DOI:10.1175/2009jcli3361.1

Kolka, R., 2012. Effects of fire and fuels management on water quality in eastern North America. In: LaFayette, Russell; Brooks, Maureen T.; Potyondy, John P.; Audin, Lisa; Krieger, Suzanne L.; Trettin, Carl C. Eds. 2012. Cumulative watershed effects of fuel management in the Eastern United States. Gen. Tech. Rep. SRS-161. Asheville, NC: US Department of Agriculture Forest Service, Southern Research Station. 282-293., 161: 282-293.

Krysanova, V., White, M., 2015. Advances in water resources assessment with SWAT-an overview. Hydrological Sciences Journal-Journal Des Sciences Hydrologiques, 60(5): 771-783. DOI:10.1080/02626667.2015.1029482

Larsen, I.J., MacDonald, L.H., 2007. Predicting postfire sediment yields at the hillslope scale: Testing RUSLE and Disturbed WEPP. Water Resour. Res., 43(11). DOI:10.1029/2006wr005560

Larsen, I.J. et al., 2009. Causes of post-fire runoff and erosion: water repellency, cover, or soil sealing? Soil Science Society of America Journal, 73(4): 1393-1407.

Legleiter, C.J., Lawrence, R.L., Fonstad, M.A., Marcus, W.A., Aspinall, R., 2003. Fluvial response a decade after wildfire in the northern Yellowstone ecosystem: a spatially explicit analysis. Geomorphology, 54(3-4): 119-136. DOI:10.1016/s0169-555x(02)00332-x

Lewis, J., Mori, S.R., Keppeler, E.T., Ziemer, R.R., 2001. Impacts of logging on storm peak flows, flow volumes and suspended sediment loads in Caspar Creek, California. Land Use and Watersheds: Human Influence on Hydrology and Geomorphology in Urban and Forest Areas, 2. Amer Geophysical Union, Washington, 85-125 pp.

Li, K.Y., Coe, M.T., Ramankutty, N., Jong, R.D., 2007. Modeling the hydrological impact of land-use change in West Africa. J. Hydrol., 337(3): 258-268. DOI:https://doi.org/10.1016/j.jhydrol.2007.01.038

Litschert, S.E., Theobald, D.M., Brown, T.C., 2014. Effects of climate change and wildfire on soil loss in the Southern Rockies Ecoregion. Catena, 118: 206-219. DOI:10.1016/j.catena.2014.01.007

Little, C., Jonas, M., 2010. Sediment impact analysis methods (SIAM): overview of model capabilities, applications, and limitations, Proceedings of the 2nd Joint Federal Interagency Conference on Sedimentation and Hydrologic Modeling, Las Vegas, NV, USA, Las Vegas, NV.

Luscz, E.C., Kendall, A.D., Hyndman, D.W., 2017. A spatially explicit statistical model to quantify nutrient sources, pathways, and delivery at the regional scale. Biogeochemistry, 133(1): 37-57. DOI:10.1007/s10533-017-0305-1

Mao, D.Z., Cherkauer, K.A., 2009. Impacts of land-use change on hydrologic responses in the Great Lakes region. J. Hydrol., 374(1-2): 71-82. DOI:10.1016/j.jhydrol.2009.06.016

Martin, S.L., Jasinski, B.L., Kendall, A.D., Dahl, T.A., Hyndman, D.W., 2015. Quantifying beaver dam dynamics and sediment retention using aerial imagery, habitat characteristics, and economic drivers. Landscape Ecology, 30(6): 1129-1144. DOI:10.1007/s10980-015-0165-9

Masui, T. et al., 2011. An emission pathway for stabilization at 6 Wm(-2) radiative forcing. Climatic Change, 109(1-2): 59-76. DOI:10.1007/s10584-011-0150-5

Matheussen, B., Kirschbaum, R.L., Goodman, I.A., O'Donnell, G.M., Lettenmaier, D.P., 2000. Effects of land cover change on streamflow in the interior Columbia River Basin (USA and Canada). Hydrol. Process., 14(5): 867-885. DOI:10.1002/(sici)1099-1085(20000415)14:5<867::Aid-hyp975>3.0.Co;2-5

Maurer, E.P., Hidalgo, H.G., 2008. Utility of daily vs. monthly large-scale climate data: an intercomparison of two statistical downscaling methods. Hydrol. Earth Syst. Sci., 12(2): 551-563.

Maurer, E.P., Wood, A.W., Adam, J.C., Lettenmaier, D.P., Nijssen, B., 2002. A long-term hydrologically based dataset of land surface fluxes and states for the conterminous United States. Journal of Climate, 15(22): 3237-3251. DOI:10.1175/1520-0442(2002)015<3237:althbd>2.0.co;2

Miesel, J. et al., 2012. Fire effects on soils in Lake States forests: a compilation of published research to facilitate long-term investigations. Forests, 3(4): 1034-1070.

Miller, J.D., Nyhan, J.W., Yool, S.R., 2003. Modeling potential erosion due to the Cerro Grande Fire with a GIS-based implementation of the Revised Universal Soil Loss Equation. International Journal of Wildland Fire, 12(1): 85-100. DOI:10.1071/wf02017

Moody, J.A., Martin, D.A., 2001a. Initial hydrologic and geomorphic response following a wildfire in the Colorado Front Range. Earth Surf. Process. Landf., 26(10): 1049-1070. DOI:10.1002/esp.253

Moody, J.A., Martin, D.A., 2001b. Post-fire, rainfall intensity-peak discharge relations for three mountainous watersheds in the western USA. Hydrol. Process., 15(15): 2981-2993. DOI:10.1002/hyp.386

Moody, J.A., Shakesby, R.A., Robichaud, P.R., Cannon, S.H., Martin, D.A., 2013. Current research issues related to post-wildfire runoff and erosion processes. Earth-Science Reviews, 122: 10-37. DOI:10.1016/j.earscirev.2013.03.004

Mooney, D.M., 2006. SIAM, sediment impact analysis methods, for evaluating sedimentation causes and effects, Proceedings of the Eighth Federal Interagency Sedimentation Conference, Reno, NV.[http://acwi. gov/8thFISC-ordering-revised. html].

Mooney, D.M., 2007. SIAM: Sediment Impact Analysis Methods, Colorado State University, 404 pp.

Moore, R.D., Wondzell, S.M., 2005. Physical hydrology and the effects of forest harvesting in the Pacific Northwest: A review. J. Am. Water Resour. Assoc., 41(4): 763-784.

Morang, A., Rosati, J.D., King, D.B., 2013. Regional Sediment Processes, Sediment Supply, and Their Impact on the Louisiana Coast. Journal of Coastal Research: 141-165. DOI:10.2112/si63-013.1

Moriasi, D.N. et al., 2007. Model evaluation guidelines for systematic quantification of accuracy in watershed simulations. Transactions of the Asabe, 50(3): 885-900.

Mukundan, R. et al., 2013. Suspended sediment source areas and future climate impact on soil erosion and sediment yield in a New York City water supply watershed, USA. Geomorphology, 183: 110-119. DOI:10.1016/j.geomorph.2012.06.021

Nakicenovic, N., Swart, R., 2000. Special report on emissions scenarios, Cambridge, UK.

Neary, D.G., Ice, G.G., Jackson, C.R., 2009. Linkages between forest soils and water quality and quantity. For. Ecol. Manage., 258(10): 2269-2281. DOI:https://doi.org/10.1016/j.foreco.2009.05.027

Neitsch, S.L., Arnold, J.G., Kiniry, J.R., Williams, J.R., 2011. Soil and Water Assessment Tool Theoretical Documentation Version 2009. TR-406, Texas Water Resources Institute, College Station, TX.

Nilsson, C. et al., 2005. Forecasting Environmental Responses to Restoration of Rivers Used as Log Floatways: An Interdisciplinary Challenge. Ecosystems, 8(7): 779-800. DOI:10.1007/s10021-005-0030-9

O'Neal, M.R., Nearing, M.A., Vining, R.C., Southworth, J., Pfeifer, R.A., 2005. Climate change impacts on soil erosion in Midwest United States with changes in crop management. Catena, 61(2-3): 165-184. DOI:10.1016/j.catena.2005.03.003

Park, J.Y. et al., 2011. Assessment of Future Climate Change Impacts on Water Quantity and Quality for a Mountainous Dam Watershed Using SWAT. Transactions of the Asabe, 54(5): 1725-1737.

Pierce, D.W., Barnett, T.P., Santer, B.D., Gleckler, P.J., 2009. Selecting global climate models for regional climate change studies. Proceedings of the National Academy of Sciences, 106(21): 8441-8446.

Potapov, P. et al., 2017. The last frontiers of wilderness: Tracking loss of intact forest landscapes from 2000 to 2013. Science Advances, 3(1). DOI:10.1126/sciadv.1600821

Powers, P.F., Cutler, H.G., 1912. A History of Northern Michigan and Its People. Lewis Publishing Company, Alcona, MI, 555 pp.

Praskievicz, S., 2016. Impacts of Projected Climate Changes on Streamflow and Sediment Transport for Three Snowmelt-Dominated Rivers in the Interior Pacific Northwest. River Res. Appl., 32(1): 4-17. DOI:10.1002/rra.2841

Pryor, S.C., Barthelmie, R.J., Schoof, J.T., 2013. High-resolution projections of climate-related risks for the Midwestern USA. Climate Research, 56(1): 61-79.

Pryor, S.C. et al., 2014. Ch. 18: Midwest. In: Melillo, J.M., Richmond, T.C., Yohe, G.W. (Eds.), Climate Change Impacts in the United States: The Third National Climate Assessment. U.S. Global Change Research Program, pp. 418-440. DOI:10.7930/J0J1012N

Quinn, F.H., 2002. Secular changes in Great Lakes water level seasonal cycles. Journal of Great Lakes Research, 28(3): 451-465.

Reeder, C.J., Jurgensen, M., 1979. Fire-induced water repellency in forest soils of upper Michigan. Canadian Journal of Forest Research, 9(3): 369-373.

Riahi, K. et al., 2011. RCP 8.5-A scenario of comparatively high greenhouse gas emissions. Climatic Change, 109(1-2): 33-57. DOI:10.1007/s10584-011-0149-y

Richardson, J., Hole, F., 1978. Influence of Vegetation on Water Repellency in Selected Western Wisconsin Soils 1. Soil Science Society of America Journal, 42(3): 465-467.

Roberts, R.G., Church, M., 1986. The sediment budget in severely disturbed watersheds, Queen Charlotte Ranges, British Columbia. Canadian Journal of Forest Research-Revue Canadienne De Recherche Forestiere, 16(5): 1092-1106. DOI:10.1139/x86-189

Robichaud, P.R., 2000. Fire effects on infiltration rates after prescribed fire in Northern Rocky Mountain forests, USA. J. Hydrol., 231-232: 220-229. DOI:https://doi.org/10.1016/S0022-1694(00)00196-7

Rothacker, L. et al., 2018. Impact of climate change and human activity on soil landscapes over the past 12,300 years. Scientific Reports, 8. DOI:10.1038/s41598-017-18603-4

Rulli, M.C., Offeddu, L., Santini, M., 2013. Modeling post-fire water erosion mitigation strategies. Hydrol. Earth Syst. Sci., 17(6): 2323-2337. DOI:10.5194/hess-17-2323-2013

Schwartz, R.C., Deadman, P.J., Scott, D.J., Mortsch, L.D., 2004. Modeling the impacts of water level changes on a Great Lakes community. J. Am. Water Resour. Assoc., 40(3): 647-662. DOI:10.1111/j.1752-1688.2004.tb04450.x

Scott, D.F., 1993. The hydrological effects of fire in South-African mountain catchments. J. Hydrol., 150(2-4): 409-432. DOI:10.1016/0022-1694(93)90119-t

Serpa, D. et al., 2015. Impacts of climate and land use changes on the hydrological and erosion processes of two contrasting Mediterranean catchments. Sci. Total Environ., 538: 64-77. DOI:10.1016/j.scitotenv.2015.08.033

Shakesby, R.A., Doerr, S.H., 2006. Wildfire as a hydrological and geomorphological agent. Earth-Science Reviews, 74(3-4): 269-307. DOI:10.1016/j.earscirev.2005.10.006

Shin, S.S., Park, S.D., Lee, K.S., 2013. Sediment and hydrological response to vegetation recovery following wildfire on hillslopes and the hollow of a small watershed. J. Hydrol., 499: 154-166. DOI:https://doi.org/10.1016/j.jhydrol.2013.06.048

Shrestha, R.R., Dibike, Y.B., Prowse, T.D., 2012. Modelling of climate-induced hydrologic changes in the Lake Winnipeg watershed. Journal of Great Lakes Research, 38: 83-94. DOI:10.1016/j.jglr.2011.02.004

Smith, J.B., 1991. The Potential Impacts of Climate Change on the Great Lakes. Bulletin of the American Meteorological Society, 72(1): 21-28. DOI:10.1175/1520-0477(1991)072<0021:tpiocc>2.0.co;2

Swank, W.T., Vose, J.M., Elliott, K.J., 2001. Long-term hydrologic and water quality responses following commercial clearcutting of mixed hardwoods on a southern Appalachian catchment. For. Ecol. Manage., 143(1-3): 163-178. DOI:10.1016/s0378-1127(00)00515-6

Taylor, K.E., Stouffer, R.J., Meehl, G.A., 2012. An Overview of CMIP5 and the Experiment Design. Bulletin of the American Meteorological Society, 93(4): 485-498. DOI:10.1175/bams-d-11-00094.1

Templeton, W.J., Jay, D.A., 2013. Lower Columbia River Sand Supply and Removal: Estimates of Two Sand Budget Components. Journal of Waterway Port Coastal and Ocean Engineering, 139(5): 383-392. DOI:10.1061/(asce)ww.1943-5460.0000188

Terranova, O., Antronico, L., Coscarelli, R., Iaquinta, P., 2009. Soil erosion risk scenarios in the Mediterranean environment using RUSLE and GIS: An application model for Calabria (southern Italy). Geomorphology, 112(3-4): 228-245. DOI:10.1016/j.geomorph.2009.06.009

Twine, T.E., Kucharik, C.J., Foley, J.A., 2004. Effects of land cover change on the energy and water balance of the Mississippi River basin. Journal of Hydrometeorology, 5(4): 640-655. DOI:10.1175/1525-7541(2004)005<0640:Eolcco>2.0.Co;2

USACE, 2007. St. Joseph River Sediment Transport Modeling Study, Detroit, MI.

USACE, 2014. Waterborne Commerce of the United States, Calendar Year 2014, Part 3 - Waterways and Harbors Great Lakes. In: Army, D.o.t. (Ed.). Corps of Engineers Institute for Water Resources, pp. 118.

USACE, 2015. Great Lakes Navigation System Update. U. S. Army Corps of Engineers Detroit District, pp. A presentation focusing on the Great Lakes region current workload, as given to Congressional Staffers in February 2015 in Washington, DC. .

van Liew, M.W., Feng, S., Pathak, T.B., 2012. Climate change impacts on streamflow, water quality, and best management practices for the Shell and Logan Creek Watersheds in Nebraska, USA. International Journal of Agricultural and Biological Engineering, 5(1): 13-34.

Verma, S. et al., 2015. Climate Change Impacts on Flow, Sediment and Nutrient Export in a Great Lakes Watershed Using SWAT. Clean-Soil Air Water, 43(11): 1464-1474. DOI:10.1002/clen.201400724

Verry, E.S., 1986. Forest harvesting and water: The Lake States experience. Water Resour. Bull., 22(6): 1039-1047.

Vincent, R.E., 1962. Biogeographical and ecological factors contributing to the decline of artic grayling, Thymallus arcticus Pallas, in Michigan and Montana, University of Michigan, Ann Arbor, MI, 179 pp.

Whitaker, A., Alila, Y., Beckers, J., Toews, D., 2002. Evaluating peak flow sensitivity to clear-cutting in different elevation bands of a snowmelt-dominated mountainous catchment. Water Resour. Res., 38(9). DOI:10.1029/2001wr000514

Whitney, G.G., 1987. An ecological history of the Great Lakes forest of Michigan. J. Ecol., 75(3): 667-684. DOI:10.2307/2260198

Wiley, M.J. et al., 2010. A multi-modeling approach to evaluating climate and land use change impacts in a Great Lakes River Basin. Hydrobiologia, 657(1): 243-262. DOI:10.1007/s10750-010-0239-2

Williams, J.R., 1975. Sediment yield prediction with universal equation using runoff energy factor. In: Service, U.S.D.o.A.A.R. (Ed.).

Williams, J.R., 1995. The EPIC Model. In: Singh, V.P. (Ed.), Computer Models of Watershed Hydrology. Water Resources Publications, pp. 909-1000.

Wischmeier, W.H., Smith, D.D., 1978. Predicting rainfall erosion losses - a guide to conservation planning. In: Agriculture, U.S.D.o. (Ed.), Washington, D.C.

Wolock, D.M., 2003. Base-Flow Index Grid for the Conterminous United States. 2003-263.

Wood, A.W., Leung, L.R., Sridhar, V., Lettenmaier, D.P., 2004. Hydrologic implications of dynamical and statistical approaches to downscaling climate model outputs. Climatic Change, 62(1-3): 189-216. DOI:10.1023/B:CLIM.0000013685.99609.9e

Wright, R.F., 1976. The impact of forest fire on the nutrient influxes to small lakes in northeastern Minnesota. Ecology, 57(4): 649-663.

Xia, Y. et al., 2012. Continental-scale water and energy flux analysis and validation for the North American Land Data Assimilation System project phase 2 (NLDAS-2): 1. Intercomparison and application of model products. Journal of Geophysical Research: Atmospheres, 117(D3). DOI:10.1029/2011jd016048

Young, R., Onstad, C., Bosch, D., Anderson, W., 1989. AGNPS: A nonpoint-source pollution model for evaluating agricultural watersheds. Journal of soil and water conservation, 44(2): 168-173.

Zhang, M.F., Wei, X.H., 2014. Contrasted hydrological responses to forest harvesting in two large neighbouring watersheds in snow hydrology dominant environment: implications for forest management and future forest hydrology studies. Hydrol. Process., 28(26): 6183-6195. DOI:10.1002/hyp.10107

Zhang, M.F., Wei, X.H., Sun, P.S., Liu, S.R., 2012. The effect of forest harvesting and climatic variability on runoff in a large watershed: The case study in the Upper Minjiang River of Yangtze River basin. J. Hydrol., 464: 1-11. DOI:10.1016/j.jhydrol.2012.05.050

Zhang, Q., Jiang, T., Chen, Y.D., Chen, X.H., 2010. Changing properties of hydrological extremes in south China: natural variations or human influences? Hydrol. Process., 24(11): 1421-1432. DOI:10.1002/hyp.7599